2012

Myocardial t1 Mapping Techniques for Quantification of Myocardial Fibrosis

Xiaopeng Zhou
Cleveland State University

MYOCARDIAL T1 MAPPING TECHNIQUES FOR QUANTIFICATION OF MYOCARDIAL FIBROSIS

XIAOPENG ZHOU

Bachelor of Chemical Engineering

Liaoning University of Petroleum & Chemical Technology

July, 2001

Master of Biochemical Engineering

Tianjin University

March, 2004

submitted in partial fulfillment of requirements for the degree

DOCTOR OF ENGINEERING IN APPLIED BIOMEDICAL ENGINEERING
at the

CLEVELAND STATE UNIVERSITY

December, 2012

This dissertation has been approved
for the Department of Chemical and Biomedical Engineering
and the College of Graduate Studies by

_____

Dissertation Committee Chairperson, Randolph M. Setser, D. Sc

_____

Department/Date

_____

George P. Chatzimavroudis, Ph.D.
Department of Chemical and Biomedical Engineering

_____

Department/Date

_____

Sandra S. Halliburton, Ph.D.
Department of Chemical and Biomedical Engineering

_____

Department/Date

_____

Melanie Kotys-Traughber, D. Sc.
Department of Chemical and Biomedical Engineering

_____

Department/Date

_____

Miron Kaufman, Ph.D.
Department of Physics

_____

Department/Date

To my family, friends, for their love and support

and

To my teachers, from whom have learned so much.

ACKNOWLEDGEMENTS

First, I would like to express my deepest gratitude to my advisor Dr. Randolph Setser for his continuous support, patience, motivation and enthusiasm for my research. His constant encouragement and immense knowledge has inspired me to achieve my goal and complete this research. I will never forget his unfailing support as I hurdle the obstacles during the course of this thesis. I am grateful to him for believing in me and giving me this opportunity.

I would also like to specially thank Dr. George Chatzimavroudis and Dr. Joanne Belovich for their help in planning my study in Cleveland State University. I would also like to thank my committee members Dr. Sandra Hallliburtion, and Dr. Miron Kaufman for helping me with their encouragement, insightful comments and guidance.

I would like to thank Philips, Cleveland State University and Cleveland Clinic for providing financial assistance to this project. I am grateful to Dr. Stefan Fischer, Dr. Melanie Traughber, Dr. Christian Stehning and Mr. Harry Friel, Hui Wang and Mohammad-hossein Kadbi from Philips for their support and suggestions. I would like to express my gratitude to Dr. Scott Flamm for his valuable insights, patience and encouragement all through my research. I thank Dr. Paul Schoenhagen and Dr. Prabhkar Rajiah for their help of recruiting patients. I thank Dr. Deborah Kwon and Dr. Patrick Collier for their help with histology analysis. I thank Ms. Megan Griffiths, scientific writer for the Imaging Institute, Cleveland Clinic, for editorial assistance of our manuscripts. I am thankful to the MRI technologists: Kathy Kohut, Angel Lawrence,

Joan Weaver, and Sharon Berry for their help with patient scans. I am thankful to every volunteer and patient recruited in our projects. I thank our secretaries Lisa Clough, Becky Laird, Darlene Montgomery for their help during the whole process.

I thank my fellow labmates: Uma Numburi, Carla Thompson, YuJaung Kim, Mitya Barreto, Kassem Soufan and Mehmet Ersoy for all the stimulating discussions, help and motivation to complete the dissertation, and for all the fun. I would also like to thank my best friends, Meng Yue and Run Hai who have been there with me whenever I needed them. Thank you to my family members for standing by me while I went crazy and stayed up days and nights on end trying to finish this on time.

MYOCARDIAL T1 MAPPING TECHNIQUES FOR QUANTIFICATION OF MYOCARDIAL FIBROSIS

XIAOPENG ZHOU

ABSTRACT

Identifying and quantifying diffuse myocardial fibrosis is important to provide insights into the relationship between myocardial fibrosis, diastolic and systolic dysfunction, as well as clinical outcomes. T1 mapping is a promising technique for noninvasively identifying diffuse myocardial fibrosis in heart failure. A quantitative T1 map provides sensitivity to the full range of T1 values and is advantageous over the traditional T1-weighted imaging by reducing the reliance on visual interpretation of the signal intensity in the myocardium. However, in-vivo myocardial T1 quantification is challenging because of cardiac and respiratory motion. During the past few years, a variety of T1 mapping techniques, including the modified Look Locker inversion recovery (MOLLI) sequence, have been developed and optimized to measure the myocardial T1 value. Importantly, there have been significant differences between the T1 values determined by various methods, and several aspects of T1 mapping are incompletely understood. The accuracy of T1 mapping is sensitive to several confounding factors, such as the types of T1 mapping acquisition sequence and individual physiologic parameters. It also remains unclear if myocardial T1 values are

constant throughout the cardiac cycle or the cyclic variation from the error of the variable flip angle (VFA) technique. Lastly, it is necessary to validate these techniques against the endomyocardial biopsy.

The work intends to validate several aspects of T1 mapping. Firstly, whether there is significant cyclic variation of myocardial T1 at 1.5T was assessed in healthy volunteers and patients without myocardial disease. Secondly, a fast 3D DFA technique with B1 correction was developed to measure T1 comparably with gold standard in a wide range of T1 values, which showed it is necessary to incorporate B1 correction at 3T. Thirdly, Look Locker and MOLLI were compared to evaluate their agreement and difference in 3 patient groups precontrast and postcontrast situations. Finally, the T1 mapping technique was applied in a group of patients with diffuse myocardial fibrosis eligible for myectomy surgery. Precontrast and postcontrast myocardial T1 values were assessed to identify and quantify myocardial fibrosis, with subsequent histological validation based on intra-operative biopsies. The extracelluar volume calculated from T1 values positively correlated with histological analysis, which can help to guide the decision-making regarding when to send patients for invasive surgery and follow changes of fibrosis in the myocardium over time with noninvasive assessment.

TABLE OF CONTENTS

Page

LIST OF TABLES

Table **Page**

LIST OF FIGURES

Figure **Page**

CHAPTER I

INTRODUCTION

Cardiovascular disease (CVD) is the disease of the heart and circulatory system. CVD is the leading threat to human health in the United States and the Western World. It is estimated by the American Heart Association that 80 million people in the United States have one or more forms of CVD. With the growing epidemic of obesity, diabetes, and hypertension, in addition to longer life expectancy, 40.5% of the US population is projected to have some form of CVD by 2030 [1].

CVD encompasses a number of specific illnesses such as coronary heart disease, heart failure (HF), cardiomyopathies, arrhythmias, stroke, arterial and pulmonary hypertension, congenital heart disease, valvular heart disease, etc [2]. Among all the forms of CVD, HF is associated with significant morbidity, mortality, and financial burden to health care services, causing over 1,000,000 hospitalizations /year in the United States [3]. HF represents a complex physiologic state characterized by a reduced cardiac output that can not meet systemic demands. The major challenges in HF management are to identify the underlying etiology and make early diagnosis [4]. Although significant advances occurred in the last 20 years to manage the systolic HF, many patients progress

to end-stage cardiomyopathies [3]. It is of particular importance to accurately and noninvasively determine the cardiac function for diagnosis and treatment of the heart diseases. Magnetic resonance imaging (MRI) is a rapidly evolving modality, providing noninvasive assessment of cardiac morphology, function, perfusion and tissue characterization for patients [2, 4]. A stepwise approach using cardiovascular MRI was proposed to evaluate and manage of patients who have HF and specific cardiomyopathis [2], which includes assessing morphology and function, characterizing the cardiomyopathy and risk stratification and therapeutic management. However, development of the means to acquire and analyze these images is still an evolving and promising area to explore clinical application.

1.1 Background

The term “cardiomyopathy” was defined as non-coronary myocardial disease by Wallace Brigden for the first time in 1957 [5]. The definition of cardiomyopathies has been evolving and updating with the development of diagnostic technology.

In 1995, World Health Organization (WHO) /International Society and Federation of Cardiology (ISFC) Task Force defined cardiomyopathies as “diseases of myocardium associated with cardiac dysfunction” [6]. The cardiomyopathies were classified according to anatomy and physiology into the following types: dilated cardiomyopathy (DCM), hypertrophic cardiomyopathy (HCM), restrictive cardiomyopathy (RCM), arrhythmogenic right ventricular cardiomyopathy/dysplasia (ARVC/D), and unclassified

cardiomyopathies. This version of definition and classification is more widely used in the years afterwards. However, classifying for heart muscle disease is exceedingly complex. With better understanding of etiology and pathogenesis, dramatic advances in diagnosis and rapid evolution of molecular genetics in cardiology, a new contemporary definition and classification of cardiomyopathies was proposed by the American Heart Association (AHA) in 2006 [7] in concert with the molecular era of cardiovascular disease. The AHA expert consensus panel defined that "Cardiomyopathies are a heterogeneous group of diseases of the myocardium associated with mechanical and/or electrical dysfunction that usually (but not invariably) exhibit inappropriate ventricular hypertrophy or dilatation and are due to a variety of causes that frequently are genetic. Cardiomyopathies either are confined to the heart or are part of generalized systemic disorders, often leading to cardiovascular death or progressive heart failure–related disability." Cardiomyopathies are classified into two groups: primary cardiomyopathies (predominantly involving the heart) and secondary cardiomyopathies (accompanied by other organ system involvement).

Determining the exact etiology is essential for directing the correct treatment and predicting survival. Cardiovascular MRI (CMR) is a rapidly evolving technology that is increasingly being used for the noninvasive imaging of the expanding HF population [8]. CMR has the potential to characterizing the myocardial and valvular structures and function, differentiating ischemic versus nonischemic cardiomyopathy, evaluating the risk stratification for therapeutic management [2].

1.2 Evaluation of Cardiomyopathies Using MRI

In comparison to other imaging modalities, including ultrasound, X-ray fluoroscopy and computed tomography (CT), MRI provides excellent spatial resolution and soft tissue contrast without radiation exposure. One of the most intriguing features of MRI is that it can provide various tissue contrasts by adjusting the parameters of the pulse sequence, such as flip angle, echo time and repetition time. For a typical MRI scan, the image contrast is predominately determined by spatially varying proton density, spin-lattice (or T1) relaxation time, and spin-spin (or T2) relaxation time. By using different pulse sequences and acquisition parameters, MRI allows us to examine myocardial function, morphology, perfusion, valvular function, myocardial tissue characterization and so on. Given its enhanced spatial resolution, improved tissue characterization, and lack of ionizing radiation, MRI has become the best of choice in the evaluation of patients with new-onset cardiomyopathy of unknown etiology.

The application of gadolinium based extracellular contrast agents can further extend the ability of MRI to discriminate ischemic from nonischemic etiologies due to different hyperenhancement patterns among the various nonischemic cardiomyopathies. Delayed enhancement (DE) MRI delineates areas of myocardial fibrosis, by imaging 10–15 minutes after gadolinium contrast administration. Delayed gadolinium retention in the interstitial space is increased in conditions with increased extracellular volume of distribution and/or decreased washout such as acute necrosis, fibrosis, infiltration and inflammation [9]. Since gadolinium shortens T1 relaxation time, it results in brighter signal intensity in the areas with increased interstitial space on inversion recovery T1-

weighted sequences [10-13]. This technique is sensitive and reproducible in the detection of myocardial scar. In an international, multicenter trial, DE MRI was associated with a sensitivity of 94–99% to detect myocardial infarction. Likewise, the accuracy of MRI for identifying myocardial infarction location (compared with infarct-related artery perfusion territory) was 99% (acute) and 91% (chronic) after contrast compared with 9% before contrast [14]. It is also important to note that the presence of DE is not specific for any cardiomyopathy. It is the location and pattern of DE that helps the final diagnosis and distinguishes the various etiologies of cardiomyopathies [15]. Multiple MRI sequences are often used in the assessment of cardiomyopathy. The combination of cine function, myocardial perfusion at rest and stress, and DE MRI helps the clinician elucidate the cause of the cardiomyopathy. It provides accurate and reproducible volumetric assessment of the left and right ventricular sizes, volumes, wall thicknesses and mass in addition to the ejection fraction with small inter- and intra-observer variability [1, 15].

1.2.1 Ischemic Cardiomyopathy

Although the 2006 AHA expert consensus panel did not support the term "ischemic cardiomyopathy", the classification of cardiomyopathies as ischemic and non-ischemic cardiomyopathy is still widely used. ICM is defined as dysfunction of the left ventricle as a result of a chronic lack of oxygen due to coronary artery disease [16]. About 1 out of 100 adults over the age of 60 have ICM. The prevalence of ICM in western countries is increasing despite improvements in prevention, diagnosis, and treatment of cardiovascular disease.

In the setting of coronary artery disease, myocardial ischemia may result in stunning, hibernation, and true infarction. Stunned myocardium occurs following an acute ischemic insult resulting in reversible contractile dysfunction. Hibernation describes chronic contractile impairment secondary to chronic hypoperfusion, where the myocardium is still viable. By either percutaneous coronary intervention or coronary artery bypass grafting, viable tissue can be revascularized and therefore myocardial contractility of the viable tissue can be improved. In contrast, patients with full thickness infarcted (scarred) tissue will not benefit from revascularization [17].

On delayed contrast enhanced T1-weighted images, infarcted tissues appear bright with decreased segmental contractile ability apparent on the corresponding cine images. On DE MR images, infarcted myocardium and fibrosis appear as high signal intensity in an area of coronary artery distribution. Since all infarctions start subendocardially and may progress towards epicardium, the subendocardium is always involved.

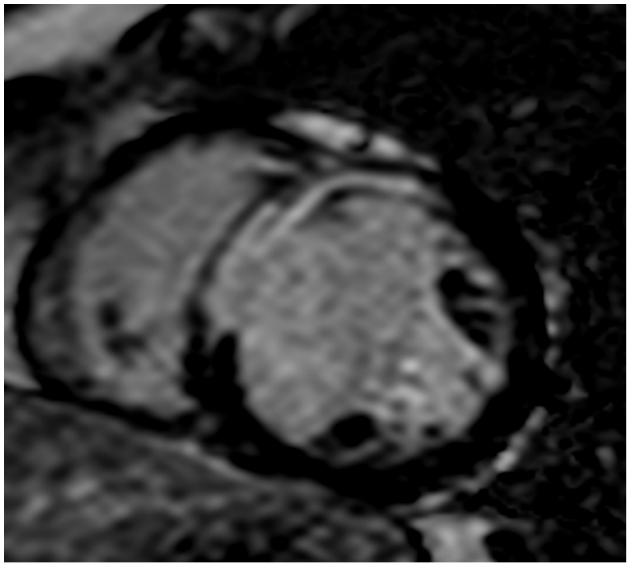

Figure 1-1:Short axis delayed enhancement images of a patient with ICM

DE MRI can be used following an ischemic event to help to distinguish between myocardial infarction (characterized by delayed contrast enhancement and segmental contractile dysfunction), viable but ischemic myocardium (characterized by segmental contractile dysfunction without delayed contrast enhancement) and normal myocardium.

The extent of myocardial delayed hyperenhancement postmyocardial infarction has important prognostic implications. It is generally accepted that the extent of transmural hyperenhancement within a myocardial segment is inversely proportional to the degree of expected functional recovery. Extensive involvement is highly predictive of a lack of functional improvement following revascularization [17]. Conversely, absence of delayed hyperenhancement within a segment of poor contractility correlates with a high likelihood of functional recovery after revascularization [11, 18].

1.2.2 Hypertrophic Cardiomyopathy

Hypertrophic cardiomyopathy (HCM) is a primary myocardial disease characterized morphologically by abnormal hypertrophied, in the absence of dilatation of the LV wall, which is usually asymmetric most prominently involving the interventricular septum with normal or reduced LV volume. Compared with normal ventricular septal measurement is 8-12 mm, the diastolic left ventricular wall thickness is 15mm or more [16]. The interventricular septum is typically more prominently involved than the left ventricular free wall, but concentric and apical hypertrophy can occur. The left ventricular volume is normal or reduced in HCM, and diastolic dysfunction is usually present. Arrhythmias and premature sudden death are common in HCM. Characteristic

histologic changes include myocyte hypertrophy and disarray, which usually corresponds to the areas of greatest hypertrophy [14, 15].

HCM is a genetic myocardial disorder with a prevalence of 1:500 [16] and probably the most frequently occurring cardiomyopathy. HCM is caused by a variety of mutations in genes encoding contractile proteins of the cardiac sarcomere. Currently, 11 mutant genes are associated with HCM, most commonly β-myosin heavy chain (the first identified) and myosin-binding protein C [7].

Typically, HCM patients display patchy, multifocal hyperenhancement occurring only within hypertrophied regions (Figure 1-2). The junction of the right ventricular free wall with the interventricular septum is frequently affected [17, 19, 20]. It is thought that the patchy enhancement is due to the presence of abundant connective tissue within the hypertrophic myocardium [21]. It has been proposed that the extent of delayed hyperenhancement may have prognostic implications, with the more severe manifestations of the disease, such as end-stage heart failure and sudden death, occurring more frequently in patients with high levels of delayed hyperenhancement reflecting high levels of myocardial fibrosis [20, 22]. However, diffuse myocardial fibrosis in HCM patients cannot be detected by DE MRI because the image contrast on DE MR images is on the basis of the difference in signal intensity between fibrotic and “normal” myocardium and such differences may not exist if the myocardial fibrosis is diffusive. Thus, the diffusive fibrosis will be nulled and not show hyperenhancement. The myocardium is thickened, and delayed enhancement is patchy.

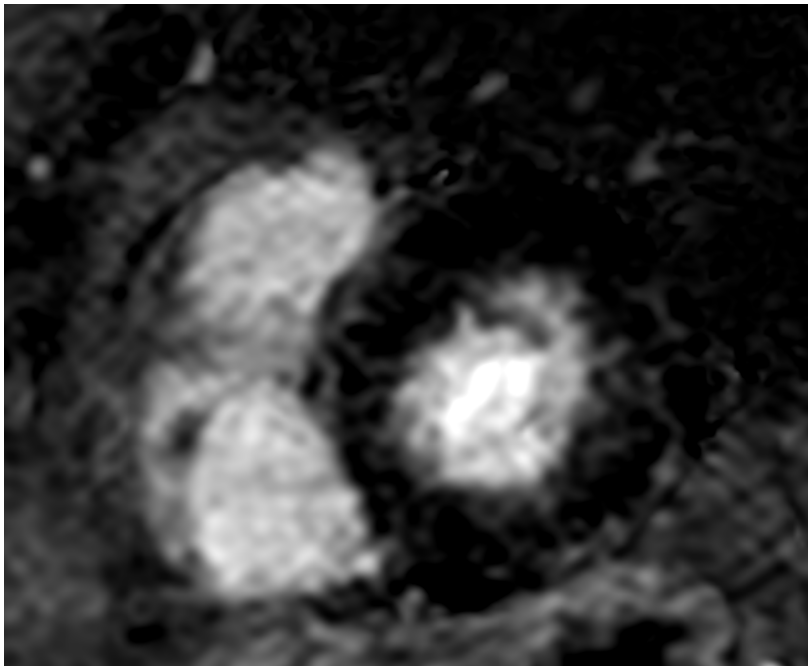

Figure 1-2:Short axis delayed enhancement images of a patient with HCM

1.2.3 Dilated Cardiomyopathy

Dilated cardiomyopathy (DCM) is characterized by ventricular chamber enlargement with an end diastolic diameter greater than 55 mm and impaired function of the left ventricle with an ejection fraction smaller than 45% or both ventricles [16]. The complete list of causes of DCM is extensive. It may be idiopathic, familial/genetic, viral and/or immune, alcoholic/toxic, or associated with recognized cardiovascular disease in which the degree of myocardial dysfunction is not explained by the abnormal loading conditions or the extent of ischemic damage [6]. DCM leads to progressive heart failure and a decline in LV contractile function, arrhythmias, conduction system abnormalities, and sudden death. Indeed, DCM is a common and largely irreversible form of heart muscle disease with an estimated prevalence of 1:2500 [7].

Patients with idiopathic dilated cardiomyopathy show either no enhancement or linear midmyocardial enhancement [13, 16]. This enhancement is explained by the presence of fibrosis. Patients with midmyocardial enhancement are at higher risk of sudden cardiac death and arrhythmias [23]. The differentiation between idiopathic dilated cardiomyopathy and ischemic dilated cardiomyopathy is important, as ischemic cardiomyopathy might be treated with revascularization and idiopathic disease might not. Late enhancement MRI will show subendocardial enhancement in patients with ischemic cardiomyopathy. Figure 1-3 shows that DCM with septal mid-wall fibrosis (left) and DCM without delayed enhancement (right) [24].

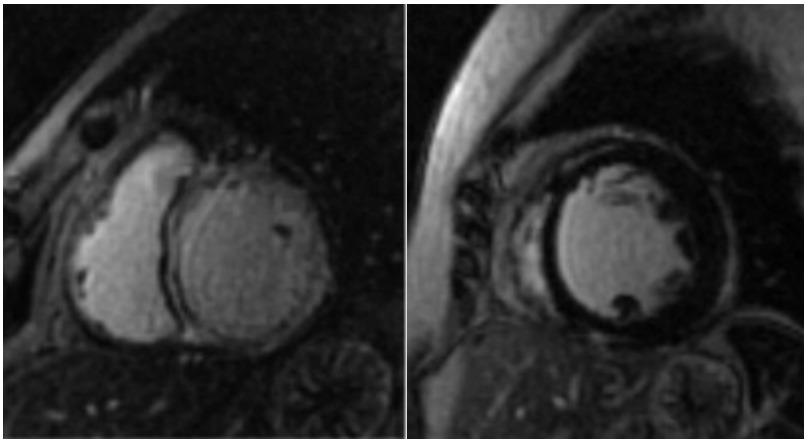

Figure 1-3:Short axis delayed enhancement images of a patient with DCM

1.2.4 Restrictive Cardiomyopathy

Restrictive cardiomyopathy is characterized by impaired ventricular filling and reduced diastolic volume of either or both ventricles with normal or near-normal systolic

function and wall thickness [6]. Hypertrophy is typically absent, although infiltrative disease (such as amyloidosis) and storage disease (such as Fabry disease) may cause an increase in left ventricular wall thickness. Systolic function usually remains normal, at least early in the disease. Increased interstitial fibrosis may be present. The most common cause of restrictive cardiomyopathy is amyloidosis. Amyloid deposits in the myocardium cause abnormal diastolic function with biatrial enlargement, concentric thickening of the left ventricle and reduced systolic function of usually both ventricles. Cardiac involvement in systemic amyloidosis occurs in up to 50% and has a poor prognosis with a median survival of 6 months [2, 16]. Restrictive cardiomyopathy is much less common than either dilated or hypertrophic cardiomyopathy. Symmetrical left ventricular hypertrophy with the classical 'zebra' pattern of DE is seen [25] on Figure 1-4.

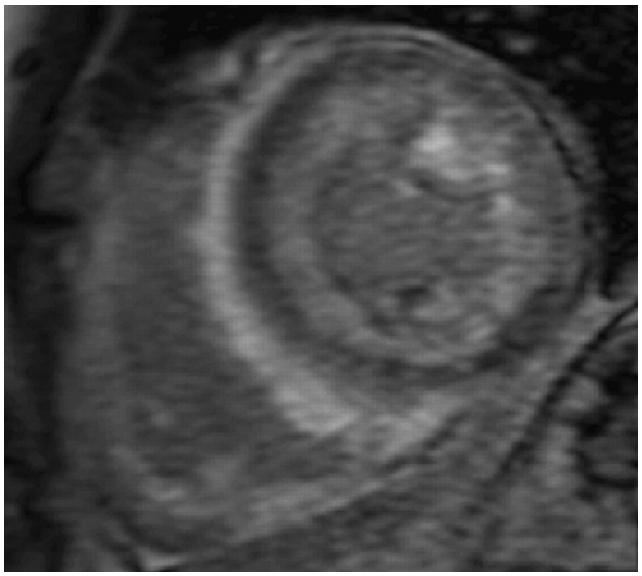

Figure 1-4:Short axis delayed enhancement images of a patient with amyloidosis

1.3 Detection and Quantification of Myocardial Fibrosis in Cardiomyopathies

Myocardial fibrosis, defined by a significant increase in the collagen volume fraction of myocardial tissue, is one of the most common histological features of the failing heart. It is caused by extracellular matrix (ECM) remodeling, which leads to increased myocardial stiffness, impaired cardiac diastolic and systolic function. Myocardial fibrosis is found in focal patterns following coronary territories in ischemic scar, but also as more diffuse myocardial fibrosis occurring in a variety of non-ischemic cardiomyopathies [26, 27].

1.3.1 Pathogenesis of Myocardial Fibrosis

Myocardial fibrosis is part of myocardial remodeling, which can be secondary to a wide range of pathologic conditions, including ischemia, pressure or volume overload, viral infection, or genetically mediated injury as in hypertrophic cardiomyopathy. Net collagen deposition is caused by an imbalance of its synthesis relative to degradation. Myocardial remodeling and fibrosis are associated with an imbalance between syntheses relative to degradation of the myocardial ECM. Several enzymes have been identified as potential mediators of myocardial ECM turnover. Among several groups of enzymes that mediate myocardial ECM turnover, the matrix metalloproteinases (MMPs) have a prominent role. The matrix metalloproteinases (MMPs) are endopeptidases, which have different substrates: MMP-1 and -13 are collagenases and MMP-2 and -9 gelatinases. The activity of the MMPs is regulated by a group of tissue inhibitors of matrix

metalloproteinase (TIMPs). The complex balance between MMPs and TIMPs, which determines ECM turnover and fibrosis, is only partially understood [28].

The distribution and characteristics of myocardial fibrosis varies according to the underlying pathology. There are three types of myocardial fibrosis: infiltrative interstitial fibrosis, interstitial reactive fibrosis and replacement fibrosis [26]. Infiltrative interstitial fibrosis is induced by the progressive deposit of insoluble proteins (amyloidosis) or glycosphingolipids (Anderson-Fabry disease) in the cardiac interstitium. Interstitial reactive fibrosis often distributes diffusively within the interstitium, but it can also be confined to the perivascular region. This type of fibrosis has a progressive onset and follows the increased collagen synthesis by myofibroblasts responding to different stimuli. It has mostly been described in hypertension and diabetes mellitus. It is also present in the aging heart, in idiopathic dilated cardiomyopathy, in left ventricular (LV) pressure-overload and volume-overload states induced by chronic aortic valve regurgitation and stenosis, and in the remote noninfarcted myocardium after infarction. Interstitial fibrosis is reversible under specific therapy and is the target for treatment. Therefore, there is clinical interest in its assessment for the management of patients with hypertension, diabetes, primary dilated cardiomyopathy, and valvular disease. Interstitial fibrosis and infiltrative fibrosis can develop further into replacement fibrosis in the later stages of disease. Under this condition, cellular damage and cardiomyocyte necrosis/apoptosis appear. This replacement fibrosis emerges once the myocyte integrity is damages, mainly consisting of type I collagen [26].

1.3.2 Endomyocardial Biopsies

Myocardial biopsy is the standard method to quantify diffuse fibrosis. This methodology enables qualitative macroscopic assessment after Masson Trichrome staining and quantitative absolute assessment of the collagen volume fraction in tissue samples by quantitative morphometry with picrosirius red, which specifically stains fibrillar collagen under polarized light. It allows absolute quantification of fibrosis in myocardial samples. However, this invasive technique is associated with a risk of significant morbidity and is prone to sampling error [29, 30]. Furthermore, fibrotic involvement of the whole LV cannot be determined [26, 29]. Development of a technique which can noninvasively quantify the diffusive myocardial fibrosis is highly critical and desirable, not just in terms of disease stratification but also in evaluating newer therapies aimed at reducing myocardial fibrosis in the treatment of heart failure.

1.3.3 Detection of Myocardial Fibrosis by DE MRI

DE MRI is a widely used and well-established powerful clinical technique used to evaluate ischemic and non-ischemic disease of the myocardium. Typically, a paramagnetic contrast agent (0.1–0.2 mmol/kg) is injected into a patient to temporarily distribute in the extravascular, extracellular, space (ve) in the myocardium [31]. Under the condition of replacement myocardial fibrosis, the myocytes have been replaced by collagen fiber and the loss of viable cardiac cells results in an increased ve where the contrast agent can accumulate in infarcted regions. The increased gadolinium concentration shortens the myocardial T1 value, making higher signal intensity in scar tissue visible when an inversion recovery sequence is set to null the normal myocardium. DE MRI was initially developed for characterization of myocardial damage after

myocardial infarction [32-35]. This technique has become the gold standard for noninvasive identification and quantification of myocardial scar tissue or replacement fibrosis. On delayed enhancement MR images, ischemic scar appears bright in a subendocardial or transmural pattern following the vascular distribution of the major coronary arteries. In nonischemic myocardial disease, the delayed enhancement usually shows non-vascular patterns and distributes diffusively, in a midwall distribution [35].

However, it is limited in its accuracy for absolute quantification of myocardial fibrosis, and the assessment of diffuse fibrosis is restricted by technical and physiopathological characteristics [26, 29]. First, with conventional DE MRI sequences, signal intensity is expressed on an arbitrary scale that differs between scans and thus, is unsuitable for direct signal quantification in cross-sectional or longitudinal comparisons. Second, image contrast is on the basis of the difference in signal intensity between fibrotic and “normal” myocardium, and such differences may not exist if the myocardial fibrosis is diffusive. Although a diffusely fibrotic myocardium would accumulate contrast agent in a similar way as in scarred myocardium, “normal” myocardium with diffuse fibrosis is “nulled” to highlight focal scar. Thus, diffuse myocardial fibrosis cannot be detected by DE MRI. As signal intensity of each single voxel is a mixture which cannot represent the difference between normal and abnormal myocardium. Collagen often diffusively deposits in non-ischemic cardiomyopathy. Such interstitial fibrosis commonly shows no regional scarring on delayed contrast enhancement images and is often missed by DE MRI.

Unlike fixed scar, diffuse myocardial fibrosis may be reversible and is a treatment target [29, 36]. Although regional fibrosis is easily imaged with CMRI there is no

noninvasive method for quantifying diffuse myocardial fibrosis. Currently, invasive biopsy is the only method to quantify diffuse fibrosis, which may cause significant morbidity and is prone to sampling error [29, 30]. Development of a technique which can noninvasively quantify the diffusive myocardial fibrosis is highly critical and desirable to stratify disease and evaluate newer therapies for the treatment of heart failure.

1.3.4 Potential of Myocardial T1 Mapping to Differentiate Myocardial Fibrosis

Diffuse myocardial fibrosis is a fundamental process in pathologic remodeling in cardiomyopathy and is postulated to cause increased cardiac stiffness and poor clinical outcomes. Evaluation of the presence and degree of myocardial interstitial fibrosis are important for diagnosis, treatment and prognosis of cardiac diseases. The degree of myocardial fibrosis is thought to play a critical role in determining a patient's risk for sudden cardiac death. However, DE MRI has limited ability to detect diffuse fibrosis and endomyocardial biopsy is invasive and prone to sampling error. Several attempts with T1 mapping techniques have been made to quantify the degree of myocardial fibrosis noninvasively [3, 29, 37].

Myocardial longitudinal relaxation time (T1) mapping is an emerging technique that could improve diagnostic accuracy of CMRI. Cardiac T1 mapping techniques enable quantification of myocardial signal directly on a standard scale. T1 time shows significant differences among different tissues and pathologies, and has shown great potential in characterizing myocardial fibrosis in the context of ischemia/infarction [38, 39] and infiltration (e.g. amyloidosis) [40]. T1 can be utilized to accentuate contrast

between normal and pathologic tissue, which is often based on differences in tissue microstructure. For example, in acute myocardial infarction, ischemic areas present edema and inflammation which results in a prolonged T1 value in these areas [38]. The elevation of T1 value could be considerable although the water content may only increase a few percent in ischemic regions [41]. Therefore T1 may be used to objectively measure changes in tissue properties and noninvasively characterize tissue as this parameter is very sensitive to the change of free water content in tissue and can differentiate the physical property of free water in tissue.

On T1 weighted images of the myocardium acquired for clinical purposes, focal differences in T1 signal are typically assessed qualitatively by visual inspection. For more precise, quantitative assessment, T1 times can be determined using multiple scans with varying T1-weighting. By calculating T1 values on a pixel-by-pixel basis, a parametric map can be reconstructed, in which pixel intensities correspond to T1 values [42]. Quantitative T1 maps can provide an absolute scale and may be advantageous over the traditional T1-weighted imaging, which is assessed using relative units and cannot be consistently compared between scans or patients [43]. T1 mapping provides sensitivity to the full range of T1, and could prescribe standardized cutoffs between “normal” and “affected” myocardium to eliminate inter- and intra-observer inconsistencies in delineation of the diseased myocardium. T1 mapping therefore is a powerful tool and holds great promises for characterizing myocardial tissue, with many potential clinical applications, such as differentiating the gray zone surrounding myocardial scar in myocardial infarction, quantifying fibrosis in patient with hypertrophic obstructive

cardiomyopathy (HOCM), and quantifying the concentrations of contrast agent within the tissue in dynamic contrast agent studies.

In vivo T1 quantification of the myocardium with modern MR systems is challenging because of cardiac and respiratory motion. A variety of dedicated cardiac pulse sequences have been developed for T1 mapping, which can be applied to characterization of diseased myocardial tissue [39, 42, 44-50]. However, the rapid cyclic cardiac motion is a significant challenge for image acquisition, validation of these techniques and comparison between techniques is still limited, requiring further evaluation of the accuracy of these techniques precontrast and postcontrast agent injection in various patient groups.

1.4 Physics of T1 Mapping Techniques

1.4.1 Spin-lattice Relaxation Time

1.4.1.1 Bloch Equation

By definition, MRI is a process involving the absorption and emission of energy by nuclei. For clinical imaging purposes, MRI exploits the magnetic property of hydrogen protons in human body as a diagnostic tool. The term “spin” is derived from the quantum mechanical description of MRI. In 1946, Felix Bloch described nuclear MR phenomenon with a set of equations [51]. Bloch assumed that the ensemble of spins

could be represented as a net nuclear magnetization (M) behaving according to the laws of classical electromagnetism. If the spins constituting M interact only with the external magnetic field (B), they will experience a torque given by the vector cross product (M×B) [51]. Because the torque of a system is equal to the time rate of change of its angular momentum, Bloch presented the motion of M could be a simple precession around B by the equation:

$$dM / dt = \gamma[M \times B] \tag{1.1}$$

If the spins interact with each other and their environment, M will not precess indefinitely around B, but will return to its original alignment with the main magnetic field (B) with the equilibrium magnitude M_0. To return back to the equilibrium state, the spin system must release its energy to the environment, which was termed as relaxation by Bloch. Two time constants (T1 and T2) were introduced by Bloch to account for the reestablishment of the thermal equilibrium of the nuclear magnetization following an RF pulse. T1 relaxation was assumed following first-order kinetics by Bloch. T1 describes the recovery of longitudinal magnetization (M_z). By adding the T1 effect to the original equation (1.1), the modified version of Bloch equation is shown:

$$dM_z / dt = (M_0 - M_z) / T1 \tag{1.2}$$

1.4.1.2 Causes of T1 Relaxation

T1 is also known as spin-lattice relaxation time and describes how fast the longitudinal magnetization recovers to its equilibrium. Regrowth of longitudinal relaxation requires a net transfer of energy from the nuclear spin system to its environment ("lattice") [51]. Because T1 relaxation requires an energy exchange, and

because all MR energy exchanges must be stimulated, T1 relaxation only can occur when a proton encounters another magnetic field fluctuating near the Larmor frequency. The source of this fluctuating field is typically another proton or electron, and the interaction is called a dipole-dipole interaction.

In order for a proton or electron to produce a fluctuating magnetic field to cause the T1 relaxation, the molecule in which it resides must be tumbling. The molecule must be rotating near the Larmor frequency to cause T1 relaxation efficiently. Thus, the tumbling rate of the molecule can affect the T1 relaxation time significantly. Small molecules (such as water) tumble too rapidly to cause effective T1 relaxation. However, when the water is in a partially bound or restricted state (as it is transiently bonded to proteins and other macromolecules), its tumbling rate may be slowed to a rate near to the Larmor frequency. Therefore, the T1 value of free water is very long and the "bound" water is much shorter [51].

The magnetic field strength affects the T1 of different molecules in a different way. For protons in highly mobile molecules (such as free water), the T1 value does not change very much because the fraction of protons precessing at Larmor frequency is not altered appreciably. For protons in molecules with intermediate or low mobility, the T1 will increase at higher field strength as the fraction of protons decreased significantly at higher Larmor frequency. For most biological tissues, there is an empirical equation suggesting that T1 increase approximately as $B^{1/3}$ [51].

1.4.2 T1 Mapping Techniques

Most currently available T1 mapping methods are based on one of 2 generic methods: variable flip angles and sampling the saturation or inversion recovery curve.

1.4.2.1 Variable Flip Angle Sequence

T1 maps can be generated using T1-weighted images with variable flip angles. The variable flip angle method can be performed with at least 2 gradient echo acquisitions with different flip angles. The radio-frequency pulse diagram of this method is shown in Figure 1-5. In this method, a pulse of tip angle θ is used to perturb the magnetization, which is then left to partially relax back to its thermal equilibrium during the short repetition time TR. As the excitation pulse angle is generally smaller than 90 degree, only a fraction of the thermal equilibrium magnetization is "tipped" into the transverse plane. This transverse magnetization is then a function of both the pulse flip angle and the amount of longitudinal relaxation that has occurred during the time interval TR [44]. An echo is formed through the use of gradients. The transverse relaxation during TE is described by the effective transverse relaxation time constant T2* and the signal intensity SI for any pixel is given by

$$\mathrm{SI} = CM_0 \exp(-\mathrm{TE}/\mathrm{T}_2^*) \frac{\sin\theta\left[1-\exp\left(-TR/T_1\right)\right]}{1-\cos\theta\exp\left(-TR/T_1\right)} \tag{1.3}$$

Where M_0 is the net magnetization at thermal equilibrium; C is a dimensionless constant representing the gain of the receiver circuit. In deriving Eq. (1-3), there are two assumptions: the pulses are applied along the same axis and a steady state has been reached. The variable flip angle method can be performed rapidly with 2 echo acquisitions, each with a different flip angle (θ_1, θ_2) and keeping other parameters same, which is called dual flip angle (DFA) method. Then T1 can be derived as

$$T_1 = -TR / \ln(m) \tag{1.4}$$

$$m = \frac{\frac{SI_1}{\sin\theta_1} - \frac{SI_2}{\sin\theta_2}}{\frac{SI_1}{\tan\theta_1} - \frac{SI_2}{\tan\theta_2}} \tag{1.5}$$

Several limitations still exist for this method such as significant errors from B0 inhomogeneity caused by not using 180 degree pulses to refocus the echo and B1 inhomogeneity from a difference between actual flip angle and the prescribed flip angle. The latter becomes more obvious at higher magnetic field strengths, such as 3T [47].

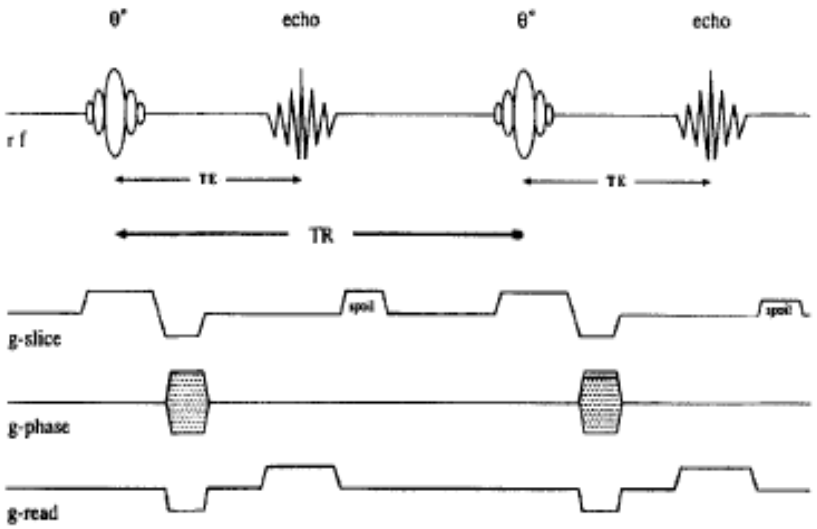

Figure 1-5: Variable flip angle, gradient-recalled echo pulse sequence

1.4.2.2 T1 Mapping with "Spin Echo" Inversion Recovery (IR- SE)

The pulse diagram for spin echo with an inversion prepulse is shown in Figure 1-6.This method uses an 180 degree pulse to invert the spins within the selected slice, then a 90 degree pulse to tip the recovered magnetization at inversion time (TI) [44] and another 180 degree pulse to form the spin echo. Sampling of the inversion recovery curve

needs to be repeated multiple times with different inversion times. The repetition time (TR) of the sequence must be long enough for the perturbed magnetization to return to its thermal equilibrium before the next 180 degree pulse. The signal intensity of the final image is proportional to the relaxed fraction of the magnetization during the TI:

$$\mathrm{SI} = CM_0 \exp(-\mathrm{TE}/\mathrm{T}_2)\left[1 - 2\exp\left(-TI/T_1\right)\right] \tag{1.6}$$

The first exponential term in Eq. (1.6) refers to the signal decay due to transverse relaxation during echo time (TE); the second exponential term accounts for T1 relaxation during inversion time interval TI. A T1 map can be generated by nonlinear, multi-parametric, least-squares fitting to Eq. (1.6) for each pixel of the image.

IR-SE sequence is the conventional method to estimate T1 because it is not affected by B0 inhomogeneity [44]. It has been known as the gold standard for computing T1 in vitro with good accuracy. However, the repetition time of the sequence must be very long, which means practically that the TR should be at least five times the longest T1 to achieve ~99% recovery of that matter. This requirement is difficult to be met in the imaging context, as the scanning time would be unacceptably long (eg, TR = 10 s in vivo). Furthermore, the imaging process needs to be repeated at least 5-6 times to acquire several images with different TIs while keeping other sequence parameters same. Therefore, a very long scanning time is necessary to ensure the acquisition of enough data points for calculating T1. A major problem encountered in making accurate T1maps based on a conventional IR-SE is the long acquisition time, making it unsuitable for routine clinical purposes. To reduce the acquisition time, turbo spin echo inversion recovery (IR-TSE) is usually used.

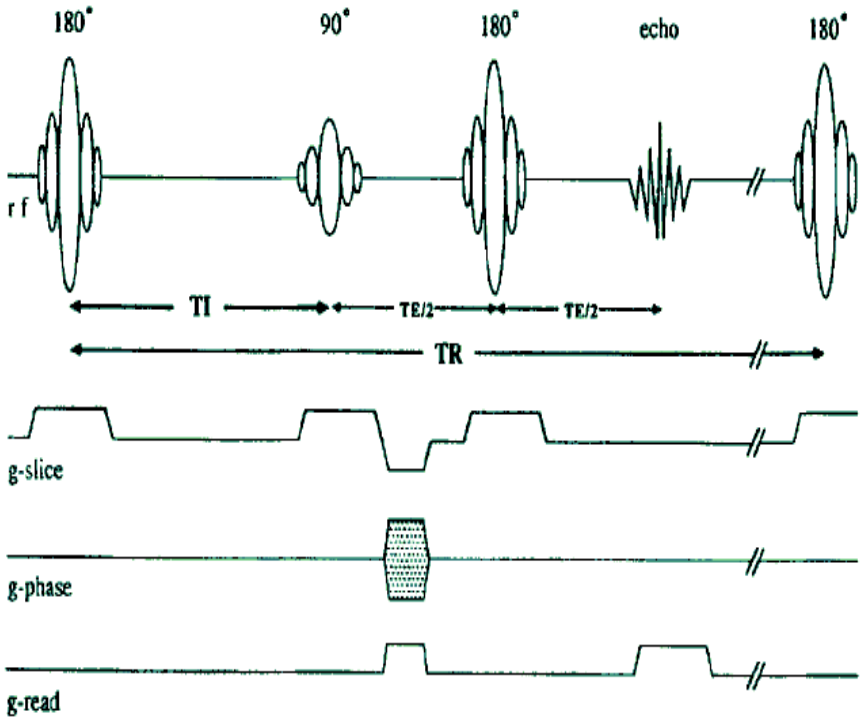

Figure 1-6: Inversion recovery spin-echo pulse sequence diagram

1.4.2.3 T1 Mapping with “Look Locker” Inversion Recovery (LL)

The LL method has been developed to accelerate the data acquisition process [52]. To calculate T1 more rapidly, it is desirable to sample the inversion recovery curve multiple times after a single inversion, rather than once as in the conventional IR-SE acquisition. The LL method employs a series of small flip angle excitation pulses after an inversion pulse to sample the inversion recovery curve with different TIs. To disturb the recovery curve minimally, usually low flip angles (7-15°) are used. The phase interval between two inversion pulses should be long enough to allow magnetization to return towards equilibrium by a sufficient pause. Look Locker has been used for cardiac applications because of its fast acquisition. Although LL has been shown to be highly

efficient, it suffers inaccuracies from the low flip angle RF pulses exciting the magnetization intermittently and not reaching the equilibrium magnetization before the next inversion pulse. Therefore, the T1 values are usually underestimated by the LL method. Another problem is the fact that the images with different TIs are acquired at different cardiac phases, therefore, manually tracking the myocardium among different phases are necessary. In addition, images are acquired continuously throughout the cardiac cycle and can be subject to cardiac motion [45]. Thus, a region of interest (ROI) would need to be drawn in a segment of the myocardium and moved along with the cardiac motion to calculate T1 in a focal area/lesion of the myocardium, which is still challenging in clinical practice. Thus, the current predominant cardiac application of Look Locker is to measure the global T1 in myocardium. This technique is not suited for measuring T1 in regionally accentuated lesions, which may not be visible in all images due to through-plane motion.

The measured data are assumed to follow a monoexponential recovery similar to IR-SE signal recovery. The difference is the recovery curve is determined by an apparent relaxation constant T1* (effective T1) not T1 in IR-SE:

$$M_Z = A - B \cdot \exp\left(-\frac{TI}{T_1^*}\right) \tag{1.7}$$

Three-parameter nonlinear curve fitting using a Levenberg-Marquardt algorithm is performed to calculate T1*. The true T1 is then calculated from T1* and the fitted parameters A and B according to T1 = T1* ((B/A) – 1).

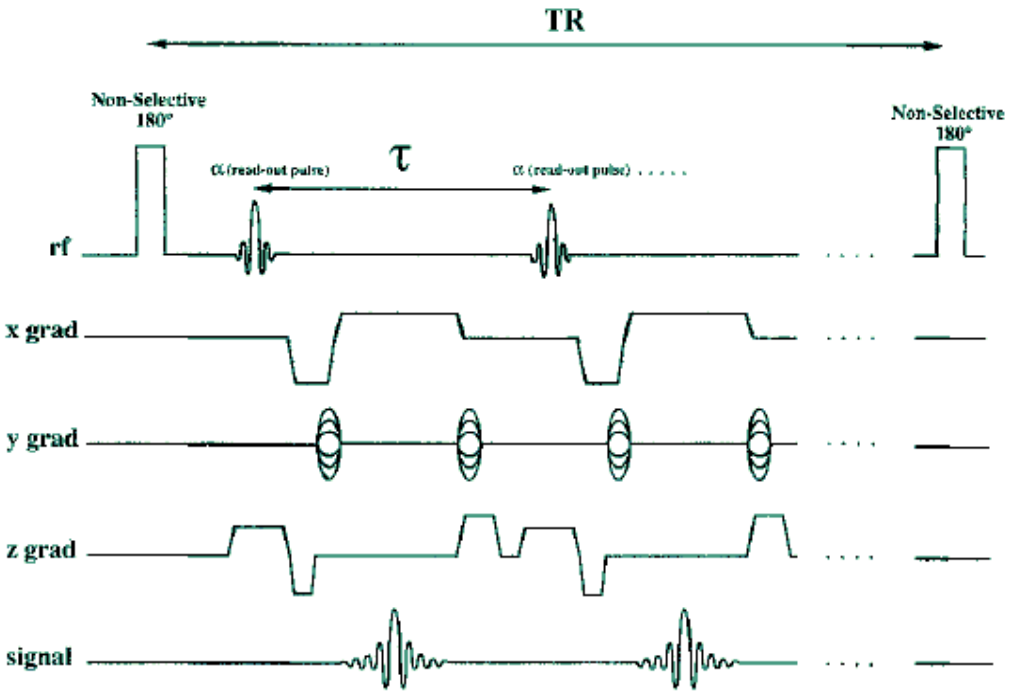

Figure 1-7: Look Locker inversion recovery pulse sequence diagram

1.4.2.4 T1 Mapping with Modified Look Locker Inversion Recovery (MOLLI)

MOLLI [45] was developed several years ago, and is a variant of LL. A series of images with different TIs from multiple LL experiments are acquired in a fixed acquisition window in the RR interval and then merged into one data set according to their inversion times. Three-parameter nonlinear curve fitting is performed and T1 is then calculated from T1* by using same equations used by LL method. The resulting T1 maps provide good T1 accuracy and high reproducibility [46] over a wide range of T1s that would cover the myocardial signal in both pre- and post-contrast agent injection acquisitions.

MOLLI requires the data for one image to be acquired in a single shot, which compensates for the cardiac motion problems of conventional LL at the expense of a

usually inferior spatial resolution. Moreover, a long cardiac acquisition window may result in the risk of cardiac motion artifacts. A very careful timing is necessary to place the acquisition window in a quiescent period of the cardiac cycle, usually at the end diastole phase.

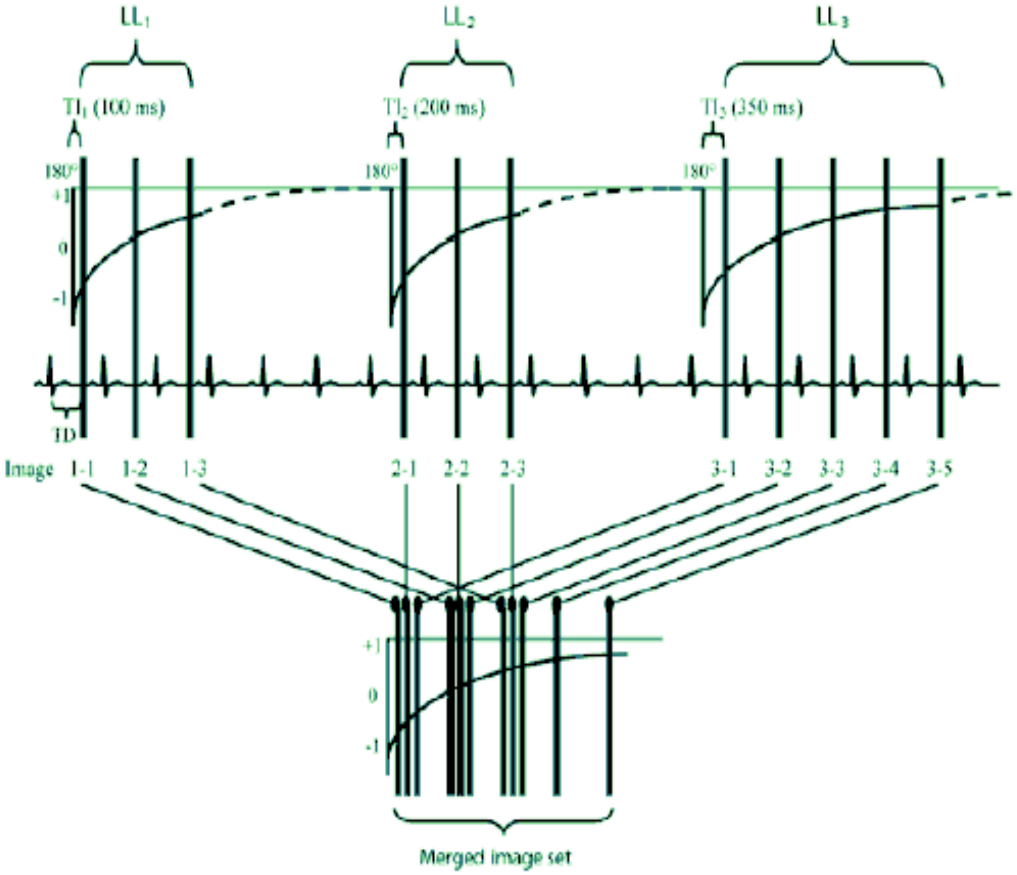

Figure 1-8: Modified Look Locker inversion recovery pulse sequence diagram

1.5 Objective and Organization of the Thesis Work

Specific remaining questions include evaluation of whether myocardial T1 values are constant throughout the entire cardiac cycle [53-55]. Such an assumption has been questioned by a recent study, which reported a cyclic variation in myocardial T1 in healthy subjects at 3T [47]. Furthermore, the accuracy of T1 mapping is confounded by several factors, such as the types of T1 mapping acquisition sequence, physiologic parameters, and presence of contrast material. Lastly, validation of T1 mapping for quantification of myocardial fibrosis is not sufficiently validated against histological analysis of myocardial biopsy. In this thesis work, we have made efforts to address these limitations.

The objective of this study is to evaluate T1 mapping techniques and develop an accurate and fast T1 mapping technique with B1 mapping correction at 3 T. Our specific aims were: 1) to evaluate whether there is clinically significant cyclic variation of myocardial T1 at 1.5 T; 2) to evaluate the accuracy of myocardial T1 measurements which may be dependent on characteristics of diseased tissues, heart rate, specific features of the T1 mapping methods, and the absolute T1 value, which is different between precontrast and postcontrast agent injection; 3) to evaluate whether the B1 mapping correction technique can improve the accuracy of T1 measurement with DFA at 3 T; 4) to correlate the noninvasive T1 mapping quantification of myocardial fibrosis with the invasive biopsy analysis.

The fulfillment of these specific aims are detailed in the following chapters (2~5). The main work of each chapter is outlined as follows: In Chapter 2, cyclic variation of myocardial T1 value was evaluated by imaging 10 volunteers and 20 patients with normal left ventricular (LV) function with MOLLI at 1.5 T. The T1 maps were obtained

at end-systole (ES), mid-diastole (MD), and end-diastole (ED) during the cardiac cycle to compare whether T1 changes at different cardiac time points.

In Chapter 3, we implemented and tested a fast T1 mapping method: dual flip angles (DFA) sequence with B1 correction at 3 T. The available sequence on our MRI scanner only allows acquiring one gradient echo image in one acquisition with a single flip angle. The sequence is changed to acquire two images with two different flip angles respectively in single acquisition using pulse programming. The T1 measurements with 2D and 3D DFA sequences were performed and the results showed that the single acquisition 3D DFA with B1 correction produced significant improvement in measuring a wide range of T1 values compared with no B1 correction at 3 T. The 3D DFA with B1 correction was then compared with the T1 measurements with the gold standard method (IR-TSE), MOLLI and LL sequences.

In Chapter 4, Look Locker (LL) and modified Look Locker inversion recovery (MOLLI) sequences for T1 mapping were compared in phantoms and in controls with normal LV function, patients with HCM, and those with ICM. Based on the results from Chapter 2, T1 value is consistent during the cardiac cycle. Therefore, only T1-weighted images at end-diastole were acquired to minimize artifacts from the cardiac motion because end-diastole is the most quiescent phase during the cardiac cycle. Phantoms were imaged with 3 T1 mapping techniques (IR-TSE as reference, LL, and MOLLI). A total of 5 controls, 16 patients with HCM, and 5 patients with ICM were imaged at 1.5 T using LL and MOLLI at 2 LV short-axis levels. T1 measurements were performed before and after contrast injection with MOLLI and LL.

In Chapter 5, histological analyses were correlated with T1 mapping results in patients with HCM. T1 measurements with MOLLI sequence were performed precontrast and postcontrast when the patients underwent MRI examinations. Myocardial ECV were calculated from noninvasive T1 measurements. Myocardial myectomy specimens were taken from the same patients during surgery. Collagen volume fraction was then determined from histological analysis of myocardial biopsies. The ECV determined from noninvasive T1 mapping technique was correlated with the collagen volume fraction from invasive method.

Further, several future research directions were suggested based on the current research in Chapter 6.

CHAPTER II

CYCLIC VARIATION IN MYOCARDIAL T1 RELAXATION TIME

2.1 Introduction

Spin-lattice (or T1) relaxation time has shown great potential in characterizing myocardial fibrosis in the context of ischemia/infarction [38, 39] and infiltration (eg amyloidosis) [40]. “Spin echo” inversion recovery (IR-SE) is the gold-standard for computing T1 in vitro [44], but long acquisition times limit its routine use for clinical cardiac applications.

A variety of methods have been developed to accelerate the image acquisition speed. Most of these methods are based on one of two generic methods using multiple T1-weighted scans: variable flip angle [47], and sampling of either saturation [44] or inversion recovery curves [44, 45, 52]. The variable flip angle method can be performed rapidly, but is subject to significant errors from B1 inhomogeneity [47]. The “Look Locker” (LL) inversion recovery method has been applied to myocardial T1 mapping by accelerating the data acquisition process [31]. With the LL method, manually tracking the

myocardium is needed to calculate T1 because the images are acquired at different cardiac phases. Furthermore, through-plane motion may compromise the accuracy of the T1 map, especially for small structures, such as myocardial lesions. Modified Look Locker inversion recovery (MOLLI) [45] is a variant of LL by improving the acquisition process to allow a series of images be acquired in a fixed acquisition window between two R-waves showed in the electrocardiogram (ECG) (RR interval).

In most T1 mapping applications, T1 maps are typically created from images acquired either at end-diastole, to minimize cardiac motion artifacts (eg MOLLI), or throughout the cardiac cycle, to reduce scan time (eg LL). There is an underlying assumption of these methods that the myocardial T1 value is constant throughout the cardiac cycle [9-11]. However, this assumption has been questioned in a recent study [5], which reported cyclic variation of myocardial T1 at 3 T of 70% in the septum and 43% in the lateral wall from end-diastole (ED) to end-systole (ES) in healthy volunteers. Myocardial blood volume (MBV) variation during the cardiac cycle was considered to contribute to the change of T1. In this study, the dual flip angle technique was used to generate cine myocardial T1 maps. The distribution of T1 was concluded to be heterogeneous throughout the cardiac cycle and could cause large variation in the mean T1. Therefore, plots of mean T1 are not optimal for comparison between subjects. However, the T1 estimation obtained by this dual flip angle technique is very sensitive to the amplitude of the RF field (B1) inhomogeneity, and the geometry and electrical properties of the human body, which can lead to errors in T1 value calculation. This error is more obvious at higher magnetic field strengths, as in this study performed at 3T. However, the MBV is only about 6% to 15% of the left ventricular (LV) mass, indicating

that the change of T1 value from MBV may not be pronounced enough to be detected, as the percentage of the change is within the standard deviation of the technique.

Development and optimization of clinical T1 mapping sequences to accurately calculate T1 values of the heart are of particular importance for the diagnosis of myocardial diseases. Therefore, it is important to evaluate T1 values at different points in the cardiac cycle to determine whether similar cyclic T1 variation is seen at 1.5T, which is more widely used in routine clinical diagnosis. T1 values were evaluated at different points in the cardiac cycle to determine whether similar cyclic T1 variation is seen at 1.5T using MOLLI, and the possible effect on the T1 mapping methods that assume constant myocardial T1 during the cardiac cycle.

2.2 Materials and Methods

2.2.1 Subjects Population

This was a prospective study in subjects without known heart disease. After Institutional Review Board approval and written informed consent was obtained from all study subjects, 10 human volunteers (n = 10, 5M/5F, age 30 ± 8 years), and 20 patients (n = 20, 16M/4F, age 52 ± 16 years) with normal left ventricular function were recruited in the study. Exclusion criteria will include pregnant females; age less than 18 years, as well as absolute contraindications to MRI (eg, pacemaker).

2.2.2 Imaging Procedure

Subjects underwent MRI examinations using a clinical 1.5 T scanner (Achieva XR, Philips Medical Systems, Best, NL). Subjects were first screened for MRI eligibility; all subjects completed the standard Cleveland Clinic Hospital System (CCHS) Safety Screening Form for MRI Patients, which is given to all patients referred clinically for MRI. ECG leads were placed on each subject's chest in order to synchronize image acquisition with heart motion. At the beginning of all studies, long-axis cine images (vector ECG-gated steady-state free precession; repetition time ms/echo time ms, 3.0/1.5; matrix, 144 ×150; slice thickness, 10 mm; 30 phases) were acquired. Then, MOLLI sequences were performed at end-systole (ES), mid-diastole (MD), and end-diastole (ED) of the cardiac cycle at two short-axis levels (mid-cavity, apical-cavity). The MOLLI sequence requires multiple single-shot scans within one breath hold (approximately 12-20 seconds). The MOLLI pulse sequence consists of three successive inversion-recovery prepared ECG-triggered LL experiments (LL1, LL2, and LL3), which were carried out with three, three, and five single-shot readouts, as described previously [45]. Undisturbed magnetization recovery was allowed for about 3 seconds between each LL experiment, with variation dependent on the subjects' heart rate, and the reconstruction and preparation time of the MR scanner. Each of the three LL experiments started with a non-slice-selective adiabatic 180° pulse, and then the first single-shot readout was performed at inversion time (LL1 ≈ 40 ms, LL2 ≈ 200 ms, and LL3 ≈ 350 ms) and at trigger delay time (TD) after the previous R-wave. Subsequent images were acquired at time TD after every R-wave in consecutive heartbeats, until the final number of images for each LL experiment was acquired, resulting in a set of 11 source images with their different

effective inversion times. Data acquisition consisted of a single-slice, single-shot, turbo-field echo (TFE) pulse sequence combined with SENSE with a reduction factor of 2, number of lines of k-space (TFE factor) = 49, dummy acquisitions = 13, partial Fourier acquisition, flip angle = 10°, repetition time (TR) = 3.9 ms, echo time (TE) = 1.95 ms, field of view (FOV) = 380 ×342 mm^2, matrix = 240 ×151, measured pixel size = 1.58 ×2.26 mm^2, slice thickness = 8 mm, and acquisition window = 191.1 ms.

2.2.3 Data Analysis

By reordering these source images according to their inversion time and merging them into one data set, T1 values can be computed for every pixel by three-parameter nonlinear curve fitting using a Levenberg-Marquardt algorithm $y = A - B \exp(-t/T1^*)$. T1 is then calculated from effective T1 (T1*) by $T1 = T1^* ((B/A) - 1)$ [45]. Reconstruction of T1 maps from MOLLI was performed off-line using software written in Matlab (The MathWorks, Natick, MA, USA). The T1 values at different time points during the cardiac cycle were also compared with each other.

A region of interest (ROI) was manually drawn in 1 image, copied to the remaining images. Curve fitting was performed using signal intensity from manually drawn ROI using Matlab to obtain the mean T1 value within the corresponding ROIs. Precontrast myocardial T1 values of two short-axis levels were compared to assess agreement of T1 values during the cardiac cycle. Regional myocardial T1 properties were further evaluated using an ROI-based approach in every subject. Four ROIs in the mid-

myocardium (septal, inferior, lateral, and anterior) were drawn according to Figure 2-1 to fit the mean signal intensity of each ROI.

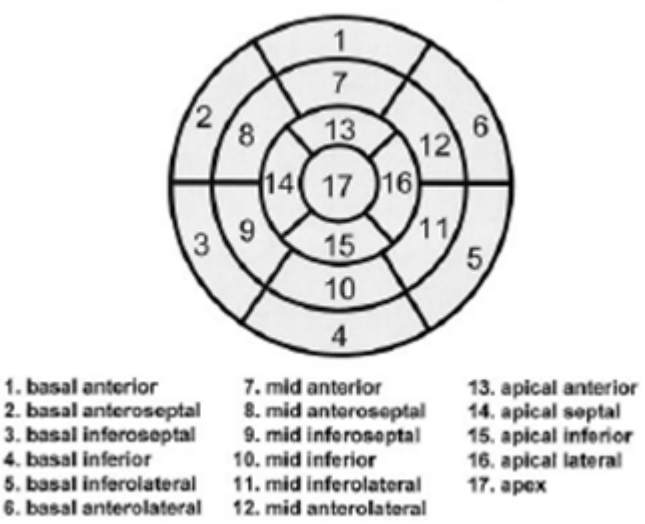

Figure 2-1: Left ventricular segmentation [56]

2.2.4 Statistical Analysis

Analysis of variance (ANOVA) was used to assess statistical significance of differences between time points and regions including myocardial T1 values from all subjects. All results are expressed as mean T1 values ± standard deviations (SD). $P<0.05$ was considered statistically significant.

For the primary analysis, the mean of the myocardial T1 values across the four locations was used in the statistical analysis. The distribution of the mean myocardial T1 values was examined and found to follow a normal distribution reasonably well. A one-way repeated measures ANOVA was performed for both the middle and apical levels. The null hypothesis was that the T1 values are the same across the three time points; the

alternative hypothesis was that the T1 values are not the same. A significance level of 0.05 was applied. If the null hypothesis was rejected, then a paired t-test was used to examine the differences between each of the time points. In secondary analysis, repeated measures ANOVA were performed for each location around the left ventricle: septal, inferior, lateral, and anterior wall. A significance level of 0.05 was applied.

2.3 Results

T1 maps were generated using software written in Matlab (The MathWorks, Natick, MA, USA) calculating T1 value pixel-wisely. Figure 2-2 shows representative T1 maps from a volunteer at 3 time points in the cardiac cycle. The trigger delays were 285 ms (ES, top), 520 ms (MD, middle) and 756 ms (ED, bottom). The color of myocardium on each T1 map is similar. Visually, there is no different among cardiac phases. Regional myocardial T1 values were further evaluated using ROI-based approach in healthy volunteers. Four ROIs in the septal, inferior, lateral, and anterior wall of the heart were drawn to fit the mean signal intensity of each ROI. The curve fitting examples of four regions of interest were shown in Figure 2-3.

A linear regression analysis was performed for precontrast T1 values and heart rate, as shown in Figure 2-4, with $T1 = -3.23 \times HR + 1160.40$ and $R^2=0.62$. Table 2-1 shows global T1 values obtained for the 10 volunteers before and after application of the correction factors. Mean T1 value before correction was $T1 = 961.2 \pm 36.3$ ms; after heart rate normalization to 60 bpm, $T1 = 966.6 \pm 22.4$ ms. Correction for heart rate was then

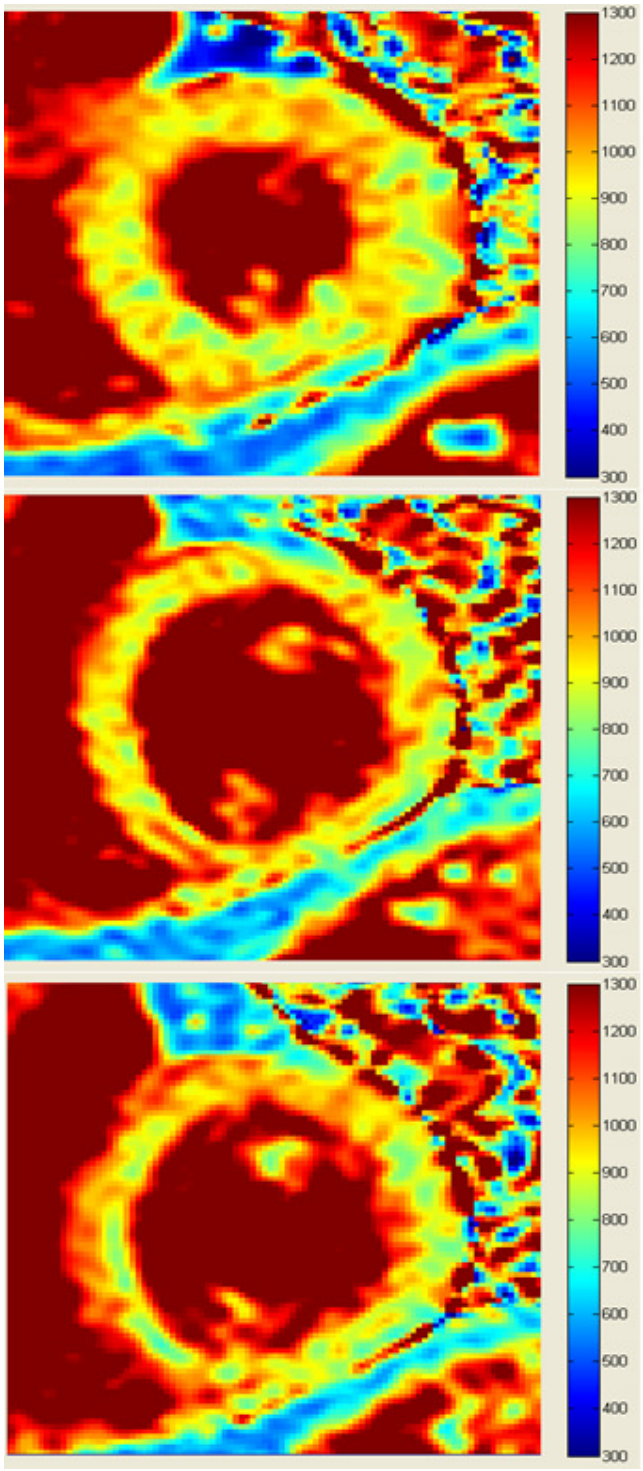

Figure 2-2:T1 maps at 3 points in the cardiac cycle from a volunteer

applied to each subject based on the linear fit. The range of uncorrected T1 values for all ROIs was 791-1034 ms in this study. After heart rate correction, the range of T1 values

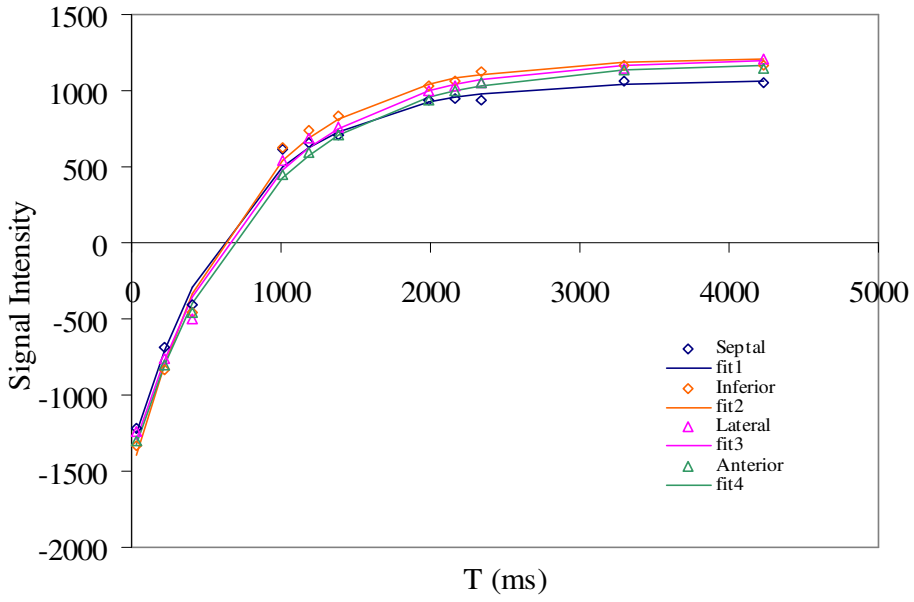

Figure 2-3: Signal intensities for each ROI were fitted to obtain the myocardial T1

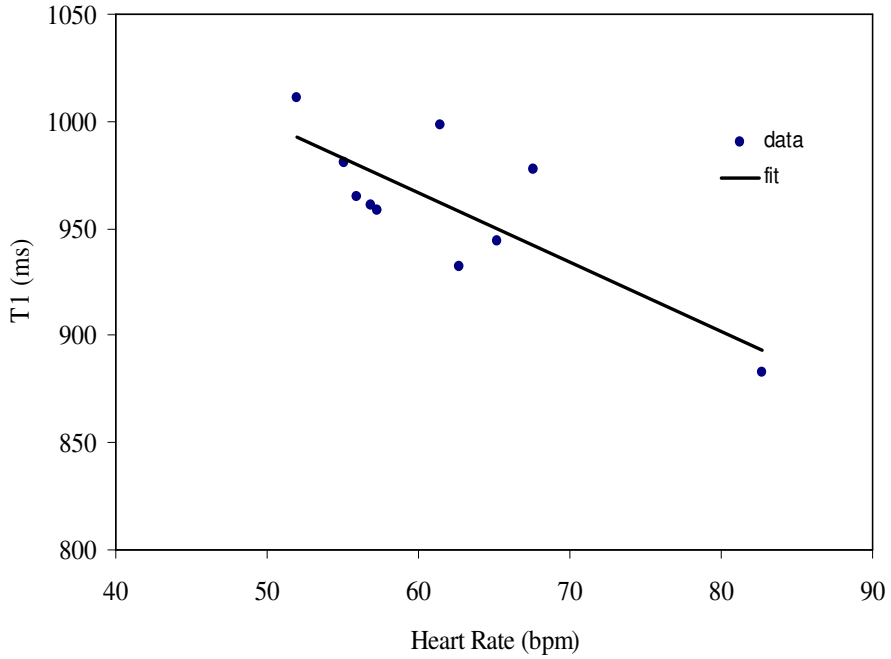

Figure 2-4:Myocardial T1 values of 10 healthy volunteers showed a negative linear relationship to heart rate (R^2=0.62)

was 859-1054 ms. Our results are consistent with previously reported T1 values measured at end diastole (862-1105 ms) [46] using the MOLLI sequence.

Table 2-1: Precontrast T1 values (ms) for 10 normal volunteers before and after correction for variation in heart rate

Volunteer number	**Heart rate (bpm)**	**T1 uncorrected (ms)**	**T1 corrected (ms)**
1	61	998	1003
2	63	932	941
3	65	944	961
4	57	961	951
5	52	1011	986
6	83	882	956
7	56	965	952
8	68	978	1002
9	57	958	948
10	55	981	965
Mean (SD)		961 (36)	967 (22)

Table 2-2 summarizes the means and standard deviations of the T1 values at each time point at the middle and apical levels. As shown in Figure 2-5, the T1 values differed significantly with cardiac cycle phase (P = 0.017) at the middle level. Specifically, the T1 values at diastole are greater than at end-systole (P = 0.037; 95% CI for the difference in T1 values is [0.9, 26.7]), and the T1 values at end-diastole are greater than at end-systole (P = 0.004; 95% CI is [9.1, 39.0]). The T1 values at diastole and end-diastole do not differ significantly (P = 0.139). For the apical level, the T1 values differ significantly over time (P = 0.001) as shown in Figure 2-5. Specifically, the T1 values at diastole are

greater than at end-systole (P = 0.048; 95% CI is [0.1, 31.2]), and the T1 values at end-diastole are greater than at end-systole (P < 0.001; 95% CI is [14.0, 38.9]). The T1 values at diastole and end-diastole do not differ significantly (P = 0.108).

Table 2-2: Mean (SD) of myocardial T1 values at three time points

	Diastole	**End-diastole**	**End-systole**
Middle level	946.8 (35.9)	956.5 (42.4)	933.0 (32.6)
Apical level	950.4 (42.4)	961.2 (38.7)	934.8 (42.4)

Comparison of regional T1 values at each ROI for each time point for both the middle and apical levels was shown in Figure 2-6. Table 2-3 summarizes the means and standard deviations of the T1 values at each location for each time point for both the middle and apical levels. At septum, the T1 values do not differ significantly over time (P = 0.126) for the middle level and the T1 values differ significantly over time (P = 0.014) for the apical level. Specifically, the T1 values at end-diastole are greater than at end-systole (P = 0.005; 95% CI is [8.2, 42.6]). The T1 values at diastole and end-diastole are not significantly different (P = 0.055), and the T1 values at diastole and end-systole are similar (P = 0.840). At inferior wall, the T1 values do not differ significantly over time (P = 0.122) for the middle level and the T1 values differ significantly over time (P = 0.016) for the apical level. Specifically, the T1 values at end-diastole are greater than at end-systole (P = 0.009; 95% CI is [9.2, 60.2]) and greater than at diastole (P = 0.017; 05% CI is [3.5, 33.3]). The T1 values at diastole and end-systole are similar (P = 0.167). At lateral wall, the T1 values do not differ significantly over time (P = 0.169) for the middle level and the T1 values do not differ significantly over time (P = 0.095) for the apical level. At anterior wall the T1 values do not differ significantly over time (P =

0.072) for the middle level and the T1 values do not differ significantly over time (P = 0.197) for the apical level.

Comparisons between the four locations, there are no differences in the T1 values at the middle level at diastole (P = 0.837), end-diastole (P = 0.778), or end-systole (P = 0.690). Similarly, there are no differences in the T1 values at the apical level at diastole (P = 0.611), end-diastole (P = 0.206), or end-systole (P = 0.635).

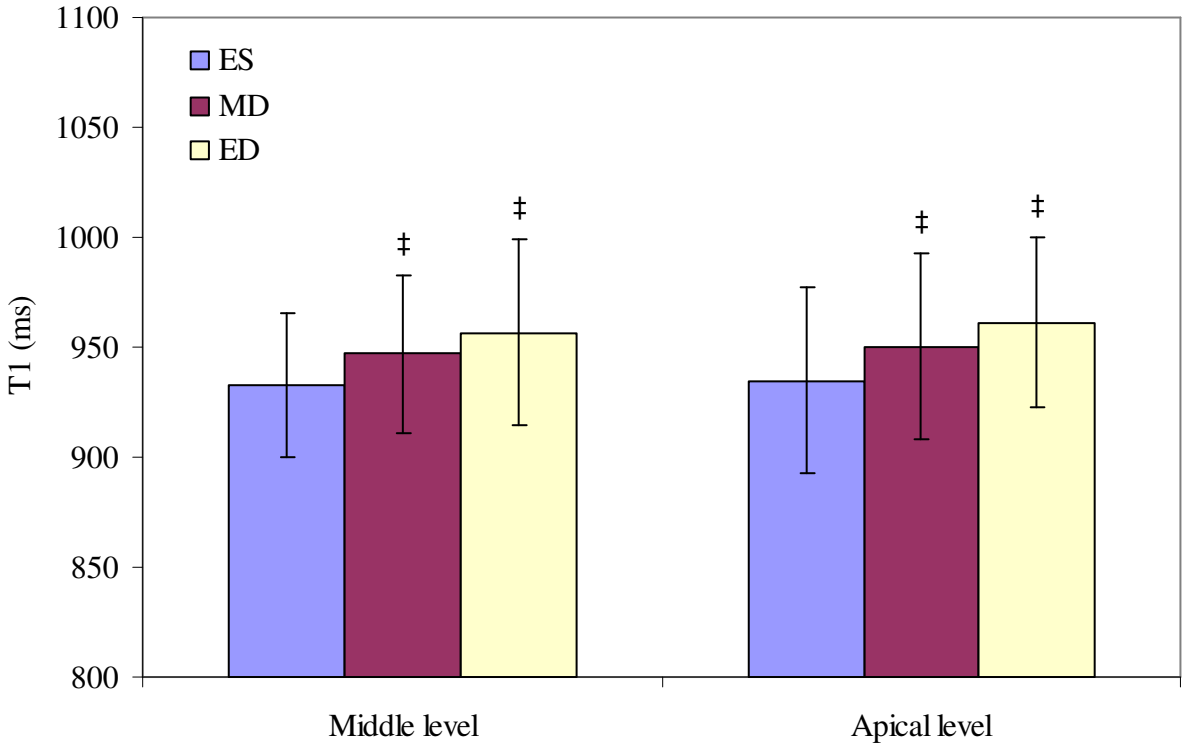

Figure 2-5:Comparison of T1 values at 3 different time points at middle and apical levels.

‡=Statistical significance of changes between time points (P<0.05 vs ES)

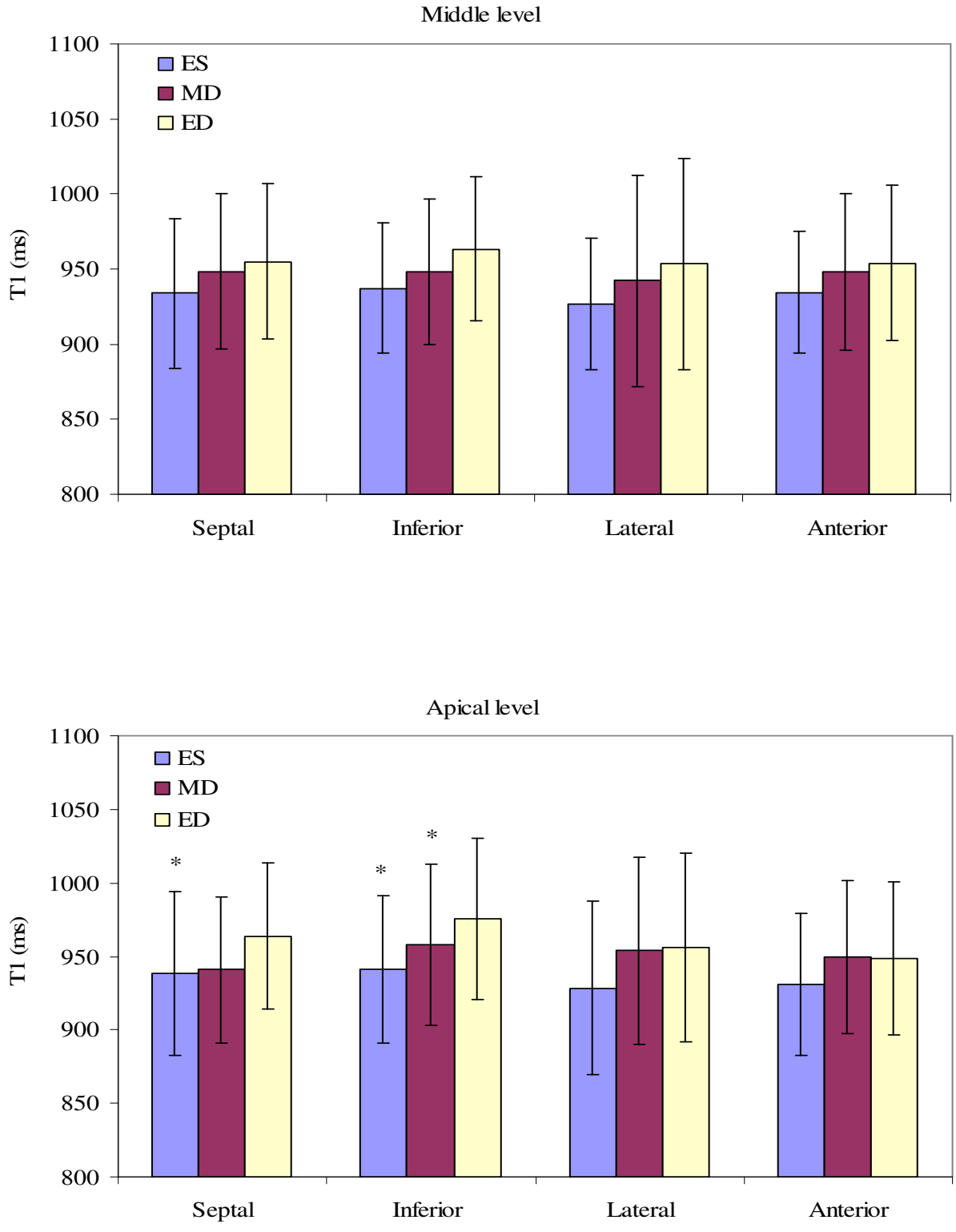

Figure 2-6:Comparison of regional T1 values at 3 different time points at middle and apical levels. *=Statistical significance of changes between time points (P<0.05 vs ED)

Table 2-3: Mean (SD) of myocardial T1 values at three time points by location

	Diastole	**End-diastole**	**End-systole**
Middle level			
Septum	948.4 (61.0)	955.1 (51.9)	933.9 (50.1)
Inferior	948.5 (49.9)	963.5 (48.4)	937.1 (43.3)
Lateral	942.3 (43.0)	953.5 (70.4)	926.5 (43.5)
Anterior	948.2 (42.7)	954.2 (52.1)	934.6 (40.8)
Apical level			
Septum	940.8 (56.9)	963.7 (49.6)	938.3 (56.0)
Inferior	957.4 (53.1)	975.9 (54.8)	941.2 (50.4)
Lateral	953.7 (69.2)	956.3 (64.0)	928.6 (59.3)
Anterior	949.4 (49.7)	948.9 (52.1)	930.9 (48.4)

2.4 Discussion

In this study, myocardial T1 values from 10 volunteers and 20 patients were measured using MOLLI at three different time points of the cardiac cycle. At both the middle and apical levels, end-systolic T1 values differed significantly from mid-diastole and end-diastole. However, the T1 values at mid-diastole and end-diastole did not differ significantly from one another. Also, the largest difference between time points was approximately 39 ms, which is within the standard deviation of the T1 mapping technique in use. Furthermore, our results are similar to those of a recent study [46] which reported T1 values from 862-1105 ms using MOLLI.

Although we found that differences in T1 were statistically significant among time points, we do not feel these differences are clinically significant. For instance, some of the variation in our results could be explained by increased cardiac motion at end

systole relative to mid-diastole and end-diastole. Overall, these results demonstrate that T1 values are approximately constant throughout the cardiac cycle at 1.5 T; they suggest that the magnetic properties of myocardial tissue do not change significantly throughout the cardiac cycle, and T1 quantification methods such as Look Locker should be valid at 1.5 T.

A recent study examined the effect of cardiac cycle on myocardial T1 at 3 T using MOLLI [57]. Their results showed that the precontrast T1 values were 1% longer (approximately 15 ms) at diastole than systole at 3 T. Similar to the current study, this difference, although statistically significant, was not clinically significant. Furthermore, this previous study was performed at different field strength (3 T) from the current study, using a balanced steady-state free precession technique, which could explain the modest differences in results.

Our results disagree with the large variation in myocardial T1 at 3 T observed by Wansapura et al [47], who reported a drop in T1 during systole of 70% in the septum and 43% in the lateral wall. However, their study relied on a dual flip angle acquisition technique, and the variations they observed may result from the inflow of unsaturated spins during the contractile heart motion. Wansapura et al [47] concluded that changes in myocardial blood volume during the cardiac cycle contributed to the cyclic T1 variation they observed. However, myocardial blood volume is only about 6%-15% of the left ventricular mass. The change of T1 value from MBV may not be pronounced enough to be detected, as the percentage of the change is within the standard deviation of the technique. The relationship between tissue volume and vascular volume fluctuations is complex, since the capillary walls are highly permeable to water. According the

physiology of myocardial blood flow and previous studies, systolic reduction in myocardial volume [58-61] has been explained as a result of blood that is squeezed out of the coronary vasculature within the myocardium. The myocardial volume decreased during systole and reached the minimum near aortic valve closure or end systole (ES). The changes in myocardial volume during the cardiac cycle have not attracted much attention, primarily because the myocardial blood flow measured by microsphere techniques [62] would predict systolic myocardial volume reduction on the order of only 1% in canine using a motion-encoding MRI technique [60]. Toyota et al [63] observed in vascular casts of rat hearts a vascular volume change equivalent to 7–8% of the tissue volume between systole and diastole. These studies reflect the decrease of myocardium volume at ES; however, they do not seem significant enough to cause a 43%-70% drop of T1 values. In contrast, in both the current study and that of Kawel et al [57], the decrease in T1 from diastole to systole does seem to correspond with these reported systolic changes in myocardial blood volume. There is an animal study using three-dimensional VFA T1 mapping of the mouse heart showed that T1 values ate end-diastole were almost equal to those at end-systole at 9.4 T preclinical MRI scanner [64].

The big difference of T1 values across the regions of interest was found by Wansapura et al [47], concluding this is caused by the larger difference in MBV in the septum between ED and ES compared to that in the lateral wall. However, there was no such big difference in our study. In the study of Wansapura et al [47], the dual flip angle technique was employed. The dual flip angle technique allows for fast imaging, but is prone to errors in absolute T1 measurements caused by B0 and B1 inhomogeneity, especially at higher field strength, such as 3 T. In addition, the geometry and electrical

properties of the human body can lead to errors in T1 with this technique. For instance, Sung et al [65] reported B1 field inhomogeneity over the LV yielded a flip angle distribution of 34º to 63º across the LV for a nominal flip angle of 60º, with the average flip angle about 20% lower than 60º. Although the impact on T1 accuracy is known, B1 correction of measured T1 was not employed by Wansapura et al [47].

In contrast to the dual flip angle technique, MOLLI is an established method to measure the myocardial T1 and has been more widely used in both 1.5 T and 3 T studies [42, 46, 48, 50, 66]. The normal range of human myocardial T1 values has been established with MOLLI [48] and our results using MOLLI agree well with the previous studies of normal myocardial T1 values [46]; also, we found a negative relationship between T1 values and heart rate, similar to previous study [31]. Although the correction equation we obtained differs from previous studies [31, 46], this may result from numerical differences in the source data due to differences in sample size and patient population.

Development and optimization of clinical myocardial T1 mapping sequences are of particular importance for the diagnosis of myocardial diseases. Such significance warrants further investigation of the myocardial T1 mapping at 3 T because CMR at 3 T is a rapidly maturing field and becomes more widely used. However, cardiac MR at 3 T is challenged by the increased inhomogeneity of static magnetic field B0 and transmit radiofrequency (RF) field B1. B0- and B1- map will be necessary to accurately measure the myocardial T1 values at 3 T. SDAM B1-map [67] has been further developed to simultaneously acquire B0- and B1- map in the heart within one breath-hold, which

allows the future study of cyclic variation of myocardial T1 using dual flip angle techniques with B1 map correction at 3 T and to be compared with MOLLI.

2.5 Conclusion

The MOLLI sequence was used to study the cyclic variation of myocardial T1 at 1.5 T. Although the statistically significant decrease from the diastole to systole may be caused by myocardial blood volume decrease, the decrease is not thought to be clinically significant, as the difference is within the standard deviation of the technique. Furthermore, there were no significant differences among different regions of interest of myocardial T1 values. Therefore, the magnetic properties of myocardium are fairly constant, and the accuracy of Look Locker technique should not be significantly affected from the consistently acquiring images during the cardiac cycle.

Our study is limited to 1.5 T scanner and precontrast myocardial T1 value obtained with MOLLI. The significant drop of T1 value from ED to ES in the 3 T study was performed with dual flip angle, which is a different technique from our study. This dual flip angle technique will be studied in next chapter to see its difference from MOLLI. In addition, although the same cardiac phase was set to obtain the MOLLI images in our study, the difference may occur among the images because every heart beat is different, especially when the subject has unstable cardiac frequency.

CHAPTER III

DUAL FLIP ANGLE WITH B1 MAPPING CORRECTION

3.1 Introduction

Longitudinal relaxation time, or T1, is one of the fundamental physical variables governing image contrast in magnetic resonance imaging [6]. T1 mapping is of interest in a range of areas including dynamic contrast enhanced studies of tissue perfusion, diagnosis of neurological diseases, and quantitative imaging for multi-site studies. As a result, quantitative mapping of T1 has a long history, and a wide variety of methods have been developed [68]. Comparing with those techniques based on saturation or inversion recovery techniques, variable flip angle (VFA) method can measure T1 relaxation times rapidly and accurately from a set of two or more spoiled gradient recalled-echo (SPGR) images. Therefore, VFA method is a promising method to meet the clinical requirement of time frame [69, 70]. The accuracy of this method has been tested to be similar to that achieved with conventional and accelerated techniques but with a significant reduction in imaging time [71]. Furthermore, compared to spin echo techniques this approach has the

advantage of low power deposition. The VFA spoiled gradient recalled echo approach was shown to be a practical alternative to conventional methods, providing better speed [70]. The simplest and fastest T1 measurement method is the dual flip angle technique.

A dominant source of error in the VFA approach is inaccurate knowledge of the flip angles due to transmit field B1 inhomogeneity. The method is known to be sensitive to transmit field (B1) inhomogeneity and can result in significant systematic errors in T1 estimates, especially at high field strengths. Although the impact on T1 accuracy is known [72], correction of measured T1 has been reported in only a few studies [73, 74]. Due to the complexity and long scan time requirements of mapping the B1 field, the B1 map is difficult to be acquired for cardiac imaging. Ideally, an angle set will yield the highest and most uniform precision across large T1 ranges while maintaining accuracy. To optimize the VFA method for both accuracy and precision, the influence of imperfect transmit fields and selection of flip angles should be considered [70]. The main challenge is to improve the accuracy of the VFA approach without sacrificing speed. To achieve optimal accuracy in VFA measurements requires careful selection of pulse sequence parameters and precise knowledge of the spatial variation in RF flip angle which can be obtained by B1 mapping. However, in only a few studies [20-25] correction has been reported mostly in brain imaging [20, 22, 25], mainly due to the complexity and long scan time requirements of mapping the B1 field. Although many B1 mapping methods have been developed to date, no single one has been in widespread application.

With VFA technique, more flip angles will increase the accuracy of the method; however, the scanning time will also increase. Dual flip angle (DFA) is the simplest way of VFA with only 2 different flip angles, which can achieve the highest efficiency over a

narrow T1 range. In chapter 1, MOLLI was used to evaluate the cyclic variation of myocardial T1 values. Our results are different from a study at 3 T using DFA technique. To understand better about the DFA method, and know how much the B1 inhomogeneity can affect the accuracy of T1 measurement at 3 T. The aim of this study was to develop a fast T1 mapping technique for accurate T1 quantification using the DFA method with fast B1 mapping to correct for spatial variations of the nominal FA at 3 T.

3.2 Theory

The VFA technique is based on the consecutive application of T1-weighted spoiled gradient-echo (T1 fast-field echo (T1-FFE)) sequences using different flip angles [75]. The theoretical signal intensity S of a T1-FFE sequence is a function of the equilibrium longitudinal magnetization M_0, relaxation times T1 and T2, echo time (TE), repetition time TR (TR), and flip angle [71, 76]:

$$S = M_0 \frac{(1-E_1)\sin\alpha}{1-E_1\cos\alpha} \tag{3.1}$$

Where $E_1 = \exp(-TR/T1)$.

Keeping TR and TE constant and measuring the signal induced by different FAs, one can find a straight line characterized by slope a = E_1 and intercept b = (1- E_1) by linear regression.

$$\frac{S}{\sin\alpha} = E_1 \frac{S}{\tan\alpha} + M_0(1-E_1) \tag{3.2}$$

T1 is then easily calculated as:

$$T_1 = -TR / \ln(E_1) \tag{3.3}$$

A correct calculation of T1 is only valid if the transverse magnetization is completely spoiled, longitudinal magnetization has reached a dynamic equilibrium (steady state), and the amplitude of the radiofrequency field (B1) is homogeneous over the complete field of view (FOV). Especially for a large FOV and at high magnetic field strengths, B1 field inhomogeneities represent a dominant source of error in the VFA approach [70].

3.2.1 Choice of Flip Angles

Achieving the best precision for the T1 range of interest requires optimally selecting flip angles, but the selection process remains complex, particularly for multiple angles. However, a couple of key results from previous work on this topic serve as useful guidelines [68, 70, 71, 76, 77].

Wang et al [78] reported that optimum T1 precision occurs when the TR/T1 ratio is approximately 1.1:1. Their results showed that the precision of two optimized angles can be achieved as the precision obtained using 10 flip angles with 5-fold reduction in imaging time [78]. A simple one-step method for determining the angles was proposed for a particular TR/T1 [71].

To estimate T1 from two signal intensities/points on the regression line accurately, the further the two points are separated along the line will be better if each point suffers the same uncertainty.

This separation along the ordinate can be defined as normalized dynamic range (DR) of the regression line, given by:

$$DR = \frac{S\alpha_2}{M_0 \sin(\alpha_2)} - \frac{S\alpha_1}{M_0 \sin(\alpha_1)} \tag{3.4}$$

Where α_1 and α_2 are the two flip angles and $S\alpha_1$ and $S\alpha_2$ are the signal intensities associated with α_1 and α_2.

However, the data points may not suffer the same uncertainty; rather, the precision depends on the location of the points along the line and generally decreases as the two points move away from the midpoint (defined by the location of the peak of the signal curve and given by Ernst signal ($S\alpha_E$)). This means that the precision can be related to the fractional signal of the points (FS).

$$FS = (S\alpha_1 + S\alpha_2)/2S\alpha_E \tag{3.5}$$

The two optimum flip angles are derived by maximizing the product of $DR \times FS$.

Besides determining the two ideal angles by searching for maxima in the product of $DR \times FS$, analytically predicting the optimal dual angles is possible by simplifying FS to f:

$$f = FS = S\alpha_1 / S\alpha_E = S\alpha_2 / S\alpha_E \tag{3.6}$$

T1 precision is maximized by choosing the flip angles such that $S\alpha_1 = S\alpha_2 =$ 0.71 $S\alpha_E$ at f = 0.71 [71].

The solution for the two optimal angles can be written as:

$$\alpha = \cos^{-1}\left(\frac{f^2 E_1 \pm (1 - E_1^2)\sqrt{1 - f^2}}{1 - E_1^2 (1 - f^2)} \right) \tag{3.7}$$

Therefore, when imaging for a single T1, precision can be optimized using two "ideal" angles, defined as those whose signals are 71% of the Ernst angle signal.

3.2.2 Transmit Field B1 Imaging

The transmit field B1 of a volume coil may arise substantial inhomogeneity when imaging at higher field strengths above 1.5 T. The distribution of the magnetic radiofrequency (RF) field B1 has an important influence on image quality in magnetic resonance imaging. In particular, inhomogeneities of the RF field are an essential source of error for quantification of MR parameters in MRI [79]. For the successful application of imaging and detection methods using a specially designed RF field, it is essential to know the accurate B1 distribution within a tissue sample. In general, the B1 field in whole body systems needs to be determined for each investigated object because induced RF eddy and displacement currents account for remarkable differences between the field of an empty and a loaded coil [80]. The induced currents depend on the shape of the object, its electric properties, the resonance frequency, and the polarization of the used RF coil [80]. Therefore a method for B1 determination using image data is highly

desirable. An approach to account for this inhomogeneity is to map the B1 field distribution.

A wide variety of amplitude of RF field (B1) mapping methods has been developed to date [3]; however, no single one has emerged yet in widespread application [81]. Generally, B1 mapping methods fall into two classes: signal magnitude or signal phase based. The majority of B1 mapping methods depend on changes in signal magnitude based on RF flip angle. Existing methods in this category include fitting progressively increasing flip angles [82], stimulated echoes [83], image signal ratios [84], signal null at certain flip angles [85], and comparison of spin echo and stimulated echo signals [86]. These methods suffer from combinations of the following problems: T1 dependence; long acquisition times, mainly from acquiring many images and/or a long pulse repetition time (TR) to mitigate the T1 dependence; inability to use some of these methods with slice selection or in a multislice acquisition; inaccuracy over a large range of B1, especially at low flip angles or flip angles close to 90° or 180°; and large RF power deposition in the case of B1 mapping sequences based on large flip angles or reset pulses to mitigate the T1 dependence. The most simple and straightforward of the B1 mapping methods are dual-TR method and double-angle method.

3.2.2.1 Dual TR Method (DTR)

The DTR B1 mapping technique is based on a T1-FFE sequence with a fixed flip angle and two alternating TRs (TR1 < TR2) [76, 87]. The ratio r of the observed gradient-echo signals STR1 and STR2 is a function of α, TR1, TR2, and T1:

$$r = \frac{S_{TR1}}{S_{TR2}} = \frac{1 - E_{12} + (1 - E_{11})E_{12}\cos\alpha}{1 - E_{11} + (1 - E_{12})E_{11}\cos\alpha} \tag{3.8}$$

Where E_{11} = exp (-TR1/T1) and E_{12} = exp (-TR2/T1)

Based on this equation, the flip angle α is calculated as:

$$\alpha = \arccos\left(\frac{1 - r\left(\frac{1-E_{11}}{1-E_{12}}\right)}{rE_{11} - \left(\frac{1-E_{11}}{1-E_{12}}\right)E_{12}}\right) \tag{3.9}$$

If the first-order approximation can be applied to exponential terms in Eq. (3.9), exp (-TR/T1) ≈ 1-TR/T1, it can be simplified as:

$$\alpha = \arccos\left(\frac{1-rn}{r\left(1-\frac{TR_1}{T_1}\right) - n\left(1-\frac{TR_2}{T_1}\right)}\right) \tag{3.10}$$

Where n = TR1/TR2.

Assuming that 1-TR1/T1 ≈ 1 and 1-TR2/T1≈1 for TR1, TR2«T1 the calculation of the flip angle becomes independent of T1 and is only a function of the ratios of the measured signals r and the TRs n:

$$\alpha = \arccos\left(\frac{1-rn}{r-n}\right) \tag{3.11}$$

3.2.2.2 Double Angle Method (DAM)

The DAM method is specially designed for the in vivo measurement of the B1 field distribution in several cross sections in whole body systems within a few minutes [79]. Between the modulus of the active RF field B1(x) and the flip angle a(x) of an amplitude modulated RF pulse the following well known relationship with the pulse

shape f(t), the pulse duration time tp, and the gyromagnetic constant γ is given approximately [88]:

$$\alpha(x) = \gamma B_1(x) \int_{-t_p/2}^{t_p/2} f(t)dt \tag{3.12}$$

Where the x represents spatial position.

Two images are acquired with two different prescribed flip angles ($\alpha_1(x)$, $\alpha_2(x)$) with the following relationship:

$$\alpha_2(x) = 2\alpha_1(x) \tag{3.13}$$

The ratio of the corresponding image signal intensities I1(x)/I2(x) of two spin echo images measured with identical all other signal-affecting sequence parameters but different nominal excitation angles given by [84]:

$$\frac{I_2(x)}{I_1(x)} = \frac{\sin\alpha_2(x) f_2(T_1, TR)}{\sin\alpha_1(x) f_1(T_1, TR)} \tag{3.14}$$

This ratio is independent of the coil sensitivity, the spin density, and the transversal relaxation time T2(x). With a repetition time TR ≥ 5T, the longitudinal relaxation terms become equal 1.0 and the ratio depends only on the flip angles. T1max is the longest Tl time occurring within the investigated object. If the effects of T1 and T2 relaxation can be neglected, the flip angle distribution α_1 (x) can be calculated by the new relationship [79]:

$$\alpha_1(x) = \arccos\frac{I_2(x)}{2I_1(x)} \tag{3.15}$$

Thus, the DAM allows the determination of $\alpha_1(x)$ and consequently also of B1 (x) of an RF coil loaded with an arbitrary object. The disadvantage of this method for in vivo application is an extended scan time resulting from the condition $TR \geq 5T1max$.

However, most double-angle approaches have been limited by the requirement of long TRs and therefore long imaging times and motion compensation issues, which restricts the method to be applied in heart. Recently, saturated double angle method (SDAM) [84] for rapid B1 mapping has been introduced to map B1 field rapidly covering the heart within a single breath-hold. It combines the double angle method with a B1-insensitive magnetization-reset sequence used for saturation of the magnetization. This technique allows the B1 correction of myocardial T1 measurements using dual flip angle method in the future.

3.3 Materials and Methods

3.3.1 T1 Measurement with IR-TSE

Liquid samples with different concentrations of gadopentetate dimeglumine (Magnevist; Schering, Berlin, Germany) doped with distilled water were prepared with a range of T1 values representing precontrast and postcontrast myocardial T1 values at 3 T. These phantoms were imaged on a 3 T scanner (Ingenia; Philips Medical Systems, Best, The Netherlands) with the gold standard of T1 mapping technique (IR-TSE). The scan

parameters were TE = 70 ms, TR = 10000 ms, TI = [50, 100, 200, 400, 800, 1400, 2200, 3500, 5000] ms. TSE factor = 7. FOV = 230 × 184 mm^2, pixel size = 0.6 × 0.7 mm^2, slice thickness = 4 mm.

3.3.2 Choice of Flip Angles for DFA Method

Achieving the best precision for the T1 range of interest requires judicious selection of flip angles [70]. In order to maximize the SNR in the T1 map, the pair of flip angles which minimizes this expression has to be found numerically. The human myocardial T1 is about 1170 ms, for TR = 6.4 ms, the product of DR×FS reaches its maximum for the optimum FAs (α_{1opt} = 2°, α_{2opt} =14°) as shown in Figure 3-1.

3.3.3 T1 Measurement with DFA and LL Methods

The DFA sequence is based on the consecutive application of fast field echo sequences. In our study, this sequence was changed to realize 2 dynamic scans with two optimal flip angles determined with Eq. (3.7) in one acquisition.

T1-weighted images were acquired using a dual flip angle 2D spoiled gradient echo protocol with the following parameters: TR/TE = 6.4/3.7 ms, FA1/FA2 = [3°, 15°], FOV = 340 × 384 mm^2, pixel size = 1 × 1 mm^2, slice thickness = 6 mm.

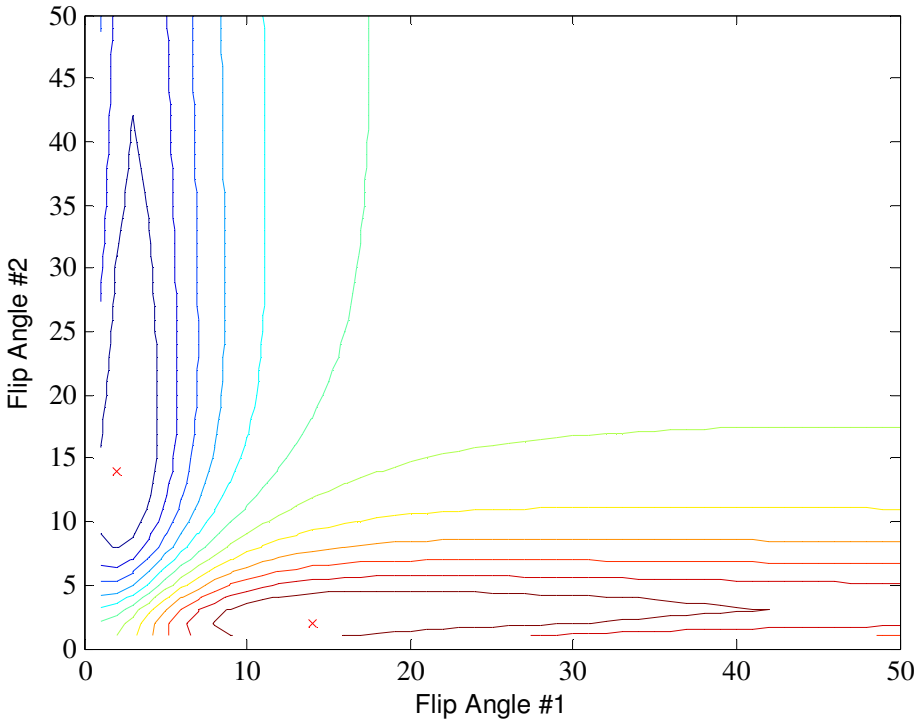

Figure 3-1:Contour plots for determining the optimal flip angles for TR = 6.4 ms and T1 = 1170 ms

Then, T1-weighted images were also acquired using a dual flip angle 3D spoiled gradient echo protocol with the following parameters: TR/TE = 6.4 ms/3.7 ms, FA1/FA2 = [2°, 11.6°], [2.5°, 14.2°], [3°, 15°], [3.1°, 17.5°], FOV = 340 × 384 mm^2, pixel size = 0.6 × 0.7 mm^2, and slice thickness = 6 mm.

All images were acquired on 3 T Ingenia MR Systems (Philips Medical Systems, The Netherlands) with anterior and posterior coil. A commercially available cardiac B1-calibration sequence, which is based on saturated dual angle method (SDAM), was performed with a simulated ECG signal. The imaging parameters were TE = shortest, flip angle = 60°, TR=1 heart beat.

T1 measurements with LL sequence were performed with the following scan parameters: flip angle, 10°; repetition time (TR), 7.7 ms; echo time (TE), 3.2 ms; measured pixel size, 2 ×2 mm^2; and slice thickness, 10 mm. After a 180° radiofrequency prepulse triggered by the R peak of ECG, gradient-recalled echo images (number of images dependent on the patient's heart rate) were acquired throughout the cardiac cycle, with a phase interval of approximately 25 ms between images.

3.3.4 T1 Measurement with MOLLI and LLN Methods

T1 measurements with MOLLI and LLN were performed on 3 T Achieva MR Systems (Philips Medical Systems, The Netherlands) Eleven MOLLI images were acquired from 3 successive IR-prepared, ECG-triggered LL experiments (LL1, LL2, and LL3) with 3, 3, and 5 single-shot readouts, respectively. Each of the LL experiments started with a 180° prepulse; the first single-shot readout was performed at inversion time (LL1 ≈ 130 ms, LL2 ≈ 267 ms, and LL3 ≈ 350 ms) and at trigger delay time (400 ms) after the previous R-wave. The scan parameters were as follows: flip angle, 35°; TR, 3.9 ms; TE, 1.95 ms; SENSE reduction factor, 2; measured pixel size, 1.9 × 2.3 mm^2; slice thickness, 10 mm; and acquisition window, 191.1 ms. LLN sequences were performed with the following scan parameters: flip angle, 10°; repetition time (TR), 7.7 ms; echo time (TE), 3.2 ms; measured pixel size, 1.9 ×1.7 mm^2; and slice thickness, 10 mm. After a 180° radiofrequency, 21 gradient-recalled echo images were acquired with a phase interval of approximately 80 ms between images (this is main difference between LL and LLN).

3.3.5 Data Analysis

The T1 calculation for IR-TSE is by three-parameter nonlinear curve fitting using a Levenberg-Marquardt algorithm is performed pixel-wise for y = A – B exp (–t/T1*). T1 is then calculated from effective T1 (T1*) by T1 = T1* ((B/A) – 1) [7]. Reconstruction of T1 maps was performed off-line using software written in Matlab (The MathWorks, Natick, MA, USA).

For MOLLI and LL sequences, curve fitting was performed using signal intensities from manually drawn ROIs using Matlab (The MathWorks, Natick, MA, USA) to obtain the mean T1 value within the corresponding ROIs.

For the DFA method, the apparent T1 values were calculated with Eq. (3.3). Due to additional effects, in particular B1 inhomogeneities and incomplete spoiling of transverse magnetization, apparent T1 values as derived from Eq. [3.3] can deviate from the real values, requiring several corrections [89]. In the presence of B1 inhomogeneities, the nominal flip angle α deviates from the real flip angle. The relative flip angle distribution b1(x,y) is determined by the ratio of the effective flip angle α_{eff} (x,y) (Eq. [12]) and the nominal flip angle α_{nom}:

$$b_1(x, y) = \frac{\alpha_{\text{eff}}(\text{x}, \text{y})}{\alpha_{\text{nom}}} \tag{3.16}$$

T1 values can be corrected by incorporating b1 information. The B1 map can be used to correct the T1 values using the following equation [76]:

$$T_1 = \frac{-T_R}{\ln\left\{\frac{S_{\alpha 1opt}/\sin(b1\cdot\alpha_{1opt}) - S_{\alpha 2opt}/\sin(b1\cdot\alpha_{2opt})}{S_{\alpha 1opt}/\tan(b1\cdot\alpha_{1opt}) - S_{\alpha 2opt}/\tan(b1\cdot\alpha_{2opt})}\right\}} \quad (3.17)$$

Where Sα1opt and Sα2opt represent the acquired signal amplitude of the T1 measurement using the optimum flip angles.

Table 3-1: T1 values (ms) of DFA (2D and 3D FFE) with and without B1 correction and IR-TSE

T1 from TSE	**Optimal FAs**	**2D DFA without B1**	**2D DFA with B1**	**3D DFA 1 Acq without B1**	**3D DFA 1 Acq with B1**
144	[2°, 11.6°]	42	61	58	85
774	[2.5°, 14.2°]	58	84	336	482
1185	[3.1°, 17.5°]	65	96	449	662
1791	[7.1°, 39.4°]	54	80	680	1011
3586	[1.4°, 8.2°]	69	105	1268	1930

3.4 Results

Optimal flip angle set are [2°, 11.6°], [2.5°, 14.2°], [3.1°, 17.5°], [7.1°, 39.4°], [1.4°, 8.2°] for T1 = 144, 774, 1185, 1791, 3586 ms with TR = 6.4 ms. Only the more central sections of the 3D slab was selected to process the data analysis. Table 3-1 compared the 2D DFA and 3D DFA with and without B1 correction. The B1

inhomogeneity is up to 20% according to the obtained B1 maps. The results of DFA, MOLLI and LL studies compared with IR-TSE are shown in Table 3-2 and Figure 3-2. The duration of MOLLI and LL data acquisitions ranged from 11 to 23s, adequate for a breath hold.

The T1 results with 2D FFE did not vary across the samples as expected, and all were much smaller compared to other methods, even after B1 correction. The 3D FFE sequences were performed with two separate acquisitions using two optimal flip angles, and two dynamic scans with two optimal flip angles in single acquisition. The T1 measurements from two separated acquisitions DFA method did not show close agreement with the gold standard method (IR-TSE). However, the single acquisition 3D DFA results showed good correlation with the gold standard method (IR-TSE). Also the results with single acquisition DFA were comparable with MOLLI and better than the LL method. Note that the accuracy of T1 measurements with 3D DFA was increased significantly with B1 correction.

Table 3-2: T1 values (ms) of 3D FFE DFA (1 acquisition [Acq]and 2 acquisitions [Acqs]) with and without B1 correction compared with IR-TSE, MOLLI and LL

T1 from TSE	**without B1**		**with B1**		**T1 from LL**	**T1 from MOLLI**	**T1 from LLN**
	3D DFA 1 Acq	*3D DFA 2 Acqs*	*3D DFA 1 Acq*	*3D DFA 2 Acqs*			
144	102	471	148	680	181	169	175
774	450	1322	678	1993	667	876	801
1185	643	1871	957	2785	863	1223	929
1791	1008	2951	1416	4146	1055	1551	1136
3586	1995	6648	2836	9464	1212	2210	1474

Without B1 correction, the T1 values are significantly underestimated compared with the gold standard. Also for the clinical interested T1 values (774 ms, 1185ms), the results with B1 correction are about 34% and 33% smaller than results with B1 correction. After flip angle corrected, the T1 values are much closer to reference T1 values for each sample especially similar results for the T1 values shorter than 1000 ms.

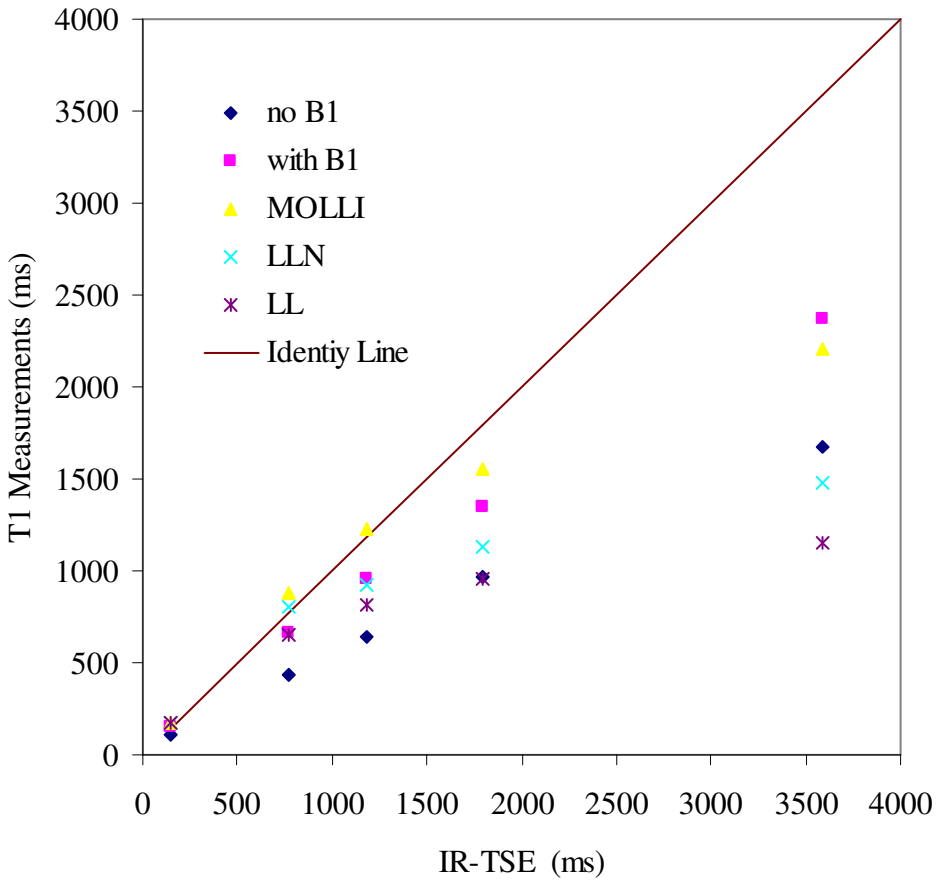

Figure 3-2:Comparison between T1 measurements with different techniques

3.5 Discussion

In this study a fast 3D T1 mapping technique based on the DFA approach to measure T1 values in a wide range was implemented and tested. The acquisition time was about 1s per slice. A fast B1 mapping technique based on SDAM was employed to correct the discrepancy of the actual flip angle from the nominal flip angle. The consecutive applications of the B1 and T1 mapping sequences enable to generate the comparable T1 measurement with MOLLI which is the most widely used myocardial T1 mapping sequence now. The described method is effective for a T1 range about 100-1200 ms, and thus the results showed that the single acquisition DFA with B1 correction is promising to measure precontrast and postcontrast myocardial T1 values in the future. However, the DFA with 2D gradient echo was not accurate and the error may be due to the inappropriate excitation pulse shape. The outer slices of a 3D sequence are often unusable since they fall at the edges of the excited slab where signal intensity and contrast are sub-optimal [90]. Previous studies showed that highly accurate T1 maps were produced only at the more central sections of the 3D slab [91, 92], therefore only the central slice was employed to avoid the inaccurate T1 measurements at the outer edges o the 3D slab.

With the VFA technique there is always a trade-off between high T1 accuracy (using more flip angles) and high temporal resolution (using fewer flip angles) [76]. As observed by Deoni et al [71], multiple averaging of T1 maps with dual flip angle technique provides higher accuracy per unit scan time than single average, multiple flip angle data. However, to apply this technique for cardiac purpose, a high temporal

resolution is required. Therefore, two optimal flip angles without signal averaging were chosen, which resulted in a temporal resolution about 1s per T1 map at a voxel size of 1× 1 ×6 mm^3.

The accuracy of the described T1 mapping technique using the DFA approach decreases continuously as T1 increases, which was also found in other 1.5 T and 3 T studies [76]. However, for the clinical interested T1 range shorter than 1500 ms, the agreement between the DFA and IR-TSE was good. According to Eq. (3.1), the acquired gradient echo signal decreased with higher T1 values. For the very long T1 value, it is important to maintain the highest possible SNR. Multiple signal averaging is one way to increase SNR; however, it was not employed in this study because to minimize the acquisition time. The SNR may also be improved by using a large slice thickness and applying RF excitation pulses with a high specific bandwidth, which resulted in improved slice excitation profiles.

The dominant source of error for T1 measurement using the VFA method is spatial variations of the nominal FA [70]. The in plane variations arise from B1 field inhomogeneities, which was up to 20% in this study. SDAM B1 mapping for cardiac triggering sequence was performed to correct the measurements. We corrected B1 field inhomogeneities by multiplying the optimal flip angles of the T1 measurement by the relative flip angle distribution b1(x,y) derived from the B1 mapping measurement [76]. This assumption holds true only in the case of a linear relationship between the nominal FA and the actual B1 amplitude of the RF pulse. For slice-selective pulses, however, linearity represents only an approximation. The deviation from the linear relationship

depends on the applied RF pulse shape. Also, image artifacts from imperfect spoiling and steady state impair accurate T1 measurements.

3.6 Conclusion

In this study we corrected B1 field inhomogeneities to improve the T1 measurements with DFA by applying fast B1 mapping technique at 3 T. The results showed that the single acquisition DFA with B1 correction produced significant improvement in measuring a wide range of T1 values than without B1 correction at high magnetic field strength. The T1 measurements with B1 correction are comparable with the MOLLI and LL sequences. For the clinical interested myocardial T1 range, the DFA with B1 calibration is in good agreement with the gold standard method (IR-TSE). The acquisition time is about 1s per slice without cardiac ECG triggering applied. However, this would result in a considerably longer acquisition time to trigger the ECG signal in human study and further research is needed to optimize this method to realize clinical application.

CHAPTER IV

MYOCARDIAL T1 MAPPING TECHNIQUES: COMPARISON OF LOOK LOCKER AND MOLLI SEQUENCES

4.1 Introduction

A variety of dedicated cardiac pulse sequences have been developed for T1 mapping, which can be applied to characterization of diseased myocardial tissue [39, 42, 44-50]. Among all the myocardial T1 mapping techniques, Look Locker (LL) was proposed in 1970 [52] and has been widely used to identify the null inversion time (TI) of myocardium for scar imaging, characterize myocardium without contrast agent injection [31], measure the myocardial T1 in patients with cardiac amyloidosis [93], and with ischemic heart [54], quantify the partition coefficient [53] and extracellular volume of myocardium [94].

The modified Look Locker inversion recovery (MOLLI) sequence has gained popularity [39, 45, 46, 48, 50] since it was developed from LL in 2004 [45]. This sequence, which obtains images at the most quiescent state of the heart, contains several important modifications from the original LL sequence, including electrocardiogram

(ECG)-synchronized acquisition in a fixed window/phase of the cardiac cycle and prolongation of the TI to fully reach longitudinal relaxation.

MOLLI is developed from LL, but has several significant modifications based on LL: 1. setting the acquisition window in the fixed cardiac cycle; 2. prolonging the TI to reach fully longitudinal relaxation. MOLLI and LL are more popular T1 mapping techniques. MOLLI is being accepted as the reference to be compared with other new techniques, such as Shortened MOLLI [50]. MOLLI should therefore be more reliable than LL in determining T1 time, but the relationship between MOLLI results and those of LL, particularly in patients with myocardial disease, has not yet been fully evaluated [95]. However, there is still unknown about the difference or agreement between these two techniques in patients. Validation and comparison between techniques is still limited, requiring further evaluation of the accuracy of these techniques pre- and post-contrast agent injection in various patient groups. Furthermore, the accuracy of T1 mapping is confounded by several factors, such as the types of T1 mapping acquisition sequence, physiologic parameters, and presence of contrast material. Examining their advantages and limitations are important to choose the more appropriate technique in certain situation. Understanding the limitations of various T1 mapping techniques as applied in cardiac imaging will help to ascertain true differences between patient groups resulting from disease. However, differences in T1 values obtained either from different pulse sequences or from different regions of the myocardium have not been well investigated.

MOLLI and LL techniques are more important clinical relevant T1 mapping techniques. In this study, we therefore sought to compare precontrast and postcontrast T1 values obtained with these two techniques in phantom studies and in patient studies that

included controls, patients with ischemic cardiomyopathy (ICM), and patients with HCM. In vitro and in vivo T1 mapping studies were performed by LL and MOLLI to evaluate the hypothesis that the accuracy of myocardial T1 measurements is dependent on the diseased tissue characteristics, heart rate, T1 mapping methods and T1 value itself which is different between before and after contrast agent injection. Static phantoms with a wide range of T1 values were scanned to measure the T1 value using LL and MOLLI. The sequences were applied to three groups of patients to be further compared the estimation of T1 values pre- and post-contrast agent injection. Our goal is to establish a protocol to accurately calculate myocardial T1 before and after injection of contrast agent in clinical setting.

4.2 Materials and Methods

4.2.1 Phantom Studies

Liquid samples with varying concentrations of gadopentetate dimeglumine (Magnevist; Schering, Berlin, Germany) doped with distilled water were prepared to meet a T1 of 200 to 2000 ms. Phantoms were imaged on a 1.5 T scanner (Achieva XR; Philips Medical Systems, Best, The Netherlands) with 3 T1 mapping techniques (IR-TSE, MOLLI, and LL) using a simulated ECG to set the heart rate at 40, 60, 80, and 100 beats per minute (bpm).

4.2.2 Subjects Population

This study was approved by the local institutional review board. A review of electronic health records identified eligible study subjects, including 5 patients (4 men, 1 woman; mean age ± SD, 44 ± 21 y) with normal left ventricular (LV) function, shape, and size (all were evaluated for thoracic aorta disease); 5 patients (3 men, 2 women; mean age ± SD, 63 ± 2 y) with ICM; and 16 patients (10 men, 6 women; mean age ± SD, 51 ± 15 y) with HCM. All patients provided written informed consent.

4.2.3 Imaging Procedure

Patients were scanned on a Philips 1.5 T scanner with a phased-array cardiac coil. Four ECG leads were placed on the chest for synchronized image acquisition. For delayed enhanced cardiac MRI, 0.2 mmol/kg of gadopentetate dimeglumine (Magnevist) was administered at an injection rate of 2 mL/s (3 patients were injected with a single dose because of impaired kidney function), followed by a 20- to 30-mL saline flush through a 20-gauge cannula placed in an antecubital vein. For patients with HCM or ICM, LL and MOLLI sequences were performed before and after (approximately 15 minutes) gadolinium administration at 2 short-axis levels (basal and mid cavity). For the normal LV function (Normal LV) patients, the postcontrast time was shorter (approximately 5 minutes) for clinical workflow.

LL sequences were performed with the following scan parameters: flip angle, 10°; repetition time (TR), 7.7 ms; echo time (TE), 3.2 ms; measured pixel size, 1.9 ×1.7 mm;

and slice thickness, 10 mm. After a 180° radiofrequency prepulse triggered by the R peak of ECG, gradient-recalled echo images (number of images dependent on the patient's heart rate) were acquired throughout the cardiac cycle, with a phase interval of approximately 80 ms between images. MOLLI sequences were performed at end-diastole to minimize cardiac motion. Eleven MOLLI images were acquired from 3 successive IR-prepared, ECG-triggered LL experiments (LL1, LL2, and LL3) with 3, 3, and 5 single-shot readouts, respectively. Each of the LL experiments started with a 180° prepulse; the first single-shot readout was performed at inversion time (LL1 ≈ 130 ms, LL2 ≈ 267 ms, and LL3 ≈ 350 ms) and at trigger delay time (400 ms) after the previous R-wave. The scan parameters were as follows: flip angle, 35°; TR, 3.9 ms; TE, 1.95 ms; SENSE reduction factor, 2; measured pixel size, 1.9 × 2.3 mm^2; slice thickness, 10 mm; and acquisition window, 191.1 ms.

4.2.4 Data Analysis

Myocardial T1 values were computed for every pixel with a 3-parameter nonlinear curve fitting using a Levenberg-Marquardt algorithm: $y = A - B \exp(-t/T1^*)$. T1 was calculated from effective T1 (T1*) with the equation $T1 = T1^* ((B/A) - 1)$ [45]. Regional analyses were also performed to compare corresponding areas between MOLLI and LL. Regions of interest (ROIs) were manually drawn in 1 image and then copied to the remaining images to calculate T1 values. A total of 6 ROIs were drawn in the mid myocardium (anteroseptal, septal, inferior, posterior, lateral, and anterior). The location of a pixel position within the myocardium was described by its position relative to the local wall thickness (relative distance to the endocardial and epicardial contour) and its

angular position relative to the wall. Care was taken to exclude epicardial structures and the blood pool from myocardial ROIs. For patients with macroscopic scar, ROIs were drawn to differentiate between scarred and remote areas. The area of all ROIs was approximately 50 pixels, but each ROI area was dependent on the size of infarcted areas in patients with delayed enhancement. The mean signal intensity of each ROI was used to calculate T1 values. All image analyses were processed offline using Matlab (The MathWorks; Natick, MA, USA).

4.2.5 Statistical Analysis

Statistical analysis was performed using SPSS 14.0 (SPSS, Inc, Chicago, IL). Paired student t-tests and Bland-Altman analyses were used to compare T1 values obtained with the MOLLI and LL techniques. A P value < 0.05 indicated statistical significance.

4.3 Results

4.3.1 Phantom Studies

For the MOLLI and LL methods, there was a systematic underestimation of T1 times longer than 1000 ms; underestimation was more pronounced for higher heart rates and longer T1 times (Table 4-1 and Figure 4-1). The duration of the breath-hold MOLLI

and LL data acquisitions ranged from 14.7 s to 23 s. T1 values calculated with MOLLI were shorter than those calculated with LL for T1 times shorter than 400 ms. The techniques produced comparable results for T1 values between 400 ms and 500 ms. For T1 times greater than 600 ms, values calculated with MOLLI were greater than those calculated with LL. LL was associated with a higher percentage of error than MOLLI.

Table 4-1: T1 values in phantoms measured with MOLLI and LL versus IR-TSE at simulated heart rates of 40 to 100 bpm

Heart Rate (bpm)	**Method**	**T1(ms)**							
	IR-TSE	**2655**	**1517**	**1094**	**854**	**760**	**448**	**251**	**194**
40	LL	1855	1307	1028	862	783	504	428	300
	MOLLI	2126	1442	1071	866	773	444	265	209
60	LL	1368	1131	932	844	770	526	444	319
	MOLLI	1977	1361	1110	885	799	464	266	210
80	LL	1106	950	815	722	683	482	416	306
	MOLLI	1652	1267	997	819	719	461	246	190
100	LL	903	858	731	655	629	467	399	306
	MOLLI	1314	1099	946	785	710	467	245	182

bpm, beats per minute; IR-TSE, inversion recovery turbo spin echo; LL, Look-Locker; MOLLI, modified Look-Locker inversion recovery.

Figures 4-2 and 4-3 show the dependence of T1 value on the simulated heart rates obtained from LL and MOLLI, respectively. For both methods, the T1 values are not dependent on heart rates when T1 values are shorter than 500 ms. This result agrees with the previous studies that showed no significant difference was found between post-contrast T1 values at different heart rates [31, 46]. However, the T1 values decreases with

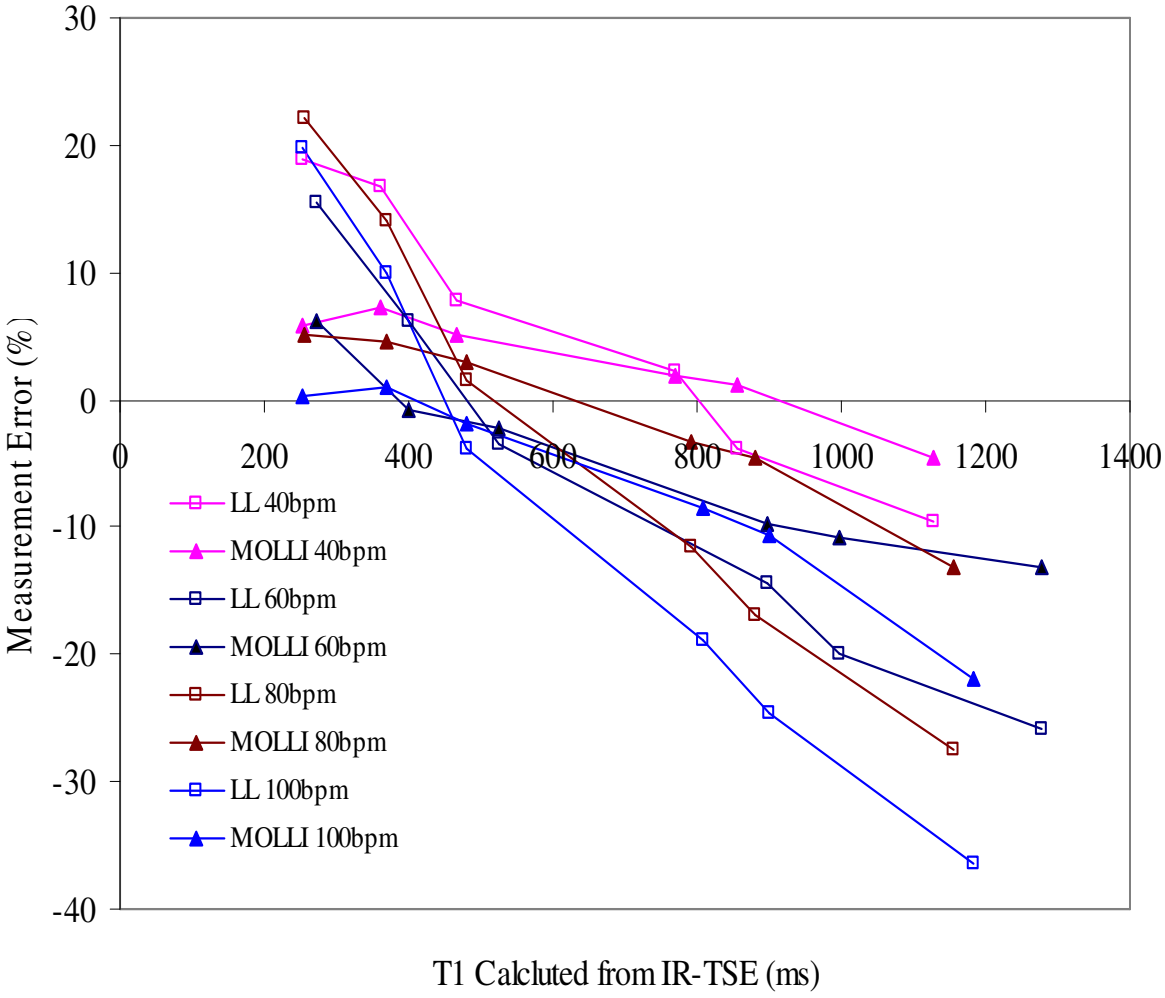

Figure 4-1: Phantom studies. Percentage error in T1 estimations (LL and MOLLI)

At various simulated heart rates versus reference values (with IR-TSE). (In the legend, L means LL, M means MOLLI, the numbers represent the heart rate)

increased heart rates when T1 values are longer than 600 ms, the dependence is more significant for longer T1. This result agrees well with the previous study [31]. The interested T1 value range is from 300-1200 ms in this study; therefore the dependence of T1 on heart rate can not be neglected for the precontrast myocardium which is in the range of 800-1200 ms.

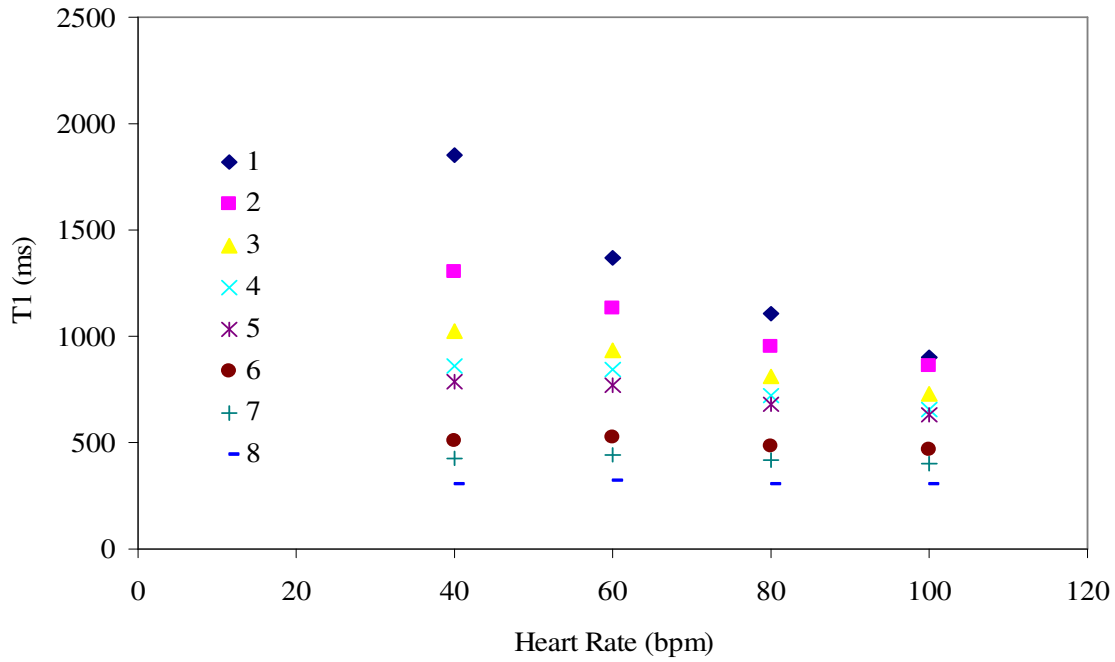

Figure 4-2: T1 estimation from LL at different simulated heart rates

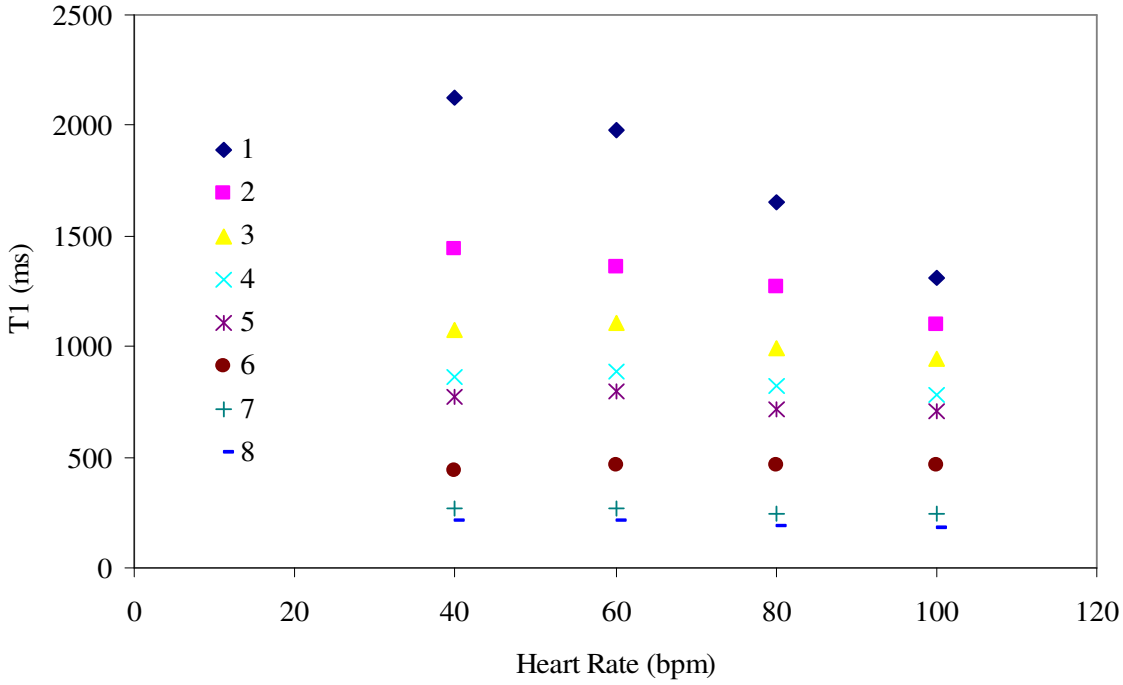

Figure 4-3: T1 estimation from MOLLI at different simulated heart rates

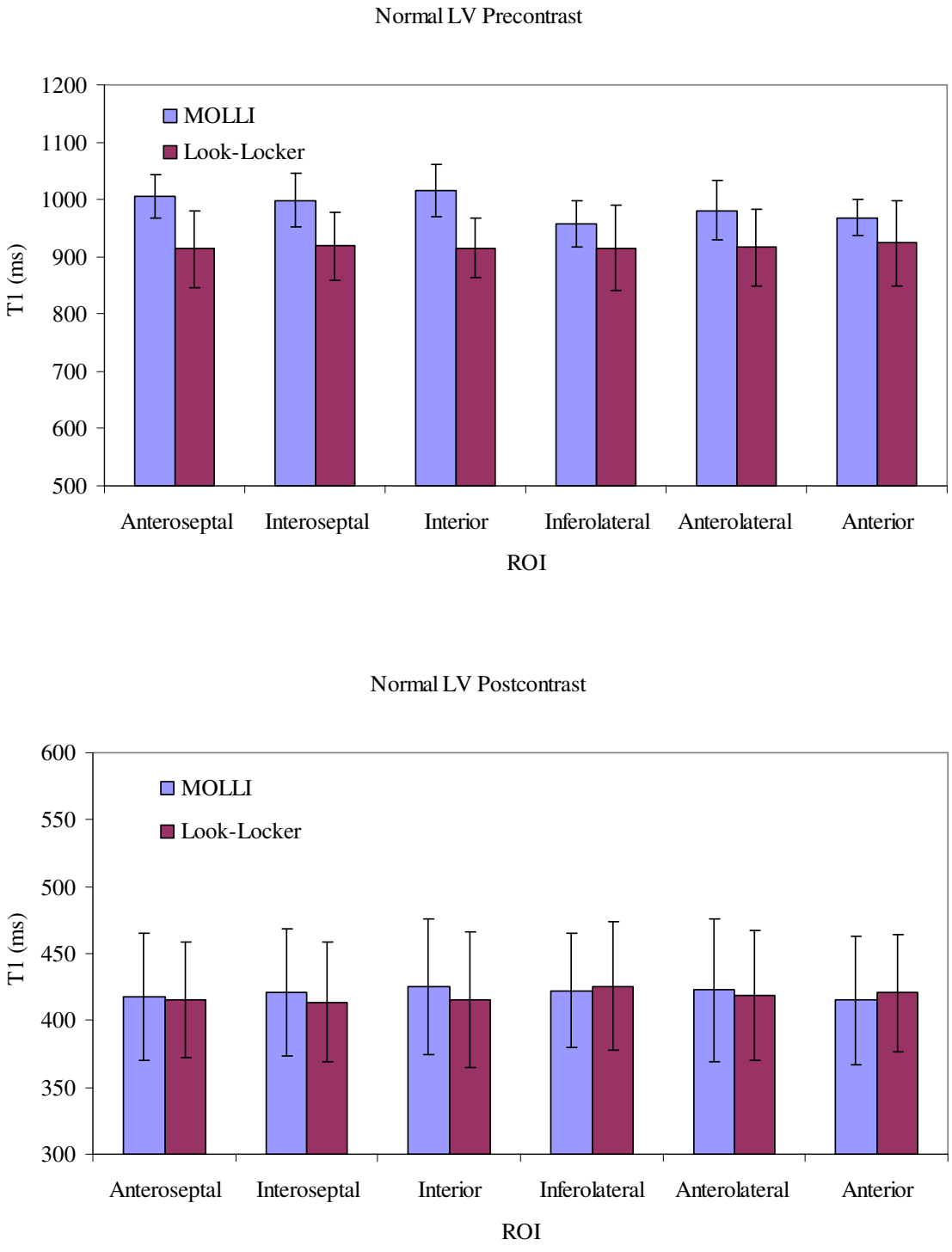

Figure 4-4: Mean myocardial T1 values for each ROI using LL compared with MOLLI for normal LV

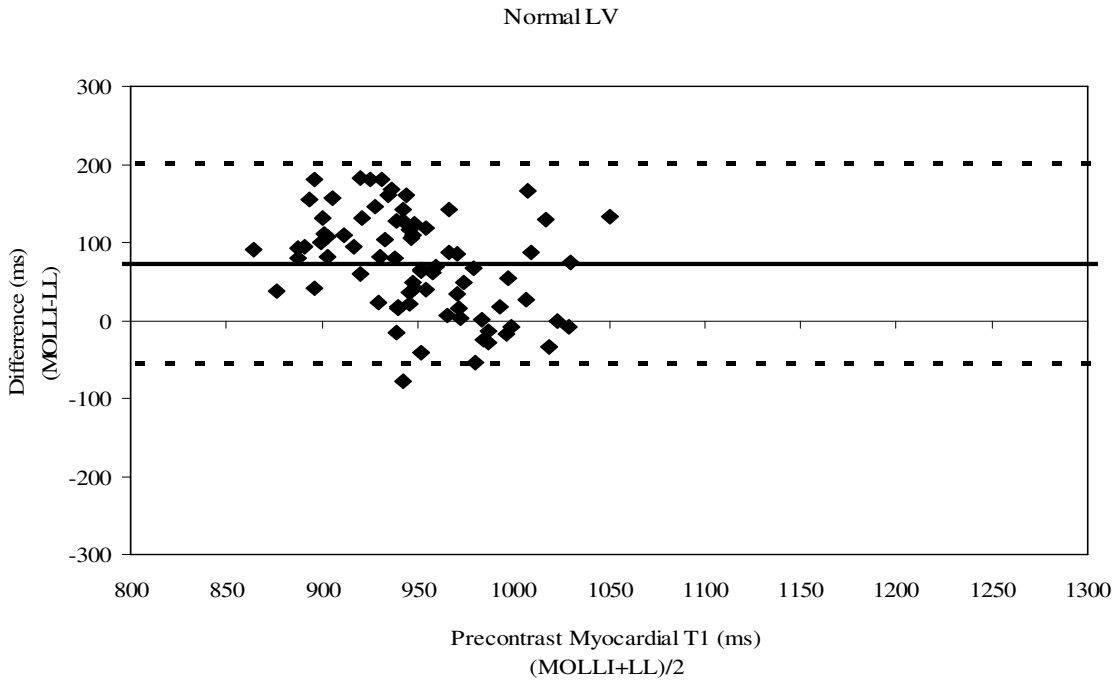

Figure 4-5: Bland-Altman analysis to express the intersequence agreement of the precontrast myocardial T1 values using LL compared with MOLLI for normal LV. The mean difference (bias) is represented by the black line and the 95% limits of agreement limit are represented by the dashed lines.

4.3.2 In Vivo Studies

In patients with normal LV, precontrast T1 measurements calculated with MOLLI were greater (983 ± 48 ms) than those calculated with LL (898 ± 69 ms; $P < 0.001$; t-test for paired comparison) as shown in Figures 4-4 and 4-5. The postcontrast measurements showed good agreement between LL (418 ± 44 ms) and MOLLI (420 ± 46 ms; $P = 0.423$) (Figures 4-4 and 4-6).

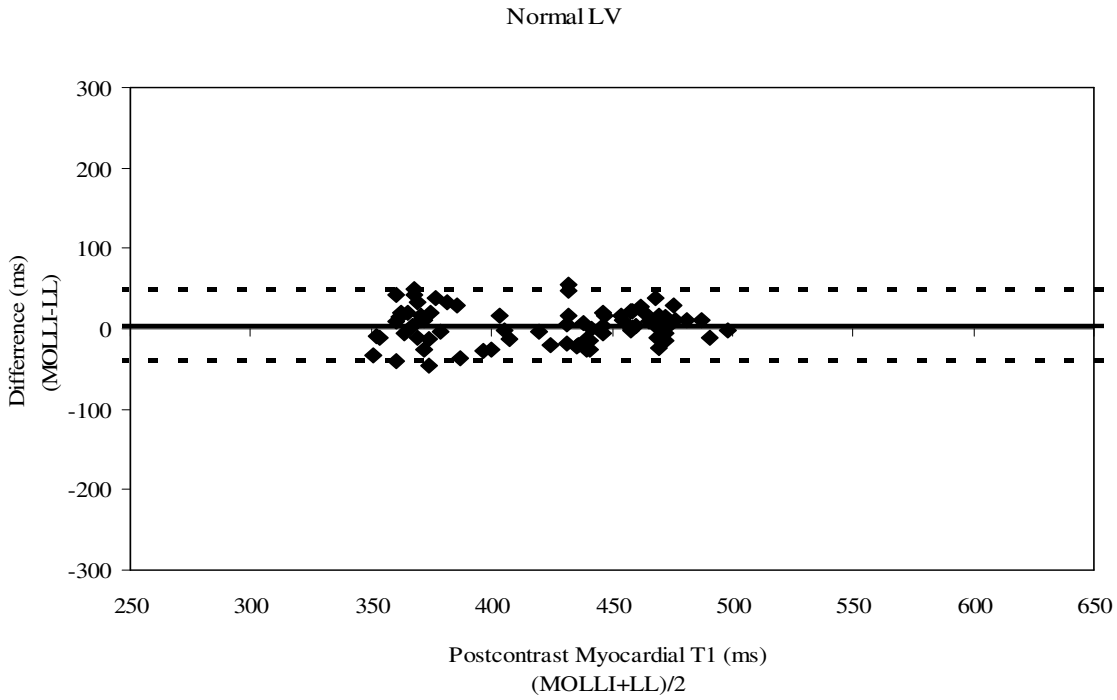

Figure 4-6: Bland-Altman analysis to express the intersequence agreement of the postcontrast myocardial T1 values using LL compared with MOLLI for normal LV patients. The mean difference (bias) is represented by the black line and the 95% limits of agreement limit are represented by the dashed lines.

In other patient groups, the precontrast myocardial T1 values obtained with MOLLI (1031 ± 78 ms) were greater than those obtained with LL (910 ± 74 ms; $P < 0.001$). Specifically, the precontrast myocardial T1 values obtained with MOLLI were greater than those obtained with LL for patients with ICM (1083 ± 136 ms vs 900 ± 112 ms; $P < 0.001$) and for patients with HCM (1029 ± 44 ms vs 917 ± 58 ms; $P < 0.001$) (Figures 4-7,4-8 and 4-9). With MOLLI, the precontrast T1 values calculated for patients with ICM (1083 ± 136 ms) and patients with HCM (1029 ± 44 ms) were greater than values for the control patients (983 ± 48 ms). However, with LL, there was no significant

difference among controls, patients with ICM, and those with HCM (898 ± 69 ms, 900 ± 112 ms, and 917 ± 58 ms, respectively).

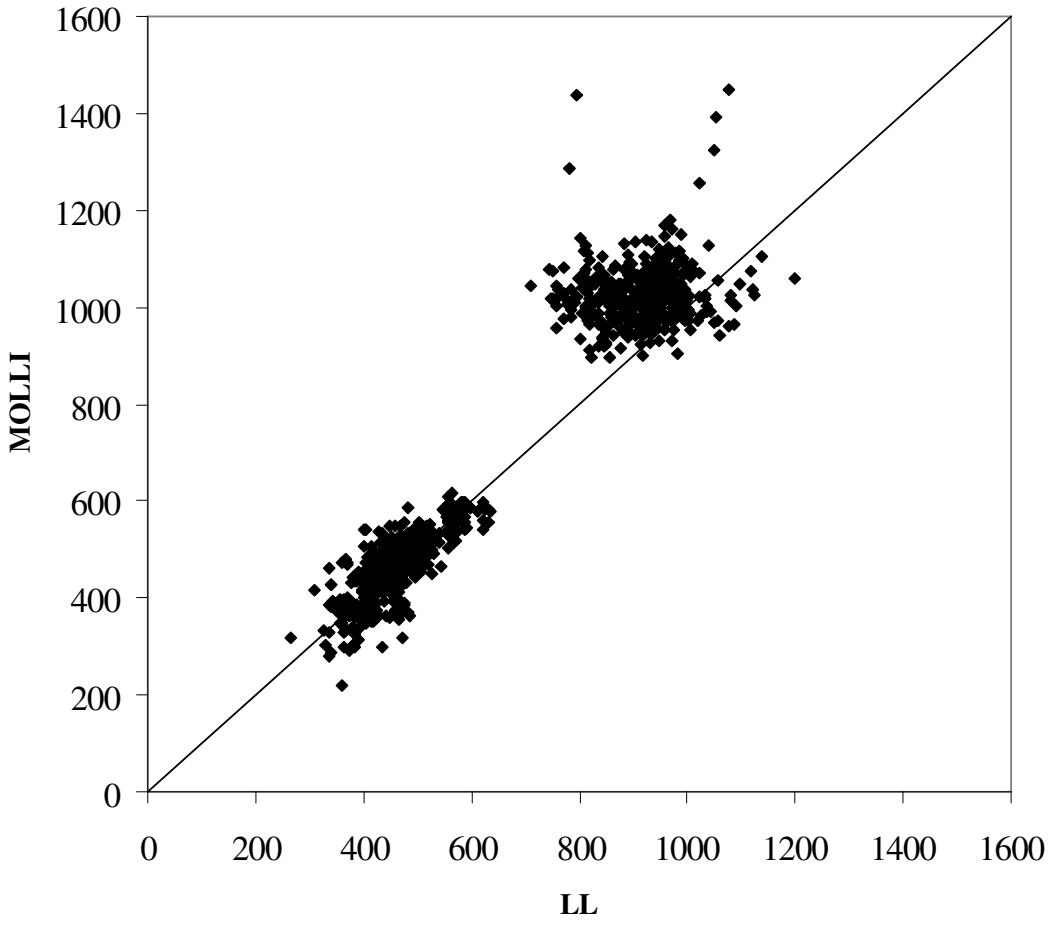

Figure 4-7: Scatterplot of myocardial T1 values obtained with LL and MOLLI

Although the paired t-test showed that post-contrast myocardial T1 values obtained with MOLLI were significantly different from those obtained with LL, the mean T1 values for MOLLI and LL were separated by less than 10 ms (474 ± 70 ms vs 465 ± 64 ms; $P < 0.001$). There was good agreement between LL (474 ± 85 ms) and MOLLI (474 ± 93 ms) postcontrast T1 measurements for patients with ICM ($P = 0.974$); however,

postcontrast values in patients with HCM were higher with MOLLI (488 ± 59 ms) than with LL (474 ± 54 ms; $P < 0.001$).

For patients with HCM or ICM, MOLLI demonstrated much longer T1 values in the infarcted area than did LL. In a representative patient with ICM, infarcted myocardium showed very long precontrast T1 values but shorter postcontrast values compared with values in remote myocardium (Table 4-2). For postcontrast images in the remote area, LL demonstrated shorter T1 values than MOLLI; however, LL demonstrated longer T1 values than MOLLI in the infarcted area.

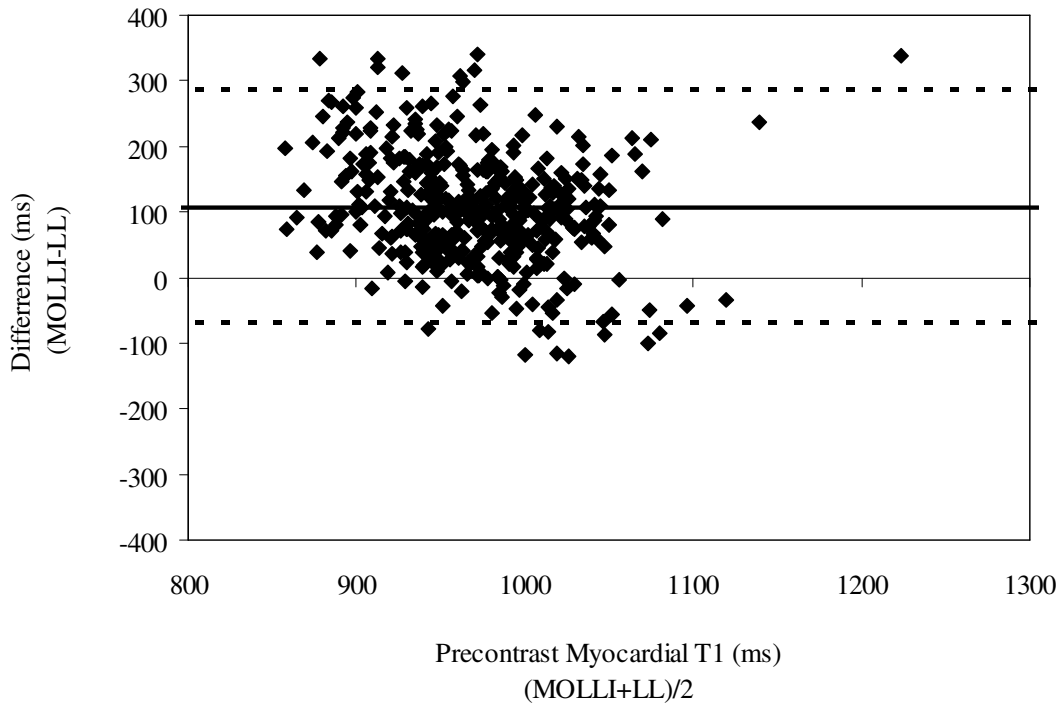

Figure 4-8: Bland-Altman analysis of myocardial precontrast T1 values obtained with LL and MOLLI for all patients. The mean difference (bias) is represented by the black line and the 95% limits of agreement limit are represented by the dashed lines.

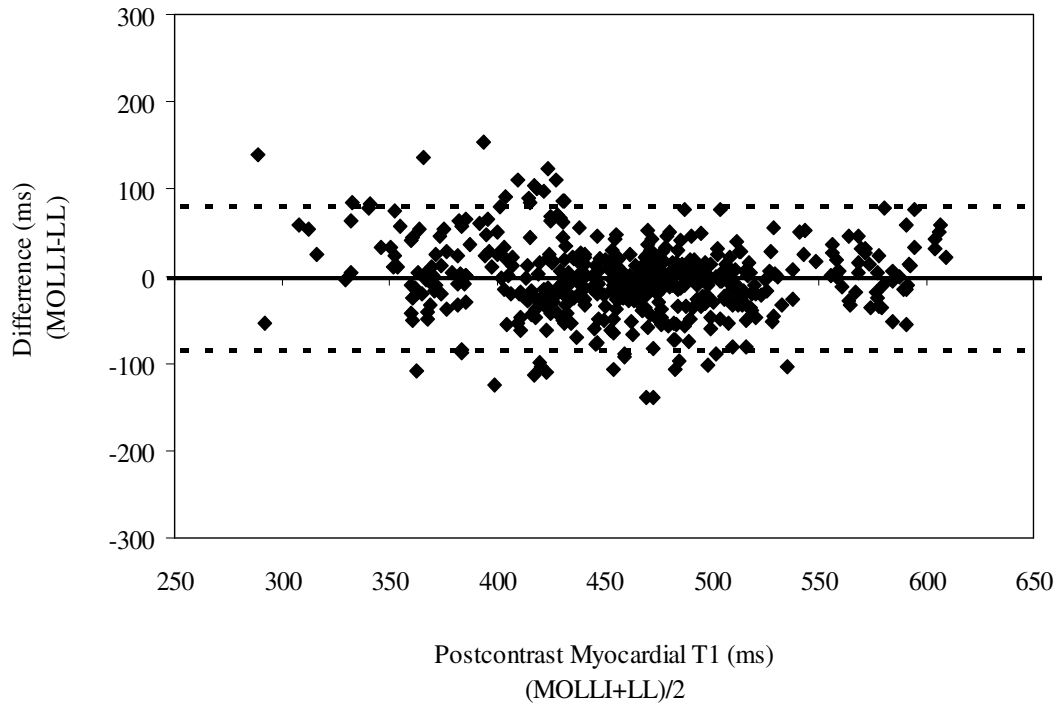

Figure 4-9: Bland-Altman analysis of myocardial postcontrast T1 values obtained with LL and MOLLI for all patients. The mean difference (bias) is represented by the black line and the 95% limits of agreement limit are represented by the dashed lines.

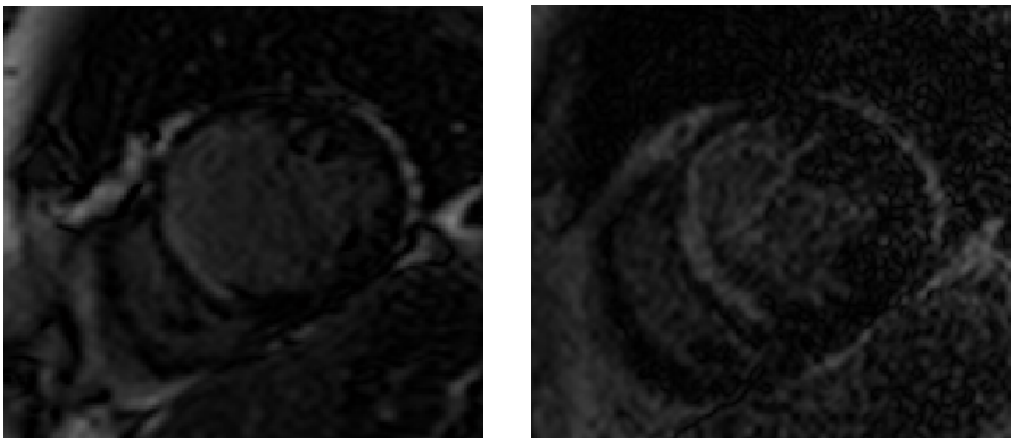

Figure 4-10: Postcontrast MOLLI (left) and LL (right) images of a patient with ICM

Table 4-2: T1 values in a patient with ICM measured with MOLLI and LL

		T1(ms)			
		Precontrast		**Postcontrast**	
		Infarcted Area	**Remote Area**	**Infarcted Area**	**Remote Area**
Basal	LL	988	941	434	571
	MOLLI	1151	995	418	600
Middle	LL	1076	929	393	572
	MOLLI	1448	1047	369	578

ICM, ischemic cardiomyopathy; LL, Look Locker; MOLLI, modified Look Locker inversion recovery.

There is different data acquisition process between LL and MOLLI. LL acquires a series of T1-weighted images from different cardiac phases. MOLLI is based on LL with the advantage of acquiring the images at the same phase within the cardiac cycle. In addition, the longest inversion time can be set much longer with MOLLI than LL, which is important to meet the requirement for the full recovery of longitudinal magnetization (about 5*T1 of the sample to be measured). For T1 times around 1000 ms at 1.5T, two cardiac cycles (about 2000 ms) would not be sufficient for magnetization to reach equilibrium with LL; thus, it caused error in estimated T1 and this error is increased with faster heart rate. Figure 4-11 showed the recovery curves of MOLLI and LL from a HCM patient. For precontrast images, the recovery of MOLLI achieved equilibrium while the recovery of LL was incomplete. For postcontrast images, the myocardial T1 time is about 500 ms and two cardiac cycles (about 2000 ms) enable almost full magnetization recovery and accurate T1 quantification can be achieved with LL. The postcontrast recovery curve of MOLLI lasted longer than the required time for fully relaxation;

therefore, the last two data points were not necessary. The magnetization tipped down by the radiofrequency pulse can recover to equilibrium state faster than the precontrast myocardium. Figure 4-11 illustrates that the data points (TI ≥2000 ms) with very long inversion time acquired with MOLLI were not necessary because the magnetization reached equilibrium before 2000 ms.

4.4 Discussion

Our data demonstrate that the MOLLI sequence shows closer agreement to IR-TSE than does LL over a wide range of T1 values in phantom studies. For myocardial T1 measurements, MOLLI and LL show close agreement in postcontrast values, but precontrast T1 values obtained with MOLLI were longer than those obtained with LL.

The LL sequence, which acquires a series of T1-weighted images from different cardiac phases, is widely used in clinical settings to identify the null TI of remote myocardium for delayed enhanced imaging. This sequence has also been used to measure myocardial T1 values in healthy volunteers [31] and various patient populations [37, 96]. MOLLI has an advantage over LL, as this sequence acquires images in a fixed phase of the cardiac cycle. In addition, the TI can be much longer with MOLLI than with LL, which allows for full recovery of longitudinal magnetization. With MOLLI, similar contours of epicardial and endocardial myocardium can be drawn for each image, thus facilitating automatic registration of corresponding areas of different images. The

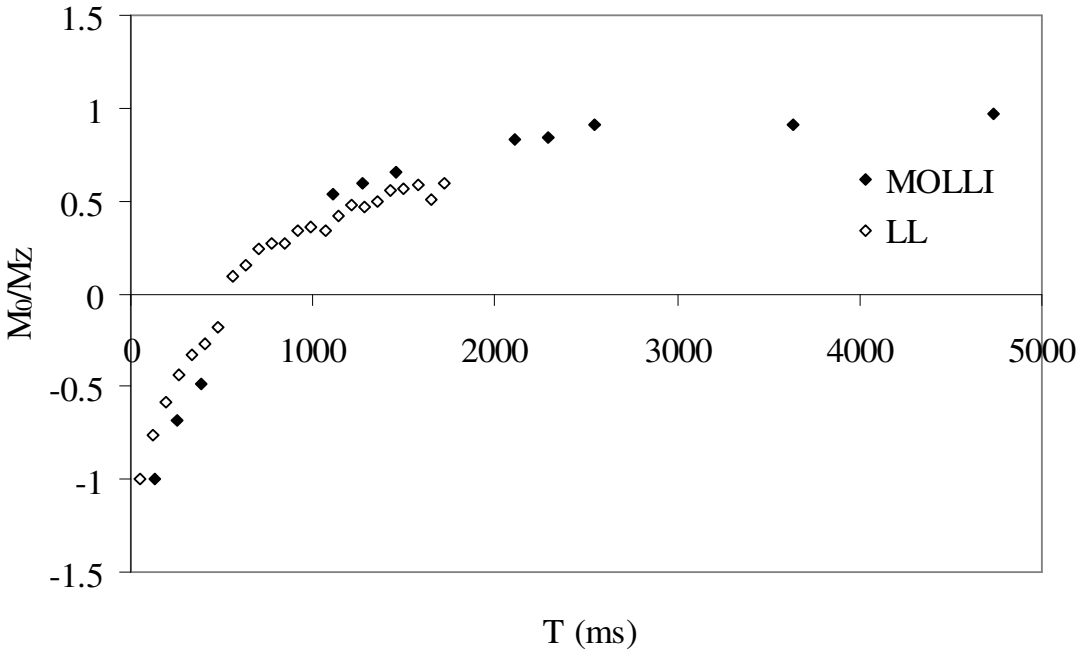

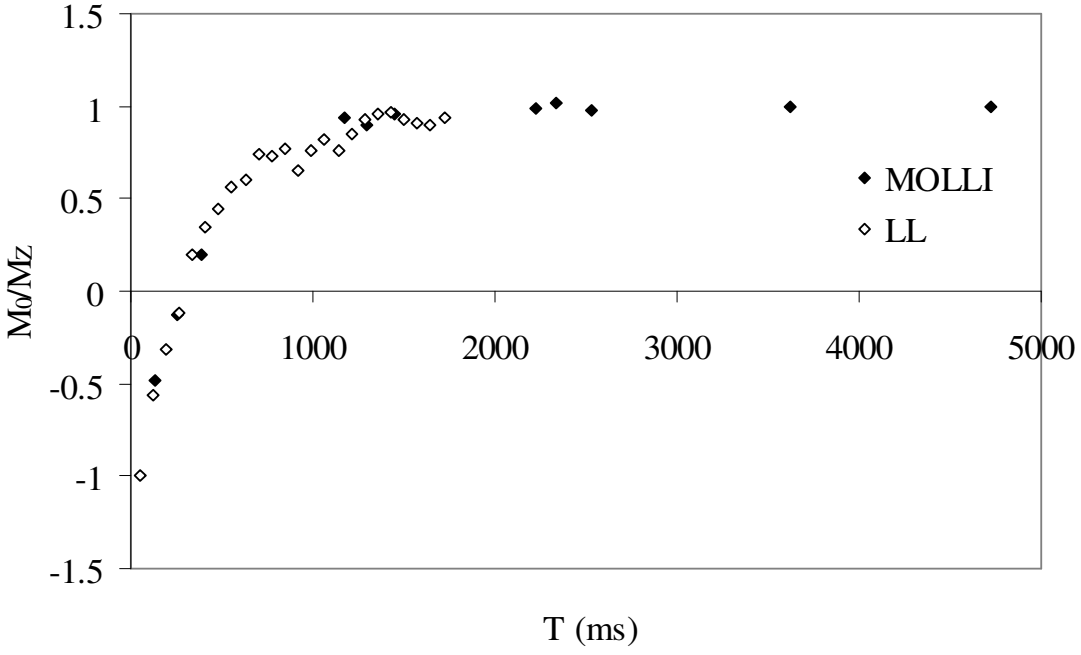

Figure 4-11: Curves of precontrast (upper) and postcontrast (bottom) myocardial T1 recovery with MOLLI and LL from a patient with HCM (HR = 65 bpm)

acquisition window for MOLLI can be set for the most quiescent stage (end-diastole) of the cardiac cycle, which reduces artifacts from cardiac motion.

Previous studies have demonstrated differences between MOLLI and LL for precontrast and postcontrast images [95, 97]. In a recent study of MOLLI and LL sequences used in imaging healthy volunteers [95], precontrast results showed that myocardial T1 values with MOLLI were longer than those with LL, results similar to those obtained in this study. Postcontrast results showed longer T1 values with LL than with MOLLI [95]; however, our results showed good agreement between MOLLI and LL sequences for postcontrast measurements in patients with normal LV. There are several potential reasons for these differences. The longest TI for LL in the previous study [95] was approximately 800 ms, whereas our longest TI for LL was approximately 1720 ms. Postcontrast myocardial T1 values can range from 300 to 600 ms depending on the timing of the postcontrast injection; for values longer than 300 ms, TI should be longer than 1500 ms to allow for full recovery of longitudinal magnetization. A multiethnic study of atherosclerosis showed good agreement between MOLLI and LL for postcontrast myocardial T1 values after correction of MOLLI for postcontrast time [97].

In our study, the MOLLI and LL sequences agreed more closely for controls than for patients with ICM or HCM. For precontrast measurements, the scarred myocardium showed longer T1 values than remote areas, and the difference between values obtained with MOLLI and LL was more significant. For postcontrast measurements, the scarred myocardium showed shorter T1 values than remote regions; the T1 values obtained with LL in scarred tissue were longer than those obtained with MOLLI.

Several previous studies have demonstrated T1 changes in diseased myocardium. In patients with chronic ischemic heart disease, T1 was found to be significantly shorter in scarred tissue than in viable tissue 2 to 50 minutes after contrast with LL [54]. However, there was no obvious difference between scarred and viable myocardium in precontrast T1 values obtained with LL, suggesting that normal and ischemic myocardium cannot be differentiated based on precontrast T1 values with LL. However, the precontrast T1 values in this study were much shorter than those found in other studies that used MOLLI [45] and LL [53]; these studies reported precontrast T1 values of approximately 1000 ms for normal myocardium. In another study, the precontrast T1 value in infarcted areas (1060 ± 61 ms) was higher than the T1 value in remote areas (987 ± 34 ms) with MOLLI, but this difference in T1 was not enough to differentiate chronic infarction areas from normal tissue [39]. Another study demonstrated a prolonged T1 value in patients with HCM (1208 ± 47 ms) at 3T compared with T1 in healthy controls (1172 ± 45 ms) [98].

In our study, there was a consistent trend toward longer precontrast T1 values for patients with ICM or HCM compared with controls. Precontrast T1 values obtained with LL were not significantly different among the 3 groups, whereas with MOLLI, pre-contrast T1 values were elevated significantly in patients with ICM (1083 ± 136 ms) and those with HCM (1029 ± 44 ms) versus controls (983 ± 48 ms). The reasons for this increase in T1 values with MOLLI in patients with ICM or HCM are unclear. Complex physical and biochemical changes during the pathological process could result in differences between diseased heart muscle and normal myocardium in the local magnetic field [99], leading to changes in local T1 values [100]. Increased myocardial T1 values in

patients with HCM may be caused by the development of diffuse fibrosis with increased collagen volume fraction. For patients with ICM, T1 elevation may be related to contractile function impairment of the scarred myocardium; T1 values are increased in hypokinetic and akinetic segments at 3T [101] .

Our study had several limitations. Several patients with HCM or ICM were injected with a single dose of contrast agent because of impaired kidney function; additionally, the postcontrast time for controls was shorter than for patients with HCM or ICM. The postcontrast T1 values were therefore not completely comparable among these groups. Only 2 short-axis slices were acquired with T1 mapping techniques, so some slices with scar on delayed enhancement images may have been missed on T1 mapping scans. Motion artifacts may have been more common in patients than in normal volunteers, as patients may have had arrhythmia or may not have been able to hold their breath as well as normal volunteers. In cases of infarcted heart, there was regional myocardial wall remodeling, leading to differences in motion pattern across the whole myocardium. Additionally, despite the advantages of the MOLLI sequence, the accuracy of quantitative pixel-by-pixel T1 estimation is compromised by several limitations, such as the single-shot acquisition method and the requirement for myocardial motion registration among frames.

4.5 Conclusion

In conclusion, the MOLLI sequence showed better agreement with the reference T1 measurement technique (IR-TSE) than did the LL sequence in both phantom and patient experiments. Although there were no obvious T1 changes between normal and diseased myocardium with LL, precontrast T1 values with MOLLI showed a consistent increase in patients with ICM or HCM compared with controls.

CHAPTER V

VALIDATION AND QUANTIFICATION OF DIFFUSE MYOCARDIAL FIBROSIS WITH T1 MAPPING AND LEFT VENTRICULAR BIOPSY

5.1 Introduction

Myocardial fibrosis has been shown to play an important role in the development and progression of systolic and diastolic cardiac failure, and is frequently seen in all forms of heart disease, including nonischemic, hypertensive, and diabetic heart disease [102-105]. Regardless of the cause of cardiomyopathy, increasing myocardial fibrosis has been shown to correlate with progressive deterioration of myocardial function [106-108]. Evaluating the extent of myocardial fibrosis may also help to predict progression to LV dilation and dysfunction in patients with valvular heart disease, which may impact decision making regarding when to send patients for surgery [109]. Furthermore, diffuse fibrosis is treatable; noninvasively evaluating therapy management is desirable to follow changes in the myocardium over time.

Although delayed contrast enhancement sequences on MRI are widely utilized for assessing regional myocardial fibrosis/scarring due to ischemic heart disease [11], this

relies on the relative difference in signal intensity between scarred and the presumed normal adjacent myocardium to generate image contrast. However, the collagen deposition is mostly diffuse in nonischemic cardiomyopathy. DE MRI can not detect the diffuse fibrosis because this technique relies on the difference in gadolinium washout kinetics between the remote and abnormal myocardium. T1 mapping technique allows the objectively showing the difference across normal and diseased tissues and has the advantage over DE MRI by circumventing the need to null the relative normal myocardium. ECV based on T1 mapping is a physiological parameter showing the extent of diffuse fibrosis intuitively.

Prior human studies have evaluated alterations in T1 relaxation due to fibrosis with T1 mapping methods [3, 42, 46, 48, 109]. Null point on DE MRI which is related with postcontrast T1 value was used as index of diffuse fibrosis [110]. This index showed shorter value in dilated cardiomyopathy and hypertrophic cardiomyopahty than controls. Iles et al [3] employed the postcontrast myocardial T1 time obtained with VAST sequence as an index of diffuse fibrosis. Postcontrast myocardial T1 times were shorter in nine heart failure patients than controls and correlated histologically collagen content on right ventricular endomyocardial biopsy. However, global T1 times were correlated to only right ventricular endomyocardial biopsy in nine special patients who had undergone heart transplant. Global postcontrast T1 values with LL were also inversely correlated with endomyocardial biopsy from right ventricle in patients with cardiomyopathy [111]. Both studies did not correlate the sites where the tissue samples were taken with the exactly regional T1 values. They may make an assumption that the diffuse myocardial fibrosis is homogenous across the myocardium and the globe T1 value can represent the

regional T1 value, while this assumption has not been validated which gave some uncertainty to this study. Iles et al [3] used VAST which is a 2D fast gradient echo sequence with variable sampling of k-space after inversion recovery prepared, which has not been well validated in the literature. Therefore, it is still unclear if the correlation found in this small group of patients represents a true histological correlation. Flett et al [29] validated equilibrium contrast CMRI (EQ–CMRI) to quantify diffuse myocardial fibrosis against the current gold standard of surgical myocardial biopsy collagen volume fraction (CVF) quantification in patients with aortic stenosis and hypertrophic cardiomyopathy. The calculated myocardial contrast volume of distribution (Vd (m)) correlated with biopsy histological analysis. However, these data are preliminary and have to be confirmed in larger and different cardiomyopathy populations. Furthermore, this method imposes a more complex image acquisition protocol that questions its applicability in the routine clinical workflow.

The purpose of this study is to validate the use of high-resolution T1 mapping with MOLLI to quantify extracellular volume (ECV) in areas of diffuse fibrosis against human operative myocardial biopsy in patients with HCM.

5.2 Materials and Methods

5.2.1 Patient Population

18 patients with hypertrophic cardiomyopathy were recruited. Height, weight, creatinine, glomerular filtration rate (GFR), heart rate, and contrast dose were recorded. The study was approved by the local ethics committee, and all subjects gave written informed consent.

5.2.2 Imaging Procedure

Subjects underwent MRI examinations using 1.5 T Achieva MR Systems (Philips Medical Systems, The Netherlands) with a prototype 32-channel coil (Invivo, USA) with a phased-array cardiac coil. MOLLI sequences were performed at end-diastole (ED) to minimize the cardiac motion, during the cardiac cycle at 2-3 short-axis levels (basal, middle and apical cavity). Data acquisition consists of a single-slice, single-shot, balanced fast-field echo (bFFE) pulse sequence combined with SENSE with a reduction factor of 2, number of lines of k-space (TFE factor) = 49, dummy acquisitions =13, partial Fourier acquisition, flip angle = 35°, repetition time (TR) = 3.9 ms, echo time (TE) = 1.95 ms, field of view (FOV) = 380 ×342 mm^2, matrix = 240 ×151, measured pixel size = 1.9 ×2.3 mm^2, slice thickness = 10 mm, and acquisition window = 191.1 ms. The MOLLI sequences were performed within in one breath hold (approximately 11 seconds depending on patients' heart rate).

For delayed enhanced CMRI, gadopentetate dimeglumine (Magnevist; Schering, Berlin, Germany) was administered at a dose of 0.15 mmol per kilogram of body weight at an injection rate of 2 mL/s, followed by a 20- to 30-mL saline flush through a 20-gauge

cannula placed in an antecubital vein. MOLLI pulse sequences were performed before and about (15 – 20 minutes) after gadolinium administration.

5.2.3 Histology

Blood specimens were acquired when the IV is placed for the MRI study. The specimens will be stored in the Prevention Research Laboratory. Hematocrit of each patient was determined from blood specimen in Cleveland Clinic Main Laboratory.

At the time of open heart surgery, the surgeon took myectomy biopsy from distal anterior wall. The tissue samples were fixed immediately in 10% buffered formalin, embedded in paraffin, routinely processed, and stained with picrosirius red and Mason trichrome to differentiate between myocardium and fibrotic areas. The tissue specimens were cut into 8 μm thick sections using a microtome. Slides were imaged at high magnification (x40) using the Aperio ScanScope digital scanner and visualized using VisionScope V10 (Aperio Technologies). A positive pixel count algorithm was applied to analyze the area and intensity of a given stain. A color deconvolution algorithm was applied to separate the image into two or three channels each corresponding to a different color in order to allow accurate measurement of the area and intensity of each color individually even where stains were superimposed. Collagen was quantified as the percentage of total endomyocardial area using Aperio software by a cardiologist. For each patient, the number of slides was different. Histology analysis was performed by Dr. Patrick Collier and then presented to the author of this dissertation.

5.2.4 Image Analysis

Regional T1 values and global T1 values from the entire myocardium, blood T1 values were obtained using cvi42 (Circle Cardiovascular Imaging Inc., Calgary, AB, Canada) to obtain the mean T1 value using curve fitting. T1 values were further processed to calculate extracellular volume fraction (ECV) using the following equations [112]. The concentration of contrast agent (CA) is directly related to the difference between the difference between precontrast and postcontrast reciprocal values of T1 (ΔR1):

$$\Delta R1 = \gamma C_{CA} = \left(\frac{1}{T1}\right)_{post} - \left(\frac{1}{T1}\right)_{pret} \tag{5.1}$$

Where γ is defined as the relaxivity of the contrast agent.

The partition coefficient for contrast agent in myocardium and blood is defined as:

$$\lambda = \frac{\Delta R1_{myocardium}}{\Delta R1_{blood}} \tag{5.2}$$

Assuming steady state between myocardium and blood, ECV and ΔR1 are related as follows:

$$\frac{ECV_{myocardium}}{\Delta R1_{myocardium}} = \frac{ECV_{blood}}{\Delta R1_{blood}} \tag{5.3}$$

The ECV of blood can be quantified as follows:

$$ECV_{blood} = 1 - hematocrit \tag{5.4}$$

Therefore, myocardial ECV can be calculated as follows:

$$ECV_{myocardium} = ECV_{blood} \times \left(\frac{1}{T1_{myocardium,post}} - \frac{1}{T1_{myocardium,pret}} \right) / \left(\frac{1}{T1_{blood,post}} - \frac{1}{T1_{blood,pret}} \right) \tag{5.5}$$

5.2.5 Statistical Analysis

All CMR data and histological images were analyzed in a blinded fashion. The correlation between the two classes of analysis was assessed using Pearson's test. $P<0.05$ was considered statistical significant. Statistical analysis was performed using SPSS version 14 (SPSS, Inc, Chicago, IL).

5.3 Results

5.3.1 Histological Biopsy Evaluation

The histological collagen volume fraction was from 0.3% to 36.9% in patients with HCM. Table 5-1 showed collagen volume fraction (CVF) quantified using Aperio software from a cardiologist. Figure 5-1 showed three representative slides with minimal,

moderate and more extensive interstitial fibrosis from left to right. Sections with collagen are yellow and myocytes appearing red.

Table 5-1: Histological analyses compared with ECV from T1 measurements

Patient	CVF from Aperio	Hematocrit	ECV from			
			Basal Anteroseptal	Basal Global	Middle Anteroseptal	Middle Global
1	3.0%	31.9	25.6%	27.1%	25.6%	31.7%
2	0.5%	37.3	23.0%	26.3%	23.0%	24.5%
3	2.8%	36.0	35.3%	33.7%	27.1%	26.4%
4	3.7%	36.6	23.8%	25.9%	25.5%	27.0%
5	4.0%	37.7	42.3%	29.8%	24.8%	26.5%
6	3.5%	46.5	24.4%	24.0%	20.0%	21.2%
7	3.0%	44.6	N/A	N/A	27.4%	28.6%
8	8.1%	46.6	20.0%	25.6%	25.6%	24.9%
9	3.9%	37.6	N/A	N/A	24.3%	22.9%
10	4.2%	42.5	26.1%	25.4%	25.5%	26.8%
11	0.3%	44.3	N/A	N/A	20.7%	21.3%
12	1.4%	43.7	25.6%	28.1%	27.5%	27.0%
13	1.8%	40.8	26.8%	26.1%	22.1%	22.8%
14	0.5%	43.7	31.6%	25.2%	25.1%	23.2%
15	3.7%	38.0	24.6%	26.2%	26.8%	28.0%
16	36.9%	38.7	40.7%	40.9%	41.9%	41.3%
17	6.5%	38.9	31.6%	30.2%	32.2%	32.5%
18	7.7%	42.2	34.5%	34.1%	34.8%	34.2%

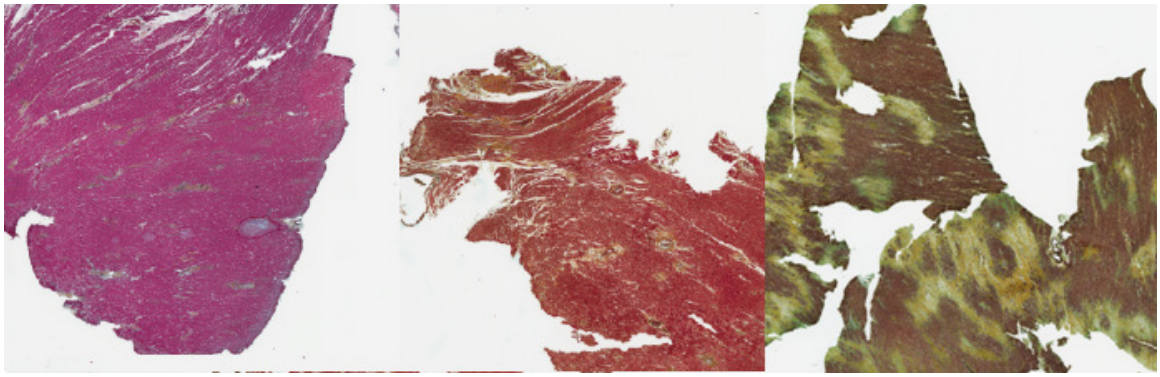

Figure 5-1: Histological images (images provided by Dr. Patrick Collier)

5.3.2 Noninvasive In Vivo MRI Measurement of Fibrosis

In this validation study, fibrosis was quantified in the anteroseptal wall of basal and middle, also global mean T1 value of the basal and middle slice. The basal anteroseptal area is missed in three patients because of the cardiac motion during the image acquisation. ECV was calculated based on the precontrast and postcontrast blood and myocardial T1 values. Four sets of ECV representing results from regional and global analyses of basal and middle slices were correlated with histological results. Figure 5-2 shows the best correlation obtained with anteroseptal region of middle slice. The coefficients are shown in Table 5-2.

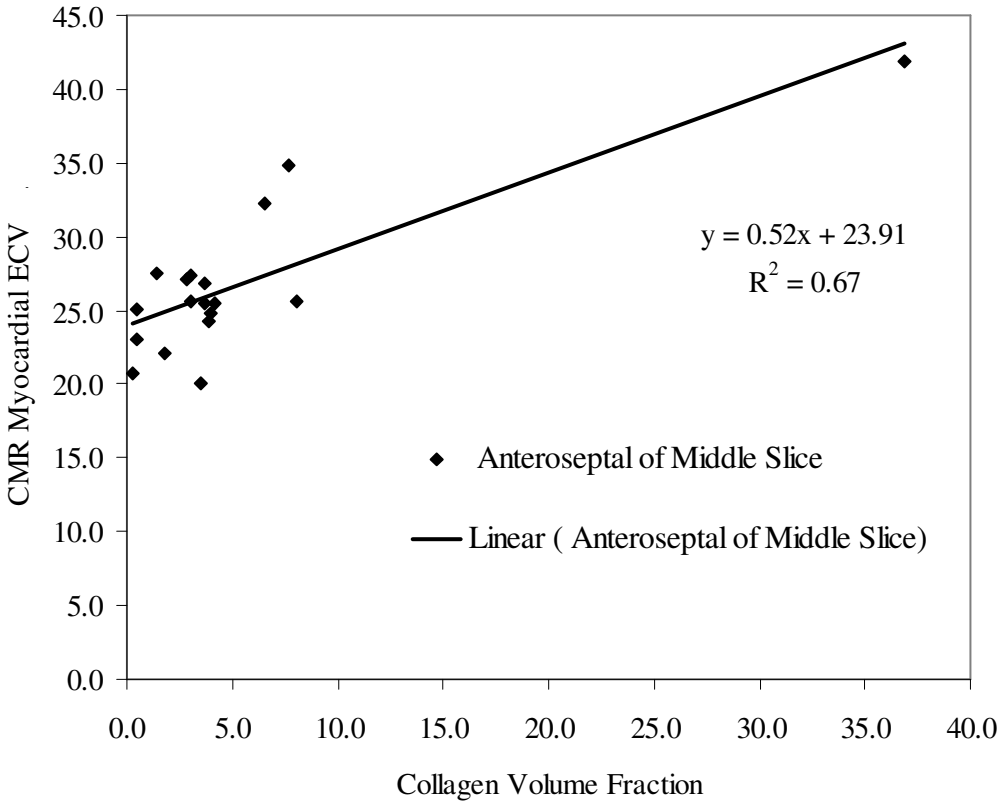

Figure 5-2:Relationship of ECV on MRI and collagen volume fraction of histological analysis

Table 5-2: Statistical correlation of histological analyses and CMRI

Analysis	**R Square**	**Pearson Coefficient**	**P Value**
Regional Basal	0.23	0.36	<0.001
Global Basal	0.61	0.40	<0.001
Regional Middle	0.67	0.52	<0.001
Global Middle	0.60	0.48	<0.001

5.4 Discussion

Our results provide histological validation for the use of ECV based on T1 mapping to noninvasively assess interstitial myocardial fibrosis in patients with hypertrophic cardiomyopathy. Higher ECV was associated with a greater degree of histologically defined interstitial fibrosis. Our current results are in agreement with previous findings related with ECV measurements with or without histology validation.

ECV calculated for normal volunteers with LL incorporating a pharmacokinetic model shows a range of 18.8%-38.0% [31]. Schelbert et al [66] calculated ECV in normal volunteer with MOLLI were in the range of 19.3%-29.2% and 18.4%-29.1% using contrast agent injection with infusion and bolus, respectively. ECV calculation with MOLLI was also performed in patients with myocardial infarction and nonischemic cardiopathy [94]. ECV was 51 ± 8% in patients with myocardial infarction which was much higher than the atypical late enhancement areas in nonischemic cardiomyopathy (37 ± 6%) and "normal appearing" myocardium (36 ± 3%). In only one study at 3 T, the mean ECV values calculated with MOLLI are 26.7 ± 1.0% for normal human subjects, which agrees well with the ECV values in normal volunteers at 1.5 T. Therefore, the normal ECV appears to approximately 25% or less. Our ECV calculated with MOLLI in patients with hypertrophic cardiomyopathy are from 20.0% - 42.3% (27.8% ± 5.4%), which means the diffuse fibrosis is not severe in most of the patients.

There has been limited previous quantitative validation of ECV based on T1 measurement methods with histopathologically demonstrated fibrosis in myectomy specimen. In only one previous report, ECV values from 18 patients with aortic stenosis

(R^2 = 0.86, Kendall Tau coefficient = 0.71) and 8 hypertrophic cardiomyopathy (R^2= 0.62, Kendall Tau coefficient = 0.52) were correlated with biopsies from LV [29]. However, the T1 mapping method in this study was not widely used in a diverse population with cardiomyopathy, and the EQ-CMR technique is complex and therefore is not easily to be added in clinical workflow. Our correlation ((R^2= 0.67, Pearson coefficient = 0.52) is comparable with this previous study although the correlation for patients with HCM in both our study and study of Flett et al [29] is not as strong as for patients with aortic stenosis, this may be due to the less diffuse nature of the fibrosis in hypertrophic cardiomyopathy [29]. We noticed the histological CVF in Flett et al [29] study were 6% to 39.38% in patients with aortic stenosis and 10.4%-30.6% in patients with hypertrophic cardiomyopathy, and were 0.3%-36.9% in our study. The histological CVF is generally lower than the ECV calculated from T1 values, which may be due to two reasons: 1) the CVF is quantified after fixation process; 2) ECV may include other extracellur matrix expansion beside collagen. In our study, the correlation of regional ECV from middle slice is better than basal slice. This may be due to the more motion at the basal slice than middle slice, and the blood ejected out from LV out tract causing artifacts on the T1 weighted images. Even the best correlation we saw in this study is not strong. Firstly, this is thought to be related with less diffuse nature of fibrosis in patients with HCM. Secondly, sample size of biopsy may be too small and three patients only have 1 slide although there are up to 3 slides for other patients. Thirdly, the precontrast blood T1 value is very long and has big standard deviation which can cause error for the ECV calculation. Finally, the image quality is impaired for patients not breath-holding well, with larger size and arrhythmia.

Although our study improved the understandings about the future clinical application of T1 mapping and ECV, there are still several limitations. Firstly, the T1 values were affected by several factors, such as changing heart rate of patients, cardiac motions causing the need for co-registration of images. Secondly, the range of ECV for patients and normal volunteers overlapped making it difficult to find the right cutoff value to differentiate the normal and diseased tissue. ECV calculation only correcting blood fraction with hematocrit, however, there are patients' specific factors (eg, glomerular filtration rates, gadolinium dose, postcontrast time) were not correct. Also the ECV of normal volunteers calculated based on T1 measurements with LL showed a wide range from 18.8% to 38.0% [31], which gives difficulty in cutting the edge of diseased and normal myocardium. Finally, the number of patients recruited is not big enough; more patients are needed to avoid the bias.

5.5 Conclusion

In conclusion, noninvasive assessment of myocardial ECV correlates moderately with interstitial fibrosis as assessed by means of invasive biopsy in patients with hypertrophic cardiomyopathy in our study. Further investigation is required to determine whether this measure can effectively guide clinical intervention and improve morbidity and mortality of patients with heart failure. Although more work needs to be done on the robustness of the technique, this technique shows promise in the quantitative evaluation

of diffuse myocardial fibrosis, and hence may have potential applications with DE MRI in heart failure, cardiomyopathy, and valvular heart disease.

CHAPTER VI

CONCLUSION AND FUTURE RESEARCH

6.1 Conclusion

Clinical validation of MRI sequences is the final and also the most important point to realize the application of the sequences in clinical application. Therefore, while T1 mapping is a promising tool to assess myocardial fibrosis when combined with DE MRI, further validation is necessary to realize the clinical application in the context of myocardial assessment in patient with suspected cardiomyopathy.

In the current thesis project, we evaluated several aspects of T1 mapping methods which were incompletely understood. Firstly, variation of myocardial T1 at 1.5 T was assessed at three time points within the cardiac cycle in healthy volunteers and patients without myocardial disease. Our results showed that although the variation is statistically significant among the different time points, the variation is less than 39 ms which is within the standard deviation of the myocardial T1 mapping technique. Therefore, we feel that this difference can not be considered clinically significant.

Secondly, a quantitative evaluation of T1 measurement with DFA based on 3D FFE with B1 correction was established and compared with gold standard method. The accuracy of T1 measurement was increased with incorporating B1 information, which supported the errorrous T1 measurements without B1 correction in the study showing severe drop of myocardial T1 value from ES to ED.

Thirdly, the two different myocardial T1 mapping techniques were compared in 3 patient groups precontrast and postcontrast to examine the difference and agreement between the techniques. These results gave guidance to interpret the clinical finding when comparing the interstudy results with MOLLI or LL.

Finally, the T1 mapping technique was applied in a group of patients with diffuse myocardial fibrosis eligible for myectomy surgery. Precontrast and postcontrast myocardial and blood T1 values were assessed to identify and quantify myocardial fibrosis, with subsequent histological validation based on LV biopsies. Our results showed positive correlation of histolocial fibrosis with ECV calculated from T1 mapping technique. Although the correlation coefficient is not strong, it showed the trend between the noninvasive and invasive methods. Larger group of patients and in multicenter settings clinical studies are needed to realize its clinical applications.

6.2 Future Research

6.2.1 3D DFA with B1 Correction in Human Studies

Optimization the method to ensure effective gradient spoiling and a steady state condition needs to be developed to meet the limitation of the acquisition time by increasing the duration of the crusher gradients (increased dephasing of transverse spin components) and applying a sufficient number of dummy excitations. Using cardiac triggering to acquire T1-weighted images at defined cardiac cycle in human subjects is necessary to realize the clinical application of DFA method.

6.2.2 Motion Registration of T1 Mapping Technique

Patient movement can result in the slices being substantially different in appearance although the same slice was selected, such as the anterosepatl region missing often at basal slice. Automatic motion registration to post processing T1-weighted images should be employed to improve the accuracy of T1 measurement and therefore ECV calculation.

6.2.3 Correct the Factors Affecting ECV Calculation

Besides the hematocrit, there are also several factors may affect the accuracy of ECV calculation, such as contrast agent dose, glomerular filtration rate, postcontrast injection time. It is necessary to incorporating these factors to further optimize this method. Further investigation is required to determine whether this measure can effectively guide clinical intervention and improve morbidity and mortality of patients with heart failure.

6.2.4 ECV Applications in 3 T and Cardiomyopathies

ECV can be applied to 3 T studies to evaluate whether it will be more sensitive than 1.5 T. Although more work needs to be done on the robustness of the technique, this technique may have potentially wide applications in heart failure, cardiomyopathy, and valvular heart disease to follow the changes of myocardium noninvasively. Longitudinal imaging of such changes could be applied to individualization of therapy by assessing treatment response in a given patient, and to the evaluation of prospective therapies for heart failure.

REFERENCES

1. Heidenreich PA, Trogdon JG, Khavjou OA, Butler J, Dracup K, Ezekowitz MD, Finkelstein EA, Hong Y, Johnston SC, Khera A, Lloyd-Jones DM, Nelson SA, Nichol G, Orenstein D, Wilson PW, Woo YJ, American Heart Association Advocacy Coordinating Committee, Stroke Council, Council on Cardiovascular Radiology and Intervention, Council on Clinical Cardiology, Council on Epidemiology and Prevention, Council on Arteriosclerosis, Thrombosis and Vascular Biology, Council on Cardiopulmonary, Critical Care, Perioperative and Resuscitation, Council on Cardiovascular Nursing, Council on the Kidney in Cardiovascular Disease, Council on Cardiovascular Surgery and Anesthesia, and Interdisciplinary Council on Quality of Care and Outcomes Research. "Forecasting the future of cardiovascular disease in the united states: A policy statement from the american heart association,"Circulation 2011;123(8):933-44.

2. White JA, Patel MR. "The role of cardiovascular MRI in heart failure and the cardiomyopathies,"Cardiol Clin 2007;25(1):71,95, vi.

3. Iles L, Pfluger H, Phrommintikul A, Cherayath J, Aksit P, Gupta SN, Kaye DM, Taylor AJ. "Evaluation of diffuse myocardial fibrosis in heart failure with cardiac magnetic resonance contrast-enhanced T1 mapping,"J Am Coll Cardiol 2008;52(19):1574-80.

4. To AC, Desai MY. "Role of cardiac magnetic resonance imaging in assessing ischemic and nonischemic cardiomyopathies,"Expert Rev Cardiovasc Ther 2012;10(2):223-33.

5. Brigden W. "Uncommon myocardial diseases; the non-coronary cardiomyopathies,"Lancet 1957;273:1179-83.

6. Richardson P, McKenna W, Bristow M, Maisch B, Mautner B, O'Connell J, Olsen E, Thiene G, Goodwin J, Gyarfas I, Martin I, Nordet P. "Report of the 1995 world health Organization/International society and federation of cardiology task force on the definition and classification of cardiomyopathies,"Circulation 1996;93(5):841-2.

7. Maron BJ, Towbin JA, Thiene G, Antzelevitch C, Corrado D, Arnett D, Moss AJ, Seidman CE, Young JB, American Heart Association, Council on Clinical Cardiology, Heart Failure and Transplantation Committee, Quality of Care and Outcomes Research and Functional Genomics and Translational Biology Interdisciplinary Working Groups, Council on Epidemiology and Prevention. "Contemporary definitions and classification of the cardiomyopathies: An american heart association scientific statement from the council on clinical cardiology, heart failure and transplantation committee; quality of care and outcomes research and functional genomics and translational biology interdisciplinary working groups; and council on epidemiology and prevention,"Circulation 2006;113(14):1807-16.

8. Karamitsos TD, Francis JM, Myerson S, Selvanayagam JB, Neubauer S. "The role of cardiovascular magnetic resonance imaging in heart failure,"J Am Coll Cardiol 2009;54(15):1407-24.

9. Lima JA. "Myocardial viability assessment by contrast-enhanced magnetic resonance imaging,"J Am Coll Cardiol 2003;42(5):902-4.

10. Amado LC, Gerber BL, Gupta SN, Rettmann DW, Szarf G, Schock R, Nasir K, Kraitchman DL, Lima JA. "Accurate and objective infarct sizing by contrast-enhanced magnetic resonance imaging in a canine myocardial infarction model,"J Am Coll Cardiol 2004;44(12):2383-9.

11. Kim RJ, Wu E, Rafael A, Chen EL, Parker MA, Simonetti O, Klocke FJ, Bonow RO, Judd RM. "The use of contrast-enhanced magnetic resonance imaging to identify reversible myocardial dysfunction,"N Engl J Med 2000;343(20):1445-53.

12. Kim HW, Farzaneh-Far A, Kim RJ. "Cardiovascular magnetic resonance in patients with myocardial infarction: Current and emerging applications,"J Am Coll Cardiol 2009;55(1):1-16.

13. McCrohon JA, Moon JC, Prasad SK, McKenna WJ, Lorenz CH, Coats AJ, Pennell DJ. "Differentiation of heart failure related to dilated cardiomyopathy and coronary artery disease using gadolinium-enhanced cardiovascular magnetic resonance,"Circulation 2003;108(1):54-9.

14. Kim RJ, Albert TS, Wible JH, Elliott MD, Allen JC, Lee JC, Parker M, Napoli A, Judd RM, Gadoversetamide Myocardial Infarction Imaging Investigators. "Performance of delayed-enhancement magnetic resonance imaging with gadoversetamide contrast for the detection and assessment of myocardial infarction: An international, multicenter, double-blinded, randomized trial,"Circulation 2008;117(5):629-37.

15. Mahrholdt H, Wagner A, Judd RM, Sechtem U, Kim RJ. "Delayed enhancement cardiovascular magnetic resonance assessment of non-ischaemic cardiomyopathies,"Eur Heart J 2005;26(15):1461-74.

16. http://www.radiologyassistant.nl/en/4a3ff48cccc37.

17. Jackson E, Bellenger N, Seddon M, Harden S, Peebles C. "Ischaemic and non-ischaemic cardiomyopathies--cardiac MRI appearances with delayed enhancement,"Clin Radiol 2007;62(5):395-403.

18. Van Hoe L, Vanderheyden M. "Ischemic cardiomyopathy: Value of different MRI techniques for prediction of functional recovery after revascularization,"AJR Am J Roentgenol 2004;182(1):95-100.

19. Choudhury L, Mahrholdt H, Wagner A, Choi KM, Elliott MD, Klocke FJ, Bonow RO, Judd RM, Kim RJ. "Myocardial scarring in asymptomatic or mildly symptomatic patients with hypertrophic cardiomyopathy,"J Am Coll Cardiol 2002;40(12):2156-64.

20. Moon JC, McKenna WJ, McCrohon JA, Elliott PM, Smith GC, Pennell DJ. "Toward clinical risk assessment in hypertrophic cardiomyopathy with gadolinium cardiovascular magnetic resonance,"J Am Coll Cardiol 2003;41(9):1561-7.

21. Moon JC, Reed E, Sheppard MN, Elkington AG, Ho SY, Burke M, Petrou M, Pennell DJ. "The histologic basis of late gadolinium enhancement cardiovascular magnetic resonance in hypertrophic cardiomyopathy,"J Am Coll Cardiol 2004;43(12):2260-4.

22. Flamm SD, Villareal RP, Hariharan R, Muthupillai R, Massumi AG, Wilson JM. "Delayed-enhancement MRI revearls myocardial fibrosis in patients with symptomatic hypertrophic cardiomyopathy,"Proc Intl Soc Mag Reson Med 2001;9.

23. Assomull RG, Prasad SK, Lyne J, Smith G, Burman ED, Khan M, Sheppard MN, Poole-Wilson PA, Pennell DJ. "Cardiovascular magnetic resonance, fibrosis, and prognosis in dilated cardiomyopathy,"J Am Coll Cardiol 2006;48(10):1977-85.

24. Iles L, Pfluger H, Lefkovits L, Butler MJ, Kistler PM, Kaye DM, Taylor AJ. "Myocardial fibrosis predicts appropriate device therapy in patients with implantable cardioverter-defibrillators for primary prevention of sudden cardiac death,"J Am Coll Cardiol 2011;57(7):821-8.

25. Deshpande A, Pakkal M, Agrawal B, Raj V. "Cardiac magnetic resonance imaging of non-ischaemic cardiomyopathy,"Postgrad Med J 2012;88(1035):38-48.

26. Mewton N, Liu CY, Croisille P, Bluemke D, Lima JA. "Assessment of myocardial fibrosis with cardiovascular magnetic resonance,"J Am Coll Cardiol 2011;57(8):891-903.

27. Jellis C, Martin J, Narula J, Marwick TH. "Assessment of nonischemic myocardial fibrosis,"J Am Coll Cardiol 2010;56(2):89-97.

28. Leong DP, Madsen PL, Selvanayagam JB. "Non-invasive evaluation of myocardial fibrosis: Implications for the clinician,"Heart 2010;96(24):2016-24.

29. Flett AS, Hayward MP, Ashworth MT, Hansen MS, Taylor AM, Elliott PM, McGregor C, Moon JC. "Equilibrium contrast cardiovascular magnetic resonance for the measurement of diffuse myocardial fibrosis: Preliminary validation in humans,"Circulation 2010;122(2):138-44.

30. Becker AE, Heijmans CD, Essed CE. "Chronic non-ischaemic congestive heart disease and endomyocardial biopsies. worth the extra?"Eur Heart J 1991;12(2):218-23.

31. Gai N, Turkbey EB, Nazarian S, van der Geest RJ, Liu CY, Lima JA, Bluemke DA. "T1 mapping of the gadolinium-enhanced myocardium: Adjustment for factors affecting interpatient comparison,"Magn Reson Med 2011;65(5):1407-15.

32. Lima JA, Judd RM, Bazille A, Schulman SP, Atalar E, Zerhouni EA. "Regional heterogeneity of human myocardial infarcts demonstrated by contrast-enhanced MRI. potential mechanisms,"Circulation 1995;92(5):1117-25.

33. Kim RJ, Chen EL, Lima JA, Judd RM. "Myocardial gd-DTPA kinetics determine MRI contrast enhancement and reflect the extent and severity of myocardial injury after acute reperfused infarction,"Circulation 1996;94(12):3318-26.

34. Ingkanisorn WP, Rhoads KL, Aletras AH, Kellman P, Arai AE. "Gadolinium delayed enhancement cardiovascular magnetic resonance correlates with clinical measures of myocardial infarction,"J Am Coll Cardiol 2004;43(12):2253-9.

35. Pack NA, Dibella EV, Wilson BD, McGann CJ. "Quantitative myocardial distribution volume from dynamic contrast-enhanced MRI,"Magn Reson Imaging 2008;26(4):532-42.

36. Zannad F, Alla F, Dousset B, Perez A, Pitt B. "Limitation of excessive extracellular matrix turnover may contribute to survival benefit of spironolactone therapy in patients with congestive heart failure: Insights from the randomized aldactone evaluation study (RALES). rales investigators,"Circulation 2000;102(22):2700-6.

37. Broberg CS, Chugh SS, Conklin C, Sahn DJ, Jerosch-Herold M. "Quantification of diffuse myocardial fibrosis and its association with myocardial dysfunction in congenital heart disease,"Circ Cardiovasc Imaging 2010;3(6):727-34.

38. Goldfarb JW, Arnold S, Han J. "Recent myocardial infarction: Assessment with unenhanced T1-weighted MR imaging,"Radiology 2007;245(1):245-50.

39. Messroghli DR, Walters K, Plein S, Sparrow P, Friedrich MG, Ridgway JP, Sivananthan MU. "Myocardial T1 mapping: Application to patients with acute and chronic myocardial infarction,"Magn Reson Med 2007;58(1):34-40.

40. Krombach GA, Hahn C, Tomars M, Buecker A, Grawe A, Gunther RW, Kuhl HP. "Cardiac amyloidosis: MR imaging findings and T1 quantification, comparison with control subjects,"J Magn Reson Imaging 2007;25(6):1283-7.

41. Walker PM, Marie PY, Mezeray C, Bessieres M, Escanye JM, Karcher G, Danchin N, Mattei S, Villemot JP, Bertrand A. "Synchronized inversion recovery-spin echo sequences for precise in vivo T1 measurement of human myocardium: A pilot study on 22 healthy subjects,"Magn Reson Med 1993;29(5):637-41.

42. Messroghli DR, Niendorf T, Schulz-Menger J, Dietz R, Friedrich MG. "T1 mapping in patients with acute myocardial infarction,"J Cardiovasc Magn Reson 2003;5(2):353-9.

43. Higgins DM, Ridgway JP, Radjenovic A, Sivananthan UM, Smith MA. "T1 measurement using a short acquisition period for quantitative cardiac applications,"Med Phys 2005;32(6):1738-46.

44. Kaldoudi E, Williams SC. "Relaxation time measurements in NMR imaging part 1: Longitudinal relaxation time,"Concepts Magn Reson 1993;5:217-42.

45. Messroghli DR, Radjenovic A, Kozerke S, Higgins DM, Sivananthan MU, Ridgway JP. "Modified look-locker inversion recovery (MOLLI) for high-resolution T1 mapping of the heart,"Magn Reson Med 2004;52(1):141-6.

46. Messroghli DR, Plein S, Higgins DM, Walters K, Jones TR, Ridgway JP, Sivananthan MU. "Human myocardium: Single-breath-hold MR T1 mapping with high spatial resolution--reproducibility study,"Radiology 2006;238(3):1004-12.

47. Wansapura J, Gottliebson W, Crotty E, Fleck R. "Cyclic variation of T1 in the myocardium at 3 T,"Magn Reson Imaging 2006;24(7):889-93.

48. Messroghli DR, Greiser A, Frohlich M, Dietz R, Schulz-Menger J. "Optimization and validation of a fully-integrated pulse sequence for modified look-locker inversion-recovery (MOLLI) T1 mapping of the heart,"J Magn Reson Imaging 2007;26(4):1081-6.

49. Blume U, Lockie T, Stehning C, Sinclair S, Uribe S, Razavi R, Schaeffter T. "Interleaved T(1) and T(2) relaxation time mapping for cardiac applications,"J Magn Reson Imaging 2009;29(2):480-7.

50. Piechnik SK, Ferreira VM, Dall'Armellina E, Cochlin LE, Greiser A, Neubauer S, Robson MD. "Shortened modified look-locker inversion recovery (ShMOLLI) for clinical myocardial T1-mapping at 1.5 and 3 T within a 9 heartbeat breathhold,"J Cardiovasc Magn Reson 2010;12:69.

51. Elster, AD, Burdette, J, H. Questions & Answers in magnetic resonance imaging. 2001. 333.

52. Look D, Locker D. "Time saving in measurement of NMR and EPR relaxation times."Rev Sci Instrum 1970;41:250-1.

53. Flacke SJ, Fischer SE, Lorenz CH. "Measurement of the gadopentetate dimeglumine partition coefficient in human myocardium in vivo: Normal distribution and elevation in acute and chronic infarction,"Radiology 2001;218(3):703-10.

54. Klein C, Nekolla SG, Balbach T, Schnackenburg B, Nagel E, Fleck E, Schwaiger M. "The influence of myocardial blood flow and volume of distribution on late gd-DTPA kinetics in ischemic heart failure,"J Magn Reson Imaging 2004;20(4):588-93.

55. Amano Y, Takayama M, Kumita S. "Contrast-enhanced myocardial T1-weighted scout (look-locker) imaging for the detection of myocardial damages in hypertrophic cardiomyopathy,"J Magn Reson Imaging 2009;30(4):778-84.

56. Cerqueira MD, Weissman NJ, Dilsizian V, Jacobs AK, Kaul S, Laskey WK, Pennell DJ, Rumberger JA, Ryan T, Verani MS, American Heart Association Writing Group on Myocardial Segmentation and Registration for Cardiac Imaging. "Standardized myocardial segmentation and nomenclature for tomographic imaging of the heart. A statement for healthcare professionals from the cardiac imaging committee of the council on clinical cardiology of the american heart association,"Int J Cardiovasc Imaging 2002;18(1):539-42.

57. Kawel N, Nacif M, Zavodni A, Jones J, Liu S, Sibley CT, Bluemke DA. "T1 mapping of the myocardium: Intra-individual assessment of the effect of field strength, cardiac cycle and variation by myocardial region,"J Cardiovasc Magn Reson 2012;14(1):27.

58. Cheng A, Langer F, Rodriguez F, Criscione JC, Daughters GT, Miller DC, Ingels NB,Jr. "Transmural cardiac strains in the lateral wall of the ovine left ventricle,"Am J Physiol Heart Circ Physiol 2005;288(4):H1546-56.

59. LeGrice IJ, Takayama Y, Holmes JW, Covell JW. "Impaired subendocardial function in tachycardia-induced cardiac failure,"Am J Physiol 1995;268(5 Pt 2):H1788-94.

60. Rodriguez I, Ennis DB, Wen H. "Noninvasive measurement of myocardial tissue volume change during systolic contraction and diastolic relaxation in the canine left ventricle,"Magn Reson Med 2006;55(3):484-90.

61. Waldman LK, Fung YC, Covell JW. "Transmural myocardial deformation in the canine left ventricle. normal in vivo three-dimensional finite strains,"Circ Res 1985;57(1):152-63.

62. Feigl EO. "Coronary physiology,"Physiol Rev 1983;63(1):1-205.

63. Toyota E, Fujimoto K, Ogasawara Y, Kajita T, Shigeto F, Matsumoto T, Goto M, Kajiya F. "Dynamic changes in three-dimensional architecture and vascular volume of transmural coronary microvasculature between diastolic- and systolic-arrested rat hearts,"Circulation 2002;105(5):621-6.

64. Coolen BF, Geelen T, Paulis LE, Nauerth A, Nicolay K, Strijkers GJ. "Three-dimensional T1 mapping of the mouse heart using variable flip angle steady-state MR imaging,"NMR Biomed 2011;24(2):154-62.

65. Sung K, Nayak KS. "Measurement and characterization of RF nonuniformity over the heart at 3T using body coil transmission,"J Magn Reson Imaging 2008;27(3):643-8.

66. Schelbert EB, Testa SM, Meier CG, Ceyrolles WJ, Levenson JE, Blair AJ, Kellman P, Jones BL, Ludwig DR, Schwartzman D, Shroff SG, Wong TC. "Myocardial extravascular extracellular volume fraction measurement by gadolinium cardiovascular magnetic resonance in humans: Slow infusion versus bolus,"J Cardiovasc Magn Reson 2011;13:16.

67. Schar M, Vonken EJ, Stuber M. "Simultaneous B(0)- and B(1)+-map acquisition for fast localized shim, frequency, and RF power determination in the heart at 3 T,"Magn Reson Med 2010;63(2):419-26.

68. Schabel MC, Morrell GR. "Uncertainty in T(1) mapping using the variable flip angle method with two flip angles,"Phys Med Biol 2009;54(1):N1-8.

69. Christensen K, Grand D, Schulman EM, Walling C. "Optimal determination of relaxation times of fourier transform nuclear magnetic resonance. determination of spin-lattice relaxation times in chemically polarized species."J Phys Chem 1974;78:1971-7.

70. Cheng HL, Wright GA. "Rapid high-resolution T(1) mapping by variable flip angles: Accurate and precise measurements in the presence of radiofrequency field inhomogeneity,"Magn Reson Med 2006;55(3):566-74.

71. Deoni SC, Rutt BK, Peters TM. "Rapid combined T1 and T2 mapping using gradient recalled acquisition in the steady state,"Magn Reson Med 2003;49(3):515-26.

72. Deoni SC, Peters TM, Rutt BK. "High-resolution T1 and T2 mapping of the brain in a clinically acceptable time with DESPOT1 and DESPOT2,"Magn Reson Med 2005;53(1):237-41.

73. Venkatesan R, Lin W, Haacke EM. "Accurate determination of spin-density and T1 in the presence of RF-field inhomogeneities and flip-angle miscalibration,"Magn Reson Med 1998;40(4):592-602.

74. Parker GJ, Barker GJ, Tofts PS. "Accurate multislice gradient echo T(1) measurement in the presence of non-ideal RF pulse shape and RF field nonuniformity,"Magn Reson Med 2001;45(5):838-45.

75. Fram EK, Herfkens RJ, Johnson GA, Glover GH, Karis JP, Shimakawa A, Perkins TG, Pelc NJ. "Rapid calculation of T1 using variable flip angle gradient refocused imaging,"Magn Reson Imaging 1987;5(3):201-8.

76. Treier R, Steingoetter A, Fried M, Schwizer W, Boesiger P. "Optimized and combined T1 and B1 mapping technique for fast and accurate T1 quantification in contrast-enhanced abdominal MRI,"Magn Reson Med 2007;57(3):568-76.

77. Wang J, Qiu M, Kim H, Constable RT. "T1 measurements incorporating flip angle calibration and correction in vivo,"J Magn Reson 2006;182(2):283-92.

78. Wang HZ, Riederer SJ, Lee JN. "Optimizing the precision in T1 relaxation estimation using limited flip angles,"Magn Reson Med 1987;5(5):399-416.

79. Stollberger R, Wach P. "Imaging of the active B1 field in vivo,"Magn Reson Med 1996;35(2):246-51.

80. Roschmann P. "Radiofrequency penetration and absorption in the human body: Limitations to high-field whole-body nuclear magnetic resonance imaging,"Med Phys 1987;14(6):922-31.

81. Sacolick LI, Wiesinger F, Hancu I, Vogel MW. "B1 mapping by bloch-siegert shift,"Magn Reson Med 2010;63(5):1315-22.

82. Hornak JP, Szumowski J, Bryant RG. "Magnetic field mapping,"Magn Reson Med 1988;6(2):158-63.

83. Akoka S, Franconi F, Seguin F, Le Pape A. "Radiofrequency map of an NMR coil by imaging,"Magn Reson Imaging 1993;11(3):437-41.

84. Cunningham CH, Pauly JM, Nayak KS. "Saturated double-angle method for rapid B1+ mapping,"Magn Reson Med 2006;55(6):1326-33.

85. Dowell NG, Tofts PS. "Fast, accurate, and precise mapping of the RF field in vivo using the 180 degrees signal null,"Magn Reson Med 2007;58(3):622-30.

86. Jiru F, Klose U. "Fast 3D radiofrequency field mapping using echo-planar imaging,"Magn Reson Med 2006;56(6):1375-9.

87. Yarnykh VL. "Actual flip-angle imaging in the pulsed steady state: A method for rapid three-dimensional mapping of the transmitted radiofrequency field,"Magn Reson Med 2007;57(1):192-200.

88. Rudolf Stollberger PW. "Imaging of the active B1 field in vivo,"Magn.Reson.Med. 1996;35:246-51.

89. Preibisch C, Deichmann R. "T1 mapping using spoiled FLASH-EPI hybrid sequences and varying flip angles,"Magn Reson Med 2009;62(1):240-6.

90. Johnson G, Wadghiri YZ, Turnbull DH. "2D multislice and 3D MRI sequences are often equally sensitive,"Magn Reson Med 1999;41(4):824-8.

91. Andreisek G, White LM, Yang Y, Robinson E, Cheng HL, Sussman MS. "Delayed gadolinium-enhanced MR imaging of articular cartilage: Three-dimensional T1 mapping with variable flip angles and B1 correction,"Radiology 2009;252(3):865-73.

92. Li W, Scheidegger R, Wu Y, Vu A, Prasad PV. "Accuracy of T1 measurement with 3-D look-locker technique for dGEMRIC,"J Magn Reson Imaging 2008;27(3):678-82.

93. Sueyoshi E, Sakamoto I, Okimoto T, Hayashi K, Tanaka K, Toda G. "Cardiac amyloidosis: Typical imaging findings and diffuse myocardial damage demonstrated by delayed contrast-enhanced MRI,"Cardiovasc Intervent Radiol 2006;29(4):710-2.

94. Ugander M, Oki AJ, Hsu LY, Kellman P, Greiser A, Aletras AH, Sibley CT, Chen MY, Bandettini WP, Arai AE. "Extracellular volume imaging by magnetic resonance imaging provides insights into overt and sub-clinical myocardial pathology,"Eur Heart J 2012;33(10):1268-78.

95. Nacif MS, Turkbey EB, Gai N, Nazarian S, van der Geest RJ, Noureldin RA, Sibley CT, Ugander M, Liu S, Arai AE, Lima JA, Bluemke DA. "Myocardial T1 mapping with MRI: Comparison of look-locker and MOLLI sequences,"J Magn Reson Imaging 2011;34(6):1367-73.

96. Ng AC, Auger D, Delgado V, van Elderen SG, Bertini M, Siebelink HM, van der Geest RJ, Bonetti C, van der Velde ET, de Roos A, Smit JW, Leung DY, Bax JJ, Lamb HJ. "Association between diffuse myocardial fibrosis by cardiac magnetic resonance

contrast-enhanced T(1) mapping and subclinical myocardial dysfunction in diabetic patients: A pilot study,"Circ Cardiovasc Imaging 2012;5(1):51-9.

97. Liu et al. "Myocardial T1 measurement: Comparison of modified look-locker inversion recovery (MOLLI) and T1 scout in the multi-ethinic study of atherosclerosis (MESA),"Journal of Cardiovascular Magnetic Resonance 2012;14(Suppl 1):265.

98. Dass S, Suttie J, Piechnik S, Ferreira V, Holloway C, Robson M, Watkins H, Karamitsos T, Neubauer S. "Non-contrast T1 mapping characterizes the myocardium beyond that achieved by late gadolinium enhancement in both hypertrophic and dilated cardiomyopathy,"Journal of Cardiovascular Magnetic Resonance 2012;14(Suppl 1):O27.

99. Williams ES, Kaplan JI, Thatcher F, Zimmerman G, Knoebel SB. "Prolongation of proton spin lattice relaxation times in regionally ischemic tissue from dog hearts,"J Nucl Med 1980;21(5):449-53.

100. Hosch W, Bock M, Libicher M, Ley S, Hegenbart U, Dengler TJ, Katus HA, Kauczor HU, Kauffmann GW, Kristen AV. "MR-relaxometry of myocardial tissue: Significant elevation of T1 and T2 relaxation times in cardiac amyloidosis,"Invest Radiol 2007;42(9):636-42.

101. Dall'Armellina E, Piechnik SK, Ferreira VM, Si QL, Robson MD, Francis JM, Cuculi F, Kharbanda RK, Banning AP, Choudhury RP, Karamitsos TD, Neubauer S. "Cardiovascular magnetic resonance by non contrast T1-mapping allows assessment of severity of injury in acute myocardial infarction,"J Cardiovasc Magn Reson 2012;14:15.

102. Kass DA. "Ventricular resynchronization: Pathophysiology and identification of responders,"Rev Cardiovasc Med 2003;4 Suppl 2:S3-S13.

103. Mann DL, Bristow MR. "Mechanisms and models in heart failure: The biomechanical model and beyond,"Circulation 2005;111(21):2837-49.

104. Querejeta R, Varo N, Lopez B, Larman M, Artinano E, Etayo JC, Martinez Ubago JL, Gutierrez-Stampa M, Emparanza JI, Gil MJ, Monreal I, Mindan JP, Diez J. "Serum carboxy-terminal propeptide of procollagen type I is a marker of myocardial fibrosis in hypertensive heart disease,"Circulation 2000;101(14):1729-35.

105. Shimizu M, Umeda K, Sugihara N, Yoshio H, Ino H, Takeda R, Okada Y, Nakanishi I. "Collagen remodelling in myocardia of patients with diabetes,"J Clin Pathol 1993;46(1):32-6.

106. Heling A, Zimmermann R, Kostin S, Maeno Y, Hein S, Devaux B, Bauer E, Klovekorn WP, Schlepper M, Schaper W, Schaper J. "Increased expression of cytoskeletal, linkage, and extracellular proteins in failing human myocardium,"Circ Res 2000;86(8):846-53.

107. Maisch B. "Ventricular remodeling,"Cardiology 1996;87 Suppl 1:2-10.

108. Sun Y, Weber KT. "Cardiac remodelling by fibrous tissue: Role of local factors and circulating hormones,"Ann Med 1998;30 Suppl 1:3-8.

109. Sparrow P, Messroghli DR, Reid S, Ridgway JP, Bainbridge G, Sivananthan MU. "Myocardial T1 mapping for detection of left ventricular myocardial fibrosis in chronic aortic regurgitation: Pilot study,"AJR Am J Roentgenol 2006;187(6):W630-5.

110. Sueyoshi E, Sakamoto I, Uetani M. "Contrast-enhanced myocardial inversion time at the null point for detection of left ventricular myocardial fibrosis in patients with dilated and hypertrophic cardiomyopathy: A pilot study,"AJR Am J Roentgenol 2010;194(4):W293-8.

111. Sibley CT, Noureldin RA, Gai N, Nacif MS, Liu S, Turkbey EB, Mudd JO, van der Geest RJ, Lima JA, Halushka MK, Bluemke DA. "T1 mapping in cardiomyopathy at cardiac MR: Comparison with endomyocardial biopsy,"Radiology 2012.

112. Messroghli DR, Nordmeyer S, Dietrich T, Dirsch O, Kaschina E, Savvatis K, O h-Ici D, Klein C, Berger F, Kuehne T. "Assessment of diffuse myocardial fibrosis in rats using small-animal look-locker inversion recovery T1 mapping,"Circ Cardiovasc Imaging 2011;4(6):636-40.